Geologic Characterization of Enigmatic Carbonate Masses in the Woodford Shale, Criner Hills Area, Oklahoma

By

DANIELLE P. MARTIN

Bachelor of Arts in Earth and Environmental Science

Wesleyan University

Middletown, CT

2014

Submitted to the Faculty of the
Graduate College of the
Oklahoma State University
in partial fulfillment of
the requirements for
the Degree of
MASTER OF SCIENCE
May, 2017

GEOLOGIC CHARACTERIZATION OF ENIGMATIC CARBONATE MASSES IN THE WOODFORD SHALE, CRINER HILLS AREA, OKLAHOMA

Thesis Approved:

Dr. Jack C. Pashin

Thesis Adviser

Dr. Natascha Riedinger

Dr. Jay M. Gregg

ACKNOWLEDGEMENTS

I would like to thank my adviser, Dr. Jack Pashin, for his guidance and encouragement throughout my graduate career. His enthusiasm and love for geology sparked a plethora of great ideas, including the basis for my master's thesis project. I've learned a great deal while studying under him. I would also like to thank Dr. Natascha Riedinger for her help with geochemistry. There were many evenings when she stayed late to guide me through procedures for sample preparation. Thank you to Dr. Jay Gregg for assistance with the fluid inclusions and cathodoluminescence microscopy and to Sahar Mohammadi for her help with the analysis of the fluid inclusions. Thank you to Dr. Bill Gilhooly at Indiana University-Purdue University Indianapolis for the analysis of the nitrogen isotopes for my project. Thank you to the Boone Pickens School of Geology and alumni, the McNair Graduate Fellowship program, the Oklahoma City Geological Society for their financial support over the years. Many thanks to the professors and my fellow students in the department who facilitated my learning over the years, especially with my thesis: Dr. Eliot Atekwana, Dr. Jim Puckette, Dr. Tracy Quan, Mercy Achang, Ibukun Bode, Kyrsti Cecil and Jingyao Meng. My family and friends have provided a great deal of emotional support throughout this journey. I would also like to thank my undergraduate adviser, Dr. Suzanne O'Connell for sparking my initial interest in geology and introducing me to academic science research.

Name: DANIELLE P. MARTIN

Date of Degree: May 2017

Title of Study: GEOLOGIC CHARACTERIZATION OF ENIGMATIC CARBONATE MASSES IN THE WOODFORD SHALE, CRINER HILLS AREA, OKLAHOMA

Major Field: GEOLOGY

Abstract: The origin of carbonate masses in the Devonian Woodford Shale in the McAlister Cemetery Quarry in south-central Oklahoma have long been an enigma. Masses range from 24 cm to 1.5 m in diameter and are sub-spherical to oblate or ellipsoidal in shape. Field, petrographic and geochemical results reveal a much more complex diagenetic history than previous research suggests. The masses formed below the sediment-water interface with varying paleoredox conditions and were altered through the complete geologic history of the Woodford Shale in the Criner Hills Uplift. The carbonate masses consist of a nucleus and surrounding outer rings. They are composed of microcrystalline calcite with microfossil pseudomorphs and intercrystalline bitumen, and a sparry rind perimeter composed of calcitic and hematitic bands. Field and petrographic evidence, and geochemical results indicate that the concretions began accreting in normal marine waters during early diagenesis preserving the precompactional sediment fabric. Masses show consistent isotopic trends from the nucleus to outer rings: Positive trends in $\delta^{13}C$ (-20.09 to -7.40‰ VPDB) and negative trends in $\delta^{18}O$ (-0.86 to -5.99‰ VPDB) and $\delta^{15}N$ (+0.51 to +10.59‰ relative to air). Isotopic trends continue in the sparry rind: Positive trends in $\delta^{13}C$ (-3.95 to +13.59‰), $\delta^{18}O$ (-5.47 to -3.06 ‰) and $\delta^{15}N$ (-6.92 to +16.78‰). High $\delta^{13}C$ values indicate that the calcitic and hematitic rind precipitated in isotopically heavy pore waters, facilitated by microbially mediated methanogenesis. Trace element concentrations (V, Ni, Mo) increase in the sparry rind, indicating increase in metal availability during rind growth. Geochemical evidence combined with field and petrographic evidence suggests that the carbonate masses underwent a broad range of events, including dissolution and mechanical reworking, possibly associated with Late Pennsylvanian and sub-Cretaceous unconformity development in the Criner Hills.

TABLE OF CONTENTS

LIST OF TABLES

Table Page

LIST OF FIGURES

Figure Page

Figure Page

CHAPTER I

INTRODUCTION

The Woodford Shale is the principal petroleum source rock in the southern Midcontinent and hosts one of the most prolific unconventional oil and gas plays in the region. The Woodford is of Late Devonian to Early Mississippian age, and extensive research has been conducted to characterize this formation as a petroleum source rock and hydrocarbon reservoir (e.g., Comer and Hinch, 1987; Johnson and Cardott, 1992; Comer, 2005). One facet of the Woodford Shale that remains an enigma is the large carbonate masses from the upper part of the Woodford section in the McAlister Cemetery Quarry (a.k.a., the McAlister Cemetery shale pit), which is an essential field trip destination in the Criner Hills of southern Oklahoma (Kirkland et al., 1992; Cardott and Chaplin 1993). These carbonate masses are a highlight of the quarry that has been viewed and discussed by innumerable geologists, yet they have not been studied in detail. Upon entering the quarry, visitors are greeted by three large, enigmatic limestone spheroids, which are perched near the edge of a small highwall overlooking the quarry (Fig. 1). These limestone spheroids were excavated from the quarry prior to the 1980's (Kirkland et al., 1992). Despite conspicuous nature of these masses, remarkably little is known about their formation and internal fabric. The purpose of this study is to produce a detailed geologic description and interpretation of origin of the spherical carbonate masses in the McAlister Cemetery shale pit.

Figure 1. The three large limestone spheroids in the McAlister shale quarry in south-central Oklahoma, positioned atop a highwall exposing a dipping panel of Woodford Shale.

This investigation is designed to facilitate a better understanding of the depositional environment and diagenetic history of the limestone masses, which may reveal new information on the origin of the Woodford Shale. The goal of this research was to characterize the depositional environment, diagenetic history, and mechanisms by which these carbonate masses formed. The major objectives were to: (1) describe the external and internal sedimentologic, biologic, and diagenetic fabrics and structures of the limestone masses, (2) analyze petrologic and geochemical indicators of depositional and diagenetic conditions, and (3) synthesize the results into a conceptual model of the origin of the carbonate masses.

Working hypotheses were formulated on the basis of the available literature and initial field observations were that the carbonate masses are (1) concretions preserving the precompactional fabric of the shale in a manner similar to coal balls or, alternatively, (2) are remnants of a primary carbonate unit that was deposited as part of the Woodford Shale, and (3) have been altered by soil-forming processes, perhaps in association with development of a Late Pennsylvanian angular unconformity and a sub-Cretaceous disconformity in the Criner Hills area (e.g., Walker, 2006). I would also like to identify where exactly in the Woodford Shale section these masses formed, being that they have apparently been observed in situ only by the quarrymen who excavated them (Kirkland et al., 1992).

Lithologic and petrographic descriptions, geochemical analyses, cathodoluminescence microscopy and fluid inclusion analysis are the tools used to test these hypotheses. Lithologic and petrographic description was intended to elucidate the composition and fabric of the limestone masses, and the remaining methods were applied to contribute to the understanding of limestone geochemistry, depositional environment, and diagenetic history.

CHAPTER II

PREVIOUS WORK

II. 1 Geologic Setting

The Late Devonian (Givetian) to Early Mississippian (Tournaisian) Woodford Shale was deposited in the southern Midcontinent during the Kaskaskia cratonic onlap event, along with other organic-rich mudrocks that accumulated across North America during the Late Devonian, including the Bakken Formation, Chattanooga Shale, and Ohio Shale (Hass and Huddle, 1965; Lambert, 1993; Ettensohn and Lierman, 2012). These organic-rich deposits are the principal petroleum source rocks in the eastern and central United States, with the Woodford Shale sourcing an estimated 70% of the oil discovered in central and southern Oklahoma (Comer and Hinch, 1987). The Woodford Shale is widespread in Oklahoma; the formation name also has been applied in the Permian Basin of western Texas and southeastern New Mexico.

In south-central Oklahoma, the Woodford Shale is a grayish-black, fissile shale with interbedded grayish-black chert beds and phosphate nodules in some parts. It ranges in thickness from 30 to 400 feet in most areas and up to 700 feet in the Southern Oklahoma Aulacogen, possibly due to tectonic overthickening (Ham, 1975; Amsden 1975). Common fossils are radiolaria, conodonts, inarticulate brachiopods, arthropods (*Angustidontus* and *Spathiocarus*), fish scales, silicified and carbonized wood, and *Tasmanites* algal cysts (Hass and Huddle, 1965).

The Woodford Shale unconformably overlies the Upper Ordovician to Lower Devonian Hunton Group (Fig. 2) in the Arbuckle Mountains, Ardmore Basin, and Criner Hills. The Hunton Group has a typical thickness of 100 to 350 feet, and an estimated 250 to 500 feet is missing due

to pre-Woodford erosion (Ham, 1975). This fossiliferous, shallow-marine carbonate unit contains multiple unconformities. The lower section (Chimneyhill Subgroup) contains skeletal limestone, the middle section (Henryhouse and Haragan-Bois d'Arc Formations) contains argillaceous and silty carbonate rocks, and the upper section (Frisco Formation) is calcarenite (Johnson and Cardott, 1992).

Overlying the Woodford Shale is Mississippian-age shale, siltstone, and carbonate (Fig. 2). The basal unit of the Mississippian System in south-central Oklahoma is the Sycamore Formation, which is composed of fine-grained, silty limestone interbedded with thin layers of dark-gray shale and lacking fossils. Thickness generally ranges from 230 to 350 feet. It is present in the southwestern portion of the Arbuckle Mountains and in parts of the Southern Oklahoma Aulacogen in the subsurface. Its absence in the northern portion of the Arbuckle Mountains is marked by an unconformity at the base of the younger Caney Shale (Ham, 1975).

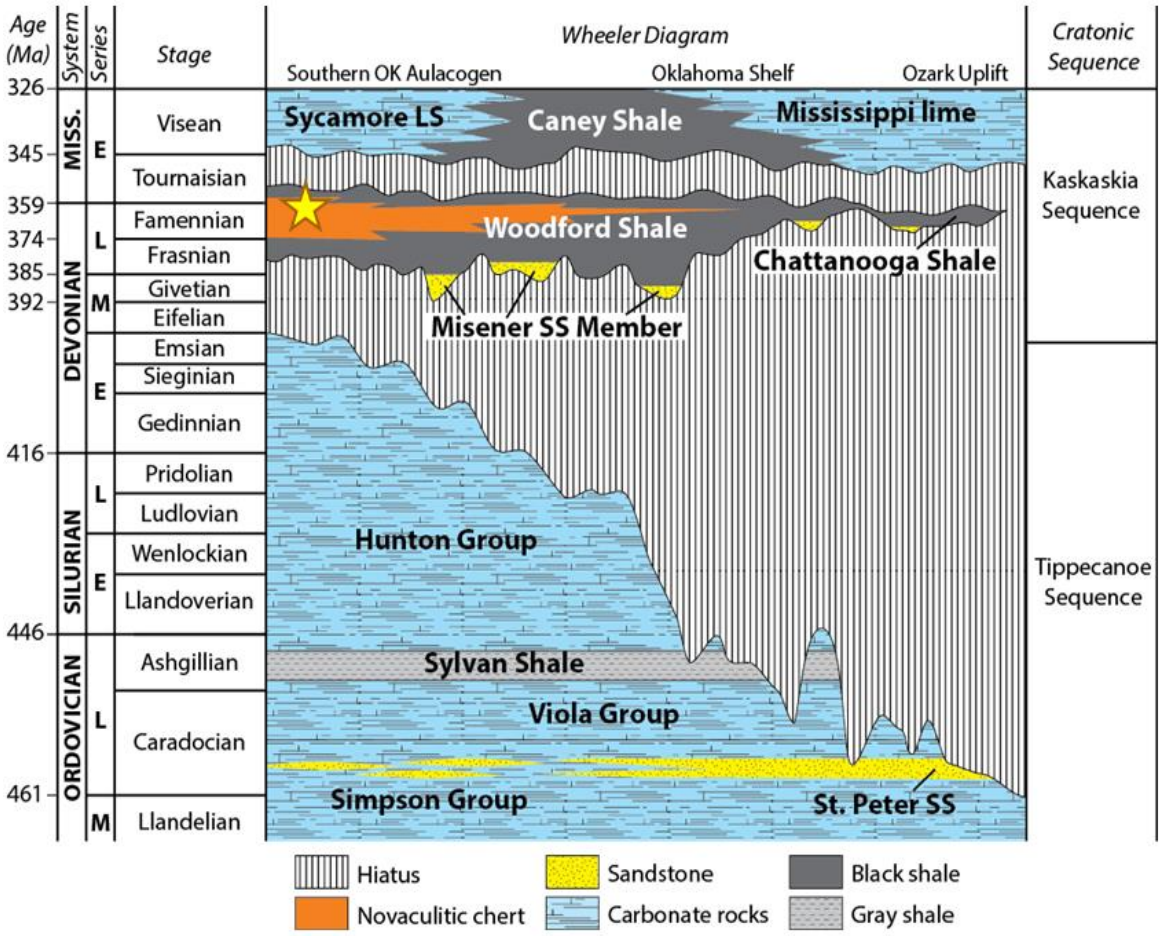

Figure 2. Generalized correlation of pre-Pennsylvanian rock units in the Southern Oklahoma Aulacogen going northeast through the Oklahoma Shelf and Ozark Uplift. The star indicates the relative position and age of the carbonate masses.

During the early and middle Paleozoic, the Anadarko and Arkoma basins were part of a broad continental shelf known as the Oklahoma Basin, which spanned most of Oklahoma and extended into six adjacent states (Johnson et. al, 1988). The Late Precambrian-Early Cambrian was marked by the formation of an Iapetan aulacogen in southern Oklahoma (Cardott and Chaplin, 1993). Deposition of shallow-marine carbonates of the Hunton Group occurred from the Silurian to Early Devonian, followed by regional exposure during the Early and Middle Devonian, which resulted in a regional unconformity that dissects Hunton strata. Subsequent deposition of clastic sediment occurred beginning with the dark shale of the Woodford. The siliceous, organic-rich black shale is thought to have occurred in response to marine transgression, development of an oxygen minimum zone, and oceanic upwelling (Comer, 1992; Kvale and Bynum, 2014; Callner, 2014; Cecil, 2016). This event was followed by shallowing of the basin and deposition of the silty limestone of the Sycamore Formation during the Mississippian (Ham, 1975; Cardott and Chaplin, 1993; Allen, 2000).

Subsidence driven by accommodation of orogenic uplifts occurred in response to the assembly of Pangaea during the Pennsylvanian, forming the Anadarko, Ardmore and Arkoma basins. The Criner Hills Uplift is a Late Pennsylvanian-Permian fault-related fold belt that formed at the southern end of the Ardmore Basin during the Wichita Orogeny (Allen, 2000) (Figs. 3, 4 and 5). The Criner Hills Uplift separates the Ardmore and Marietta basins, and the McAlister Cemetery Quarry is developed in the southwest flank of the uplift (Fig. 3, 4 and 6).

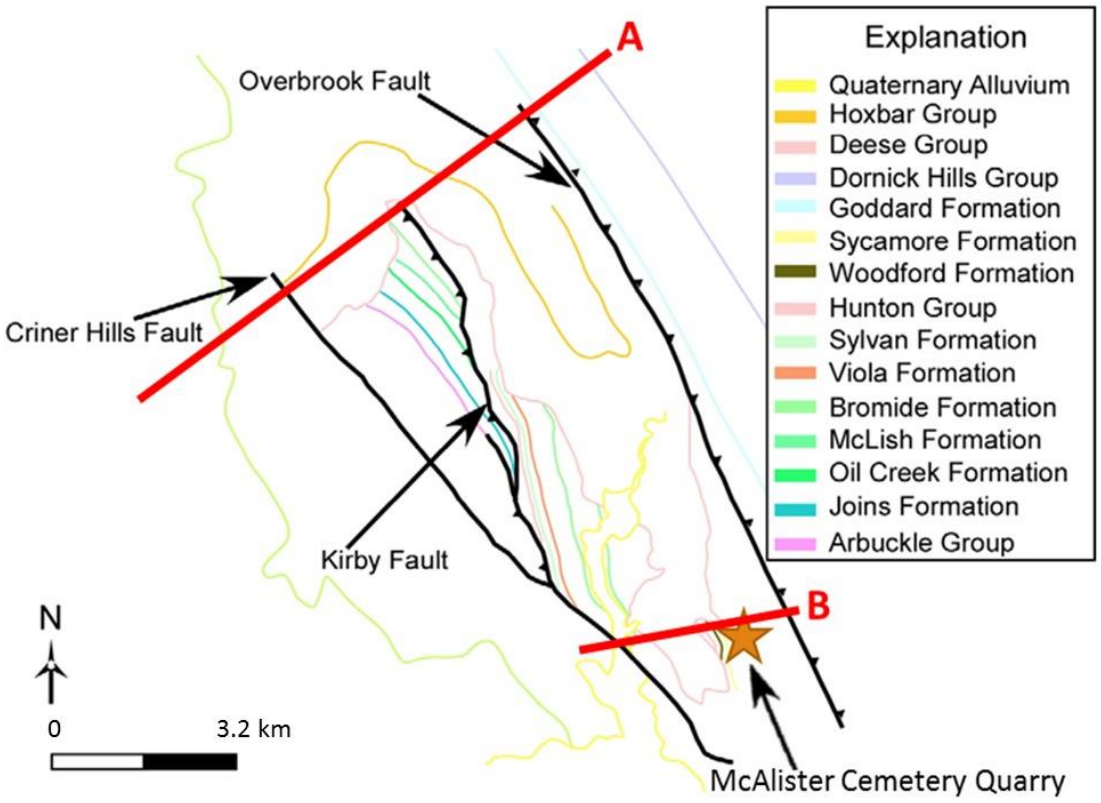

Figure 3. Geologic map depicting faults, basal contacts and the location of the McAlister Cemetery Quarry in and proximal to the Criner Hills area. Cross section lines for Figures 4 and 5 depicted in red (after Walker, 2006).

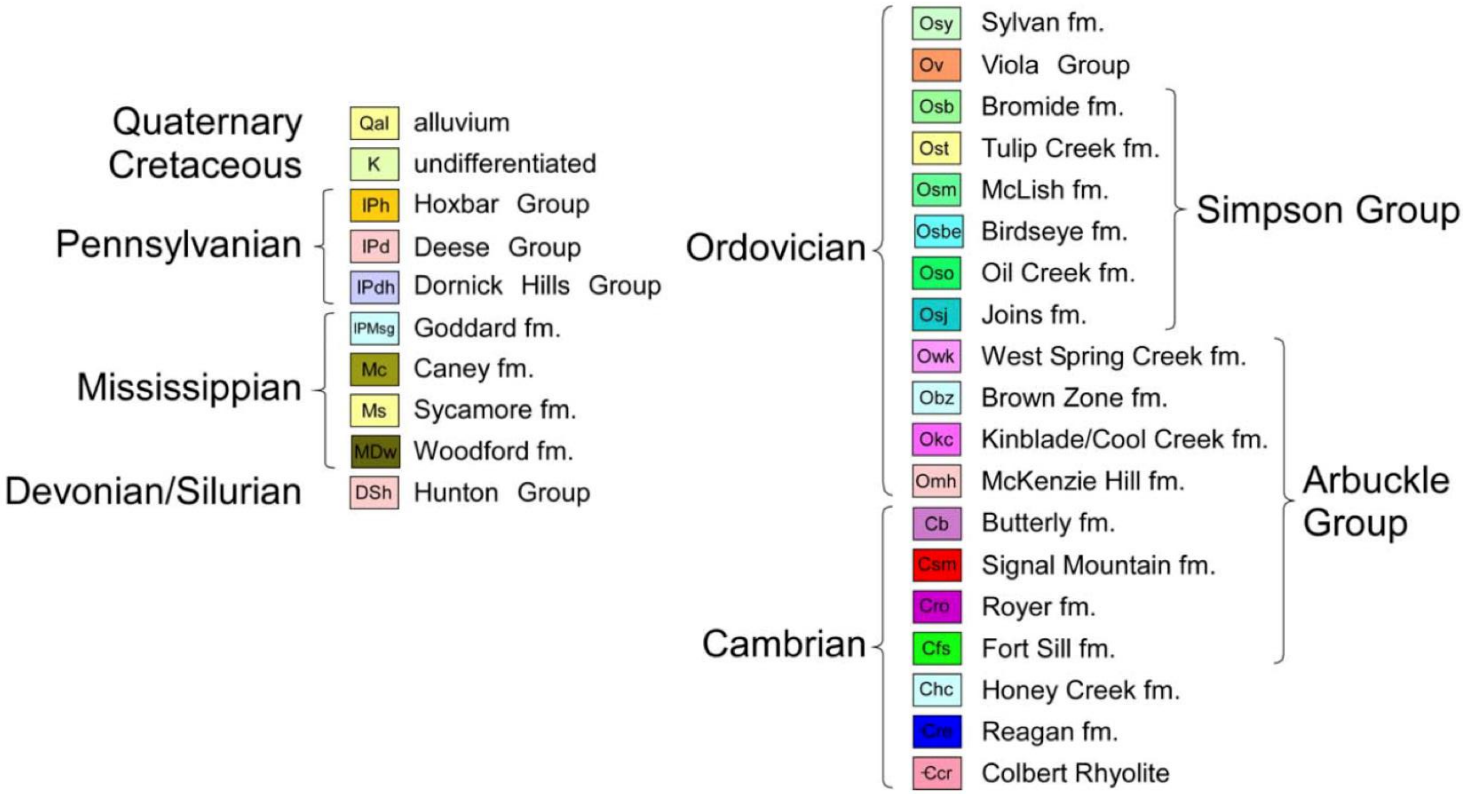

Figure 4. Explanation of the color, symbol and relative age of the stratigraphic units in the cross sections of Figures 5 and 6 (after Walker, 2006).

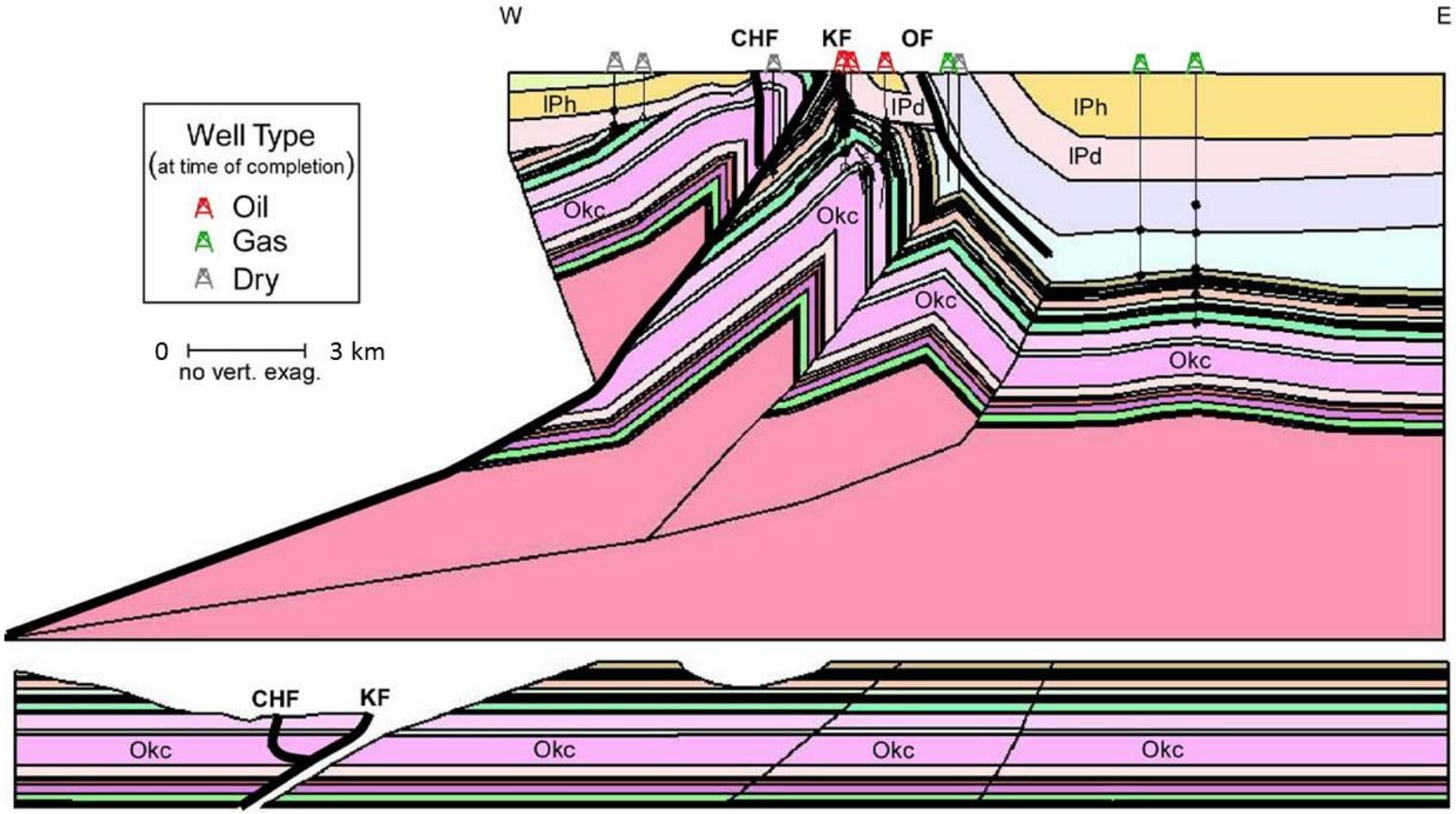

Figure 5. Regional view of balanced cross section A through the Criner Hills area and associated folded regions in south-central Oklahoma. Included are the Criner Hills Fault (CHF), Kirby Fault (KF) and Overbrook Fault (OF) (after Walker, 2006).

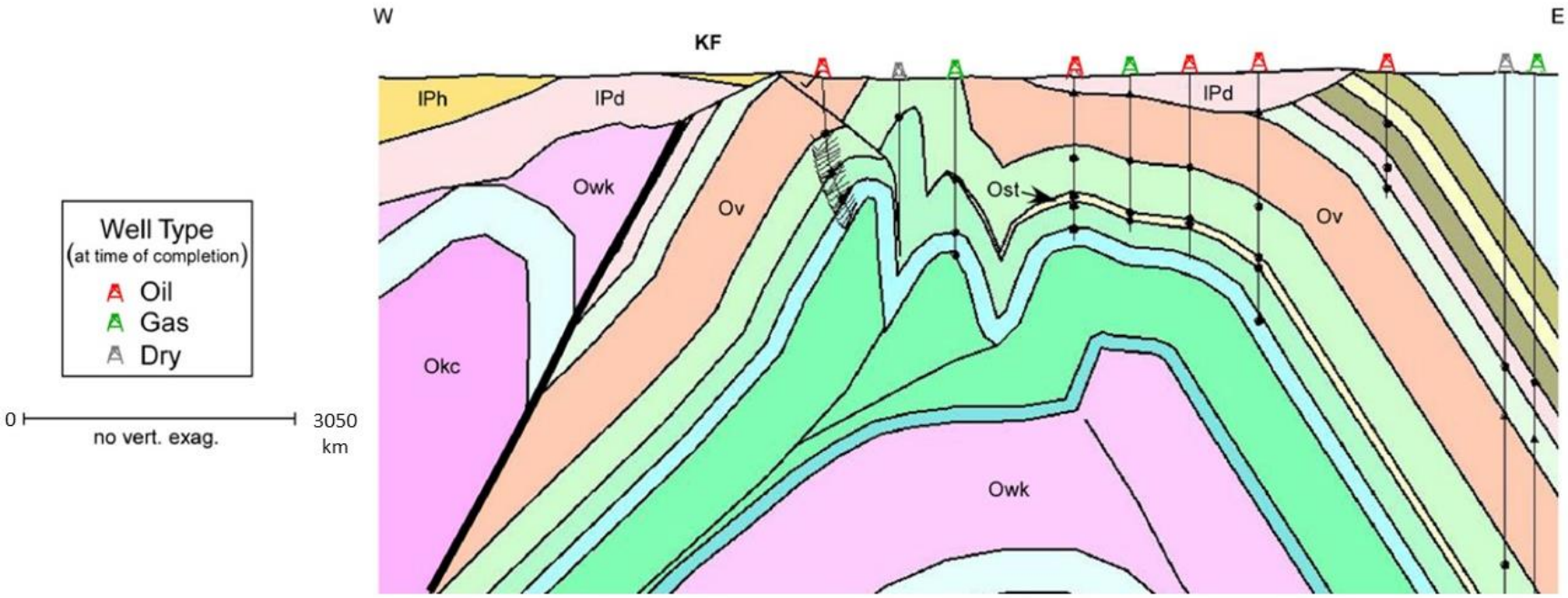

Figure 6. A balanced cross section B which traverses an area near the McAlister Cemetery Quarry (after Walker, 2006).

II. 2 Carbonate Concretions, Woodford Shale, Criner Hills Area

In addition to the large limestone masses that attract visitors to the quarry, other carbonate masses can be found at various locations throughout the pit. Kirkland et al. (1992) identified what they interpreted as seven calcite concretion in the Woodford Shale that are exposed in the McAlister Cemetery Quarry in September of 1986, after they had been excavated from the base of a phosphate nodule zone in the upper 50 feet of the Woodford Shale (Fig. 7A and 7B). This locality remains the only location where these types of masses are known in the Woodford. Kirkland et al. (1992) described the masses as spectacular calcite "concretions" averaging ~1.5 m in diameter. They noted a coating of calcite spar on some concretions and phosphate nodules embedded within the masses; they determined that the masses are composed mainly of coarsely crystalline calcite with minor amounts of quartz. Siliceous sponge spicules and radiolarian tests were observed throughout a core taken from one of the masses, along with sparse pyrite crystals (note that what Kirkland et al. 1992 determined to be sponge spicules may be simple radiolarian tests). The 2.5-cenimeter-diameter core recovered by Kirkland et al. (1992) contains a phosphate nodule 5-cm from the surface and bedding becomes increasingly faint towards the center of the mass.

The presence of bedding is the basis for the first hypothesis that the limestone masses preserve the precompactional fabric of the shale. No concretionary nucleus was identified in the core, but the Kirkland et al. (1992) suggested that the core might not have passed through the center of the concretion. They hypothesized that the masses formed within the upper part of

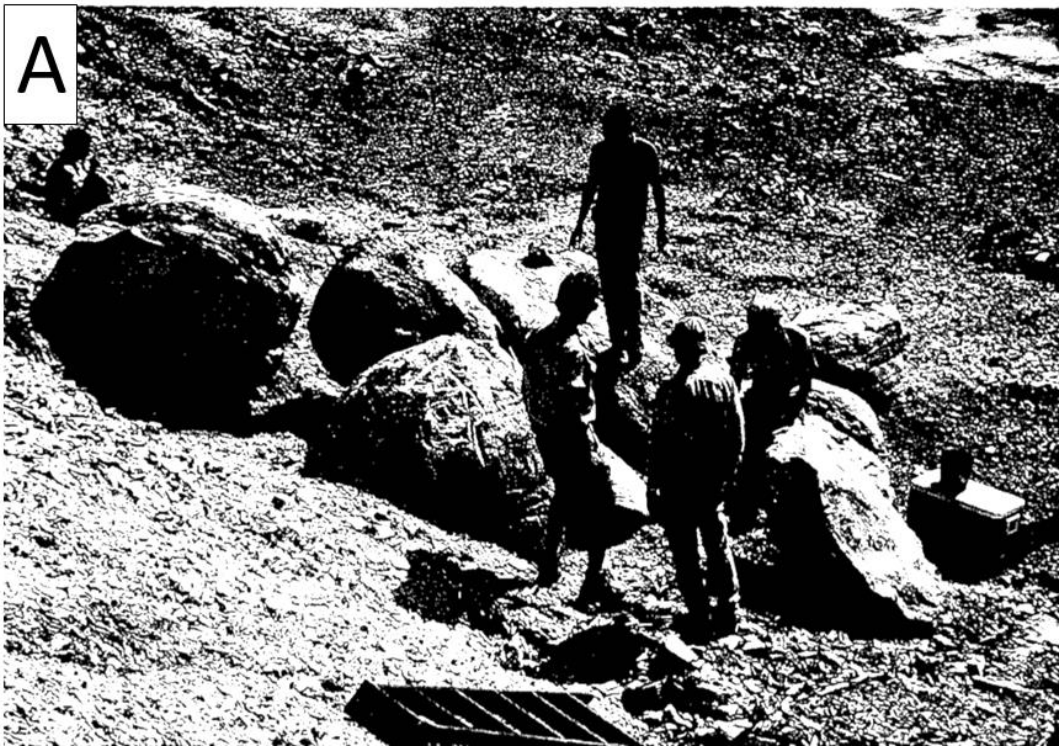

Figure 7. Seven carbonate concretions in the McAlister Cemetery Quarry after they were moved to a central area within the quarry in September 1986 (Kirkland et al., 1992). Note present-day condition of three masses in the quarry in August 2015 in Fig 1.

the sediment column by cementation and replacement, similar to how the phosphate nodules formed.

Puckette et al. (2013) referred to the masses as "bullion" concretions. They also observed phosphate nodules within these masses, along with well-preserved radiolarian tests that are readily observed in thin section. Preservation of undegraded and uncompacted tests with spines intact also helped to form my initial hypothesis of the concretions preserving the precompactional fabric of the shale.

II. 3 Carbonate Concretions, Ohio Shale

Devonian-age carbonate masses are not restricted to the Woodford Shale in south-central Oklahoma. Similar concretions are known from the Devonian shale section in other regions, including as those discovered in the Ohio Shale near Columbus, Ohio (Criss et al., 1936; Clifton, 1957). Carbonate concretions (0.3 to 3 meters in diameter) occur near the base of the Huron Member of the Ohio Shale, which is widespread in the Appalachian Basin (Fig. 8). Unlike the Woodford Shale carbonate masses, the Ohio Shale concretions were discovered in situ in the host mudrock and exhibit more internal deformation, with conical depressions in some concretions. The Huron carbonate masses become more ellipsoidal or oblate as they increase in size, with the largest ones averaging 2.7 meters in width and 1.8 meters in height and having funnel-shaped depressions in the tops and bottoms. The in situ concretions contain joints in places and cone-in-cone structures at the outer edges, and the host shale drapes under and over the concretions. Well-defined horizontal laminae occur in the main body of the concretions. The laminae constitute alternating light and dark layers with the latter

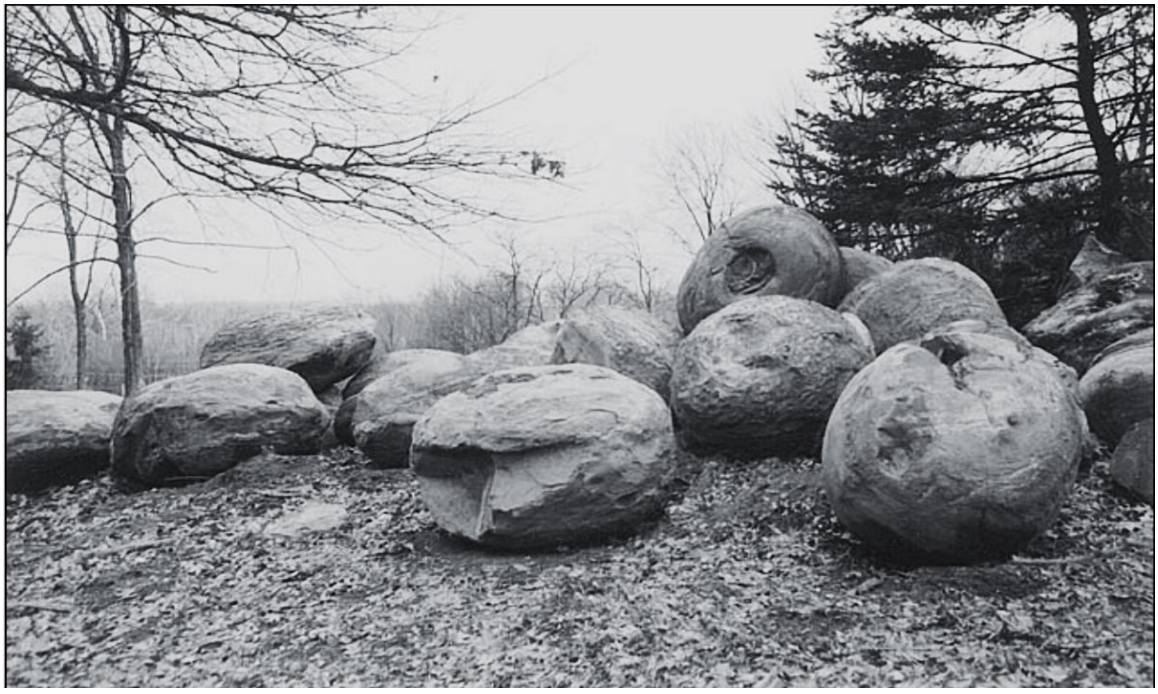

Figure 8. Carbonate concretions ("Huron boulders") excavated from the Huron member of the Ohio Shale in Columbus, Ohio (from Hansen, 1994)

being chert and the bands curving towards the center at the outer edges of the concretions. Marcasite is observed as a half-inch band on the outer edge of some masses (Edwards and Baker, 1951; Siesser, 1978; Alvi and Winterhal, 2001). The concretions are composed of mostly secondary materials of calcite, dolomite, pyrite and silica in a very fine matrix of carbonate, silica and organic matter. The centers are composed of mostly calcite but also contain some fluorite, barite, or celestite. Bands and patches of chert and chalcedony occur throughout the concretions, along with detrital quartz grains. Fossil material present throughout the masses includes plant spore cases and *Tasmanites*. Ostracods, unidentified spicules, well-preserved fish bones and ancient fossil wood (*Dadoxylon newberryi*) are found in the centers of some of the concretions. Replacement of minerals and fossils are common and can be identified through zoned calcite crytsals, optically oriented areas of matrix and doubly replaced plant matter (replaced first by calcite and then by quartz).

Clifton (1957) suggested that these masses formed during the early stages of burial after deposition of the host sediment but before the compaction was complete. The concretion grew outward from a nucleolus as crystallization and compaction commenced. The horizontal laminae in the concretions formed by replacement of mud laminae in its pre-compacted state by secondary crystals.

CHAPTER III

ANALYTICAL METHODS

Limestone samples were collected from the McAlister Cemetery Quarry, which is located northwest of Overbrook in Carter County, Oklahoma (Fig. 9). Three large carbonate masses (~1.5 m in diameter) are located at 34.07814° N., 97.15544° W. on top of a small highwall (Fig. 1). These bodies were left undisturbed because they are prominent geological attractions. We instead collected samples from large limestone masses near a small tailings pond (34.07837° N., 97.155023° W.). In addition, three small limestone balls (23 to 33 centimeters in diameter; 7 to 27 kg in weight) were retrieved from the quarry spoils next to the main highwall (34.07780° N., 97.15463° W). Seven samples were collected from the quarry (Fig. 10). Samples from the large masses were recovered by hammer. The three smaller limestone spheroids were the largest masses recovered intact and carried out of the quarry. Although there is a significant size difference between the smaller and larger limestone spheroids, they appear to be analogous: similar surficial features to the large limestone units were observed such as bedding, phosphate nodules, calcite rinds, carbonate-rimmed vugs, replaced fossils, and ferruginous staining.

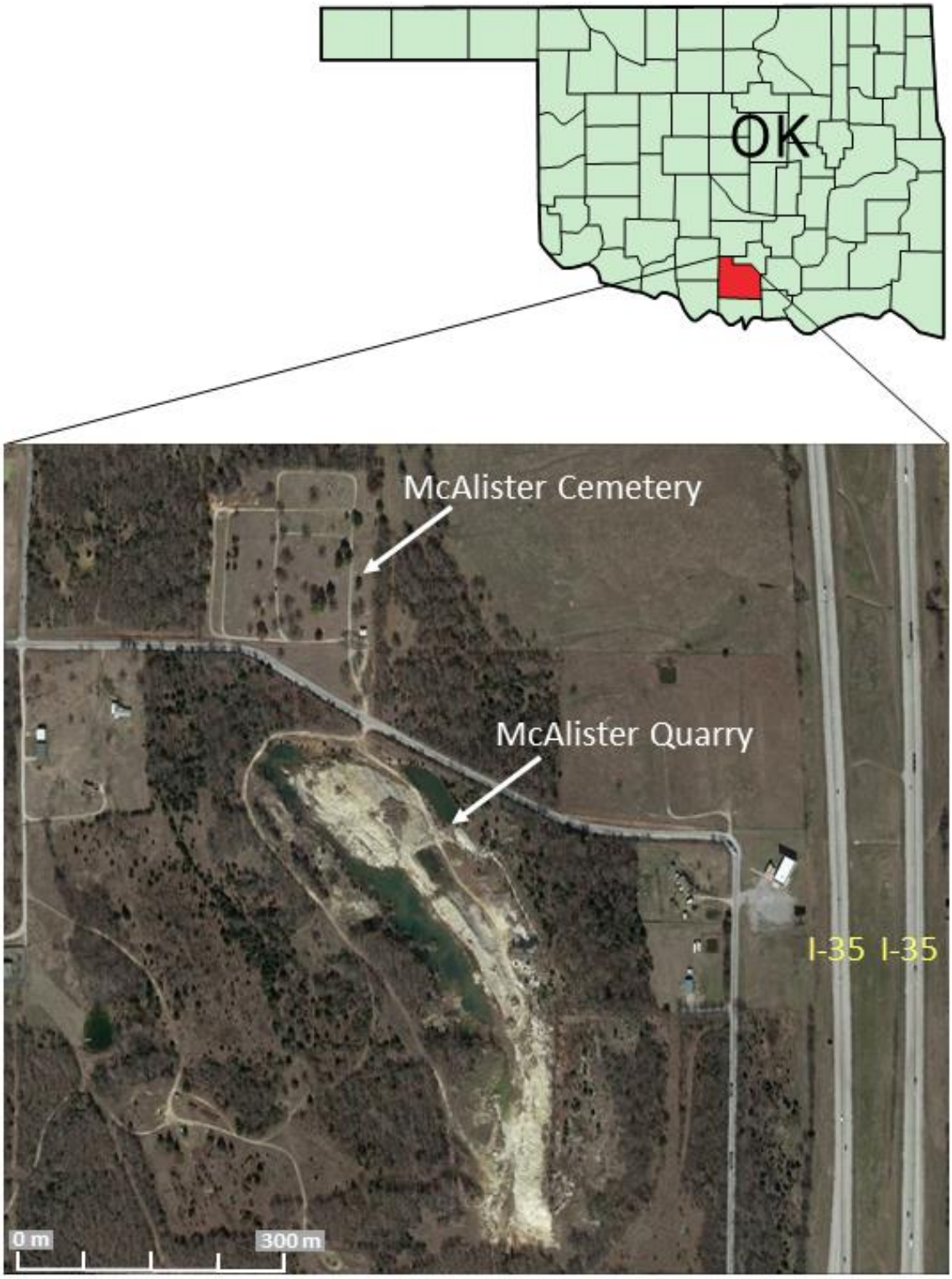

Figure 9. Location map of the study area, McAlister Cemetery Quarry, in Carter County, OK.

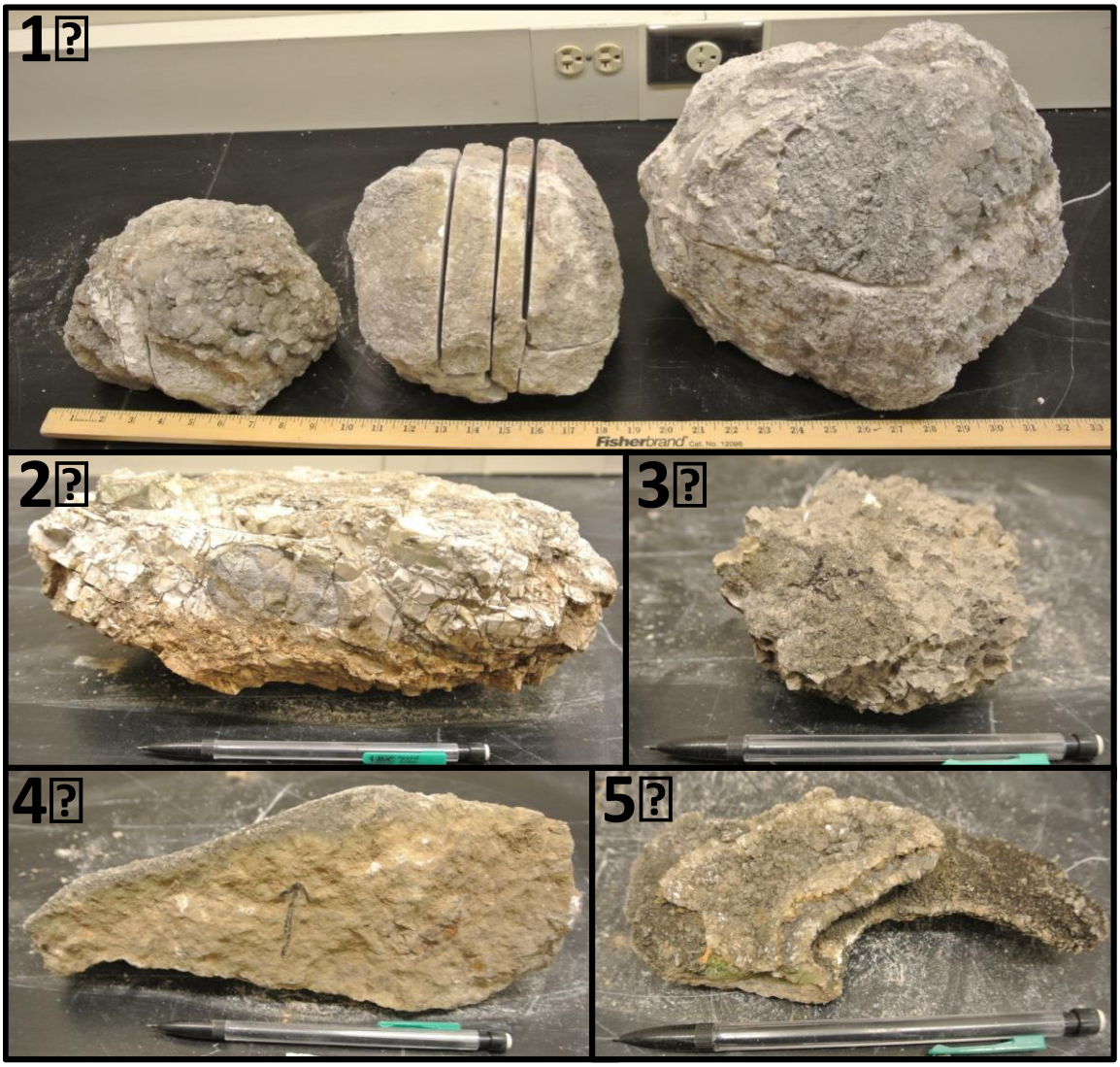

Figure 10. Samples from the McAlister Cemetery Quarry: 1) Three small limestone masses, 2) chert-bearing layer from large limestone mass, 3) outer rind of large limestone mass, 4) outer portion of large limestone matrix and 5) calcite vug fill.

Basic lithologic descriptions of the carbonate masses and hand samples were made in order to characterize rock type and sedimentary structure. Samples collected in the field were slabbed and polished, and billets were cut and sent to a third-party laboratory for thin section preparation. Most thin sections were stained with an alizarin red to distinguish calcite from other carbonate minerals. To classify the rock type, analyze rock composition, fabric, and cementation, 32 thin sections were made. Thin sections were described for mineralogy, rock fabric, texture, crystal orientation and fossil content using a Nikon polarizing petrographic microscope with a spectrophotometer attachment. This aided in reconstructing the depositional and diagenetic history of the units.

Two samples were examined using a CITL MK5-1 cold cathode optical cathodoluminescence (CL) system mounted on an Olympus-BX51 petrographic microscope to identify differences in the sample composition that are not visible under plane polarized light. With this technique samples are exposed to a high-energy electron beam that stimulates the emission of photons with wavelengths in the visible spectrum corresponding to the crystal make up. Compositional changes during crystal growth, such as changes in water chemistry, iron content, and magnesium content, can be highlighted with CL (Boggs and Krinsley, 2006).

One doubly polished fluid inclusion thick section was prepared from a billet made from the outer calcitic and hematitic rind of the largest concretion and was then thoroughly examined under high magnification (up to 80x mag) for fluid inclusions. During formation or recrystallization of diagenetic minerals, vacuoles may be filled with the formation water and trapped in within the crystal. Using microthermometry techniques, such as determining the melting point and bubble point of fluids and hydrocarbons, information may be obtained about the temperature, pressure and composition of the fluids that formed the mineral (Roedder, 1984).

Samples for isotope geochemistry were taken from each of the three small carbonate

masses using a carbide-coated drill bit and diamond-coated carbide drill bit. One transect of samples through each mass was collected, beginning at the nucleus, or center, and ending in the outer rind. The masses display faint concentric layering that differs slightly in color, and this layering was used to determine sample distribution, with one sample taken from each layer. A total of 29 samples were collected for $\delta^{13}C$, $\delta^{18}O$, and $\delta^{15}N$ stable isotopic analyses. Powdered samples were sent to the University of Miami, where $\delta^{13}C$ and $\delta^{18}O$ isotopic ratios were determined using a common acid bath interfaced to a Finnigan-MAT 251 isotope ratio mass spectrometer (IRMS). Values were corrected for interference and then reported on a per mil basis relative to the Vienna Pee Dee Pee (V-PDB) standard. Analytical precision of the isotopic ratio values is +/- 0.08‰.

Nitrogen stable isotope values were obtained from the powdered samples using an IRMS at Indiana University-Purdue University Indianapolis (IUPUI). Values were calibrated using standards USGS 40 ($\delta^{15}N$ = -4.52‰), IAEA N1 ($\delta^{15}N$ = 0.4‰), and RM 8704 ($\delta^{15}N$ = 4.01‰). Replicate analyses of standards revealed an analytical precision of 0.2 ‰. The elemental composition of the sample (%N) was determined using the thermal conductivity detector (TCD) on the elemental analyzer and calibrated with a size series of acetanalide (10.36 %N).

Samples were analyzed for major elements, specifically Mg, Al, P, Ca, Ti, Mn and Fe, and for trace elements, such as Sr, Ba, V, Cr,Co, Ni, Cu, Zn, As, Zr, Mo, Hf, Pb, Th, and U. Only V, Ni and Mo results were interpreted in this project. Minor and trace elements may be substituted into the crystal lattice when a crystal grows from a solution. The presence and relative concentration of some of these elements indicate the level of redox in the environment of deposition and subsurface processes associated with diagenetic alteration.

Concentrated HCl of trace metal grade was added to the powdered samples to dissolve carbonate, and then concentrated HNO_3 was added for the partial destruction of organic matter

present. Hydrofluoric acid (HF) was added only to the shale standard to remove silica bonds. Next, an Aqua Regia (HNO_3:HCl = 1:3 v/v) solution was added to isolate the heavy metals from the rock matrix. Between each step, samples were sonicated for 15 minutes, heated overnight at 120 to 140°C, and then evaporated to a viscous slurry form. Sample solutions were then dissolved with 50% HNO_3 and diluted with Milli-Q water. Dark particles of apparent resistant organic origin were separated from the solution by centrifuging the sample solution and pipetting the excess liquid. Samples were then analyzed for trace metal concentrations using an Inductively Coupled Mass Spectrometer (ICP-MS), Thermo Scientific iCAP Qc, at Oklahoma State University in Stillwater, OK.

CHAPTER IV

RESULTS

IV. 1 Lithologic Descriptions: Hand Sample

The large limestone masses at the McAlister Cemetery Quarry have a diameter of about 1.5 m and are subspherical to bullion-shaped (i.e., oblate discoids) (Figs. 11-13). The three smaller masses collected from the field range from 24 cm to 33 cm in diameter and are subspherical in shape (Fig. 10). In hand sample, freshly broken pieces of the limestone matrix have a distinctly sparry texture, yet polished slabs reveal a texture resembling micrite (Fig. 14-17). Hand sample slabs show layering in the matrix radiating from an apparent nucleus with red-staining in areas. Concentric lamellae resembling bedding, that pinches towards the edge of a mass, was observed on the surface of one of the large masses (Fig.13). One mass contains numerous thin to medium beds of chert in the exterior of the mass that become slightly divergent toward the heart of the mass (Fig. 18). Relief along the surfaces of the masses provides some indication of bedding although the layering that is apparent on the exterior of many masses is not visible in the interior (Figs. 14-17). Chert, calcite spar and shale layers can be seen on the outer portions of both small and large masses (Figs. 12-17, 19). Chert takes multiple forms in these samples, including bedding and layers on the outer mass surface. Samples of outer mass layers are composed of fractured white chert and fractured phosphate lenses with possible partial chert replacement, as suggested by hardness (Fig. 21)

Phosphate is observed as nodules and lenses, on the surface and embedded centimeters within the mass surface (Figs. 13, 17, 20, 22, 23). Spherical phosphate nodules up to 3.1 cm in diameter are scattered through the masses (Fig. 17).

Body fossils were observed in the masses and in the phosphate nodules; they include bivalves and solitary rugose corals up to 5 cm in length (Figs. 23, 24).

Isopachous cement is preserved as partial rims on the large masses in the quarry, and vugs within the masses also are lined by isopachous cement (Figs. 24, 25). The cement contains alterations of calcitic and hematitic bands. Some vugs within the masses are also completely filled with sparry calcite (Figs. 14, 15, 17).

A surficial rind can be seen lining both large and small carbonate masses. In slab samples the rind is composed of alternating calcitic and hematitic bands, like the isopachous cemented vugs, in addition to coarse calcite crystals (up to 2.3 cm) covering the outer surface of some masses (Figs, 14-17, 24, 26).

Figure 11. A large oblate-shaped mass, where on the upper left side appears to be an amalgam of two concretionary masses, probably two carbonate masses that were in close depositional proximity and grew together. Located on the high wall (lat. 34.078131°, long. -97.155499°).

Figure 12. Large carbonate mass positioned on top of the highwall within the McAlister Cemetery Quarry. Covering the mass is a band of calcite spar and phosphate nodules embedded throughout the surface of the mass. Located on the high wall (lat. 34.078164°, long. -97.155324°).

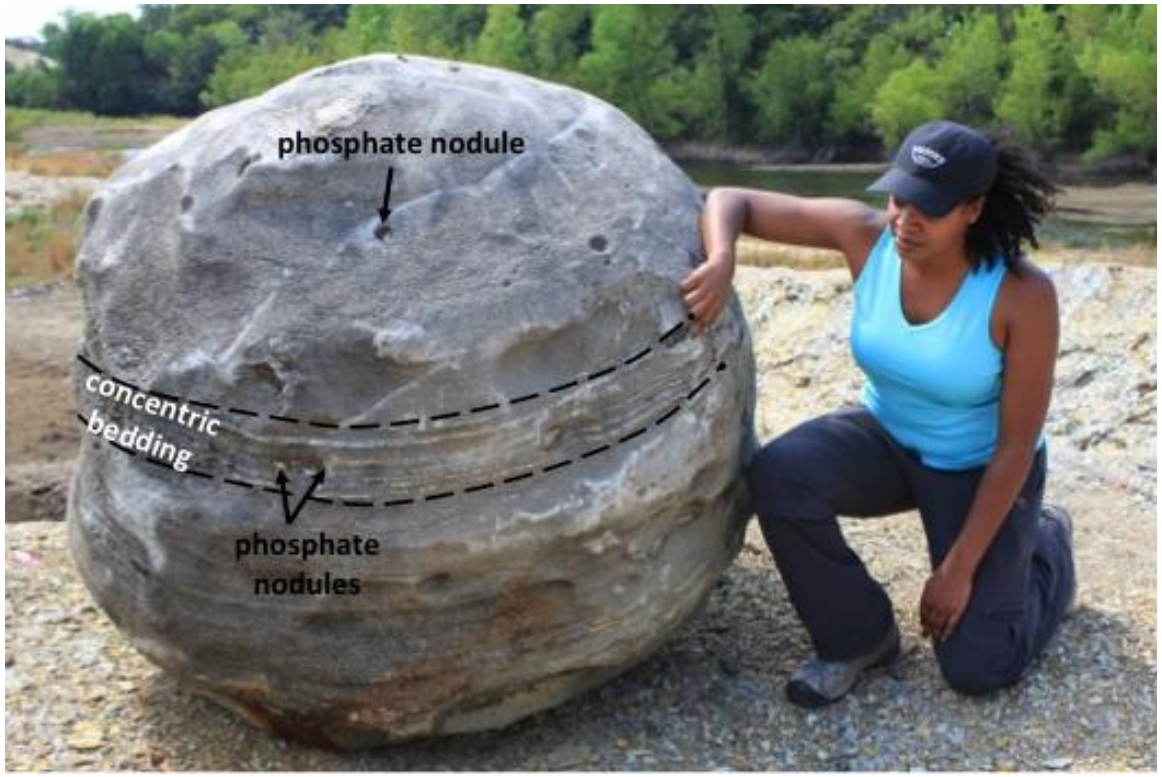

Figure 13. Carbonate mass atop highwall with concentric bedding which, pinches on the edges. Phosphate nodules are common embedded in the surface of the mass. Located on the high wall (lat. 34.078137°, long. -97.155438°).

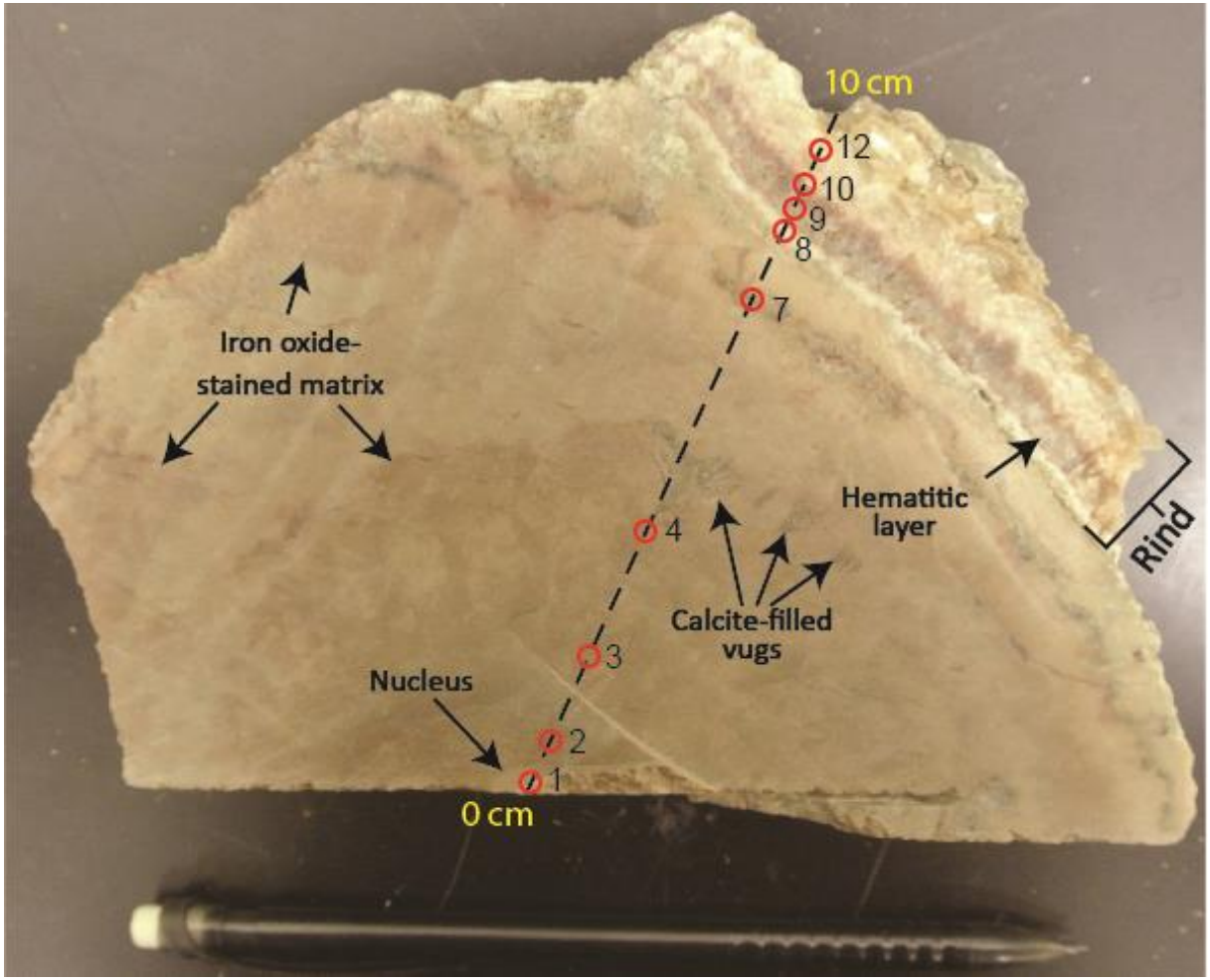

Figure 14. Polished slab from Mass 1 (the smallest mass from Sample Group 1 in Fig. 10) containing a nucleus, outer rings, iron-oxide stained matrix, calcite-filled vugs and sparry rind with hematitic layer. Red circles denote sample locations for geochemical analysis.

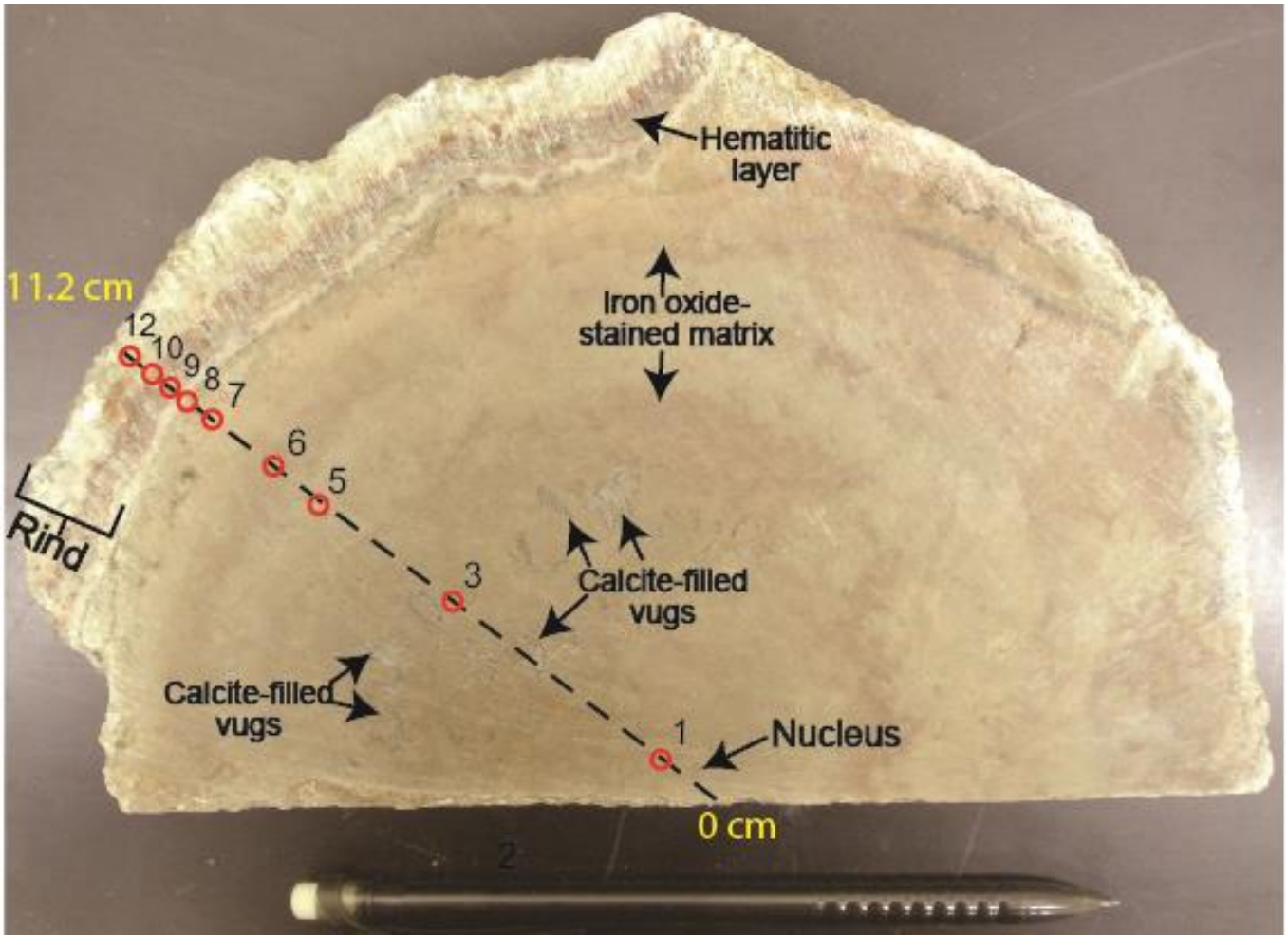

Figure 15. Polished slab from Mass 2 (intermediate mass from Sample Group 1 in Fig. 10), containing a nucleus, outer rings, iron-oxide stained matrix, calcite-filled vugs and sparry rind with hematitic layer. Red circles denote sample locations for geochemical analysis.

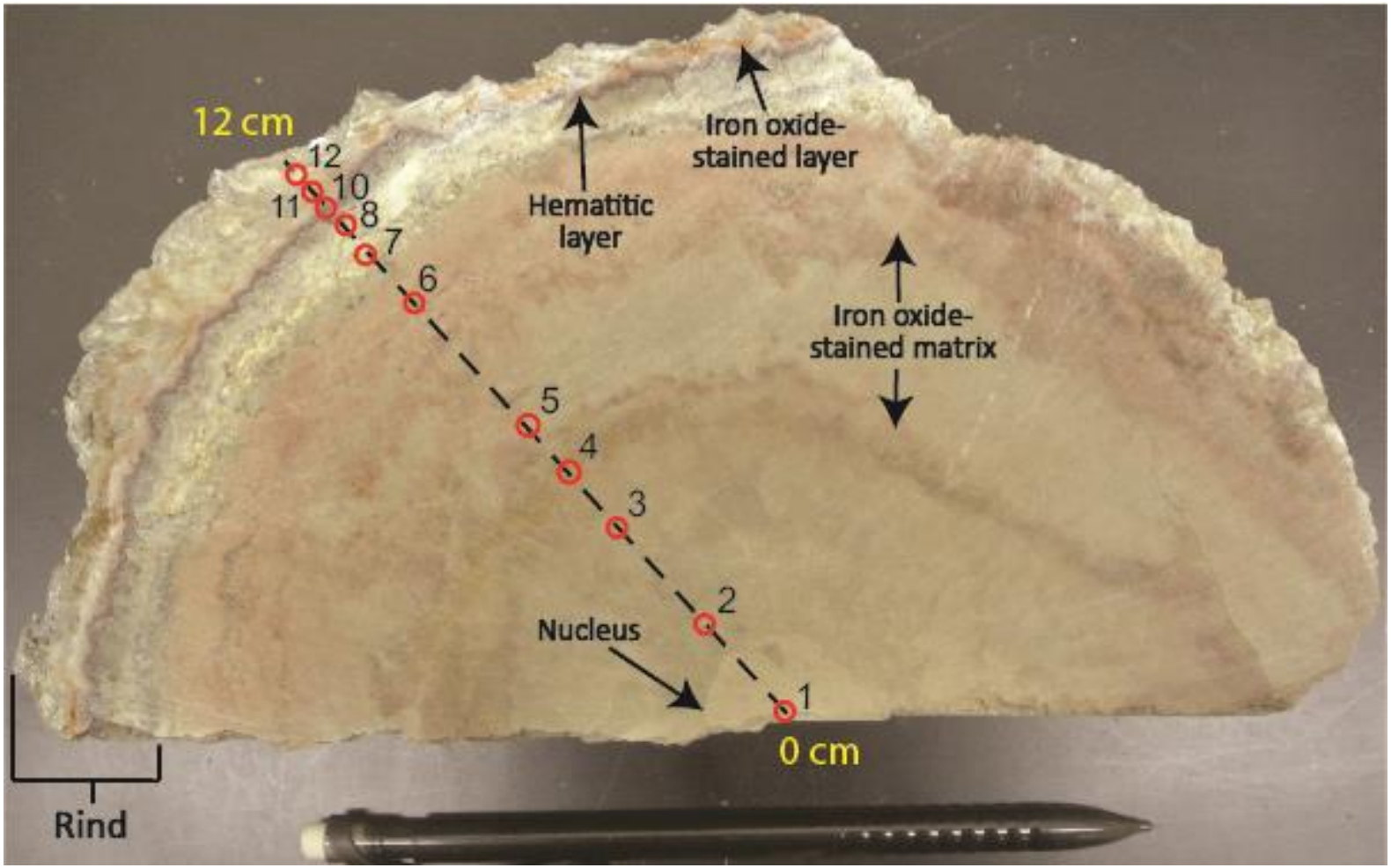

Figure 16. Polished slab from Mass 3 (the largest mass from Sample Group 1 in Fig. 10) containing a nucleus, outer rings, iron-oxide stained matrix and sparry rind with hematitic and iron oxide-stained layers. Red circles denote sample locations for geochemical analysis.

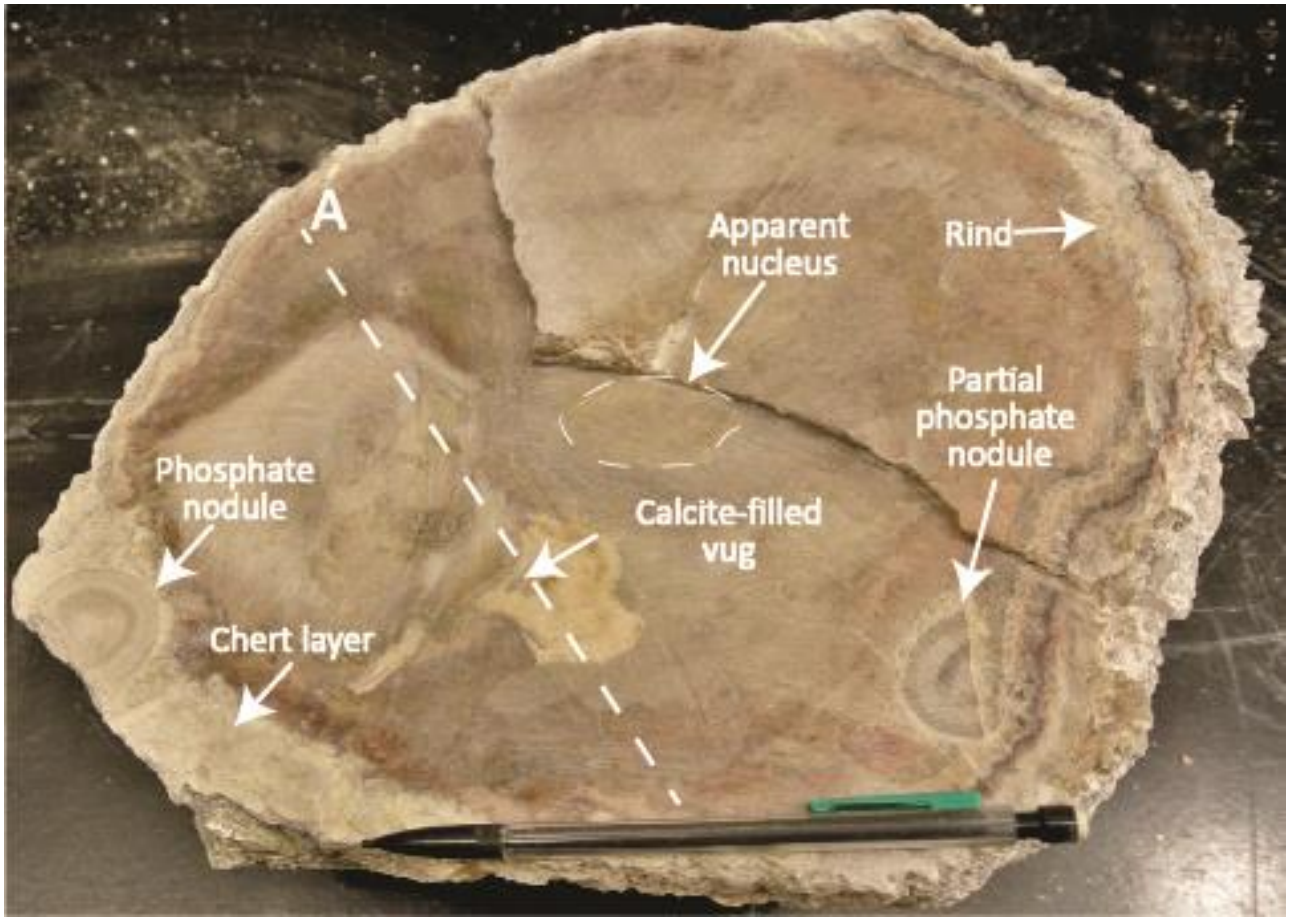

Figure 17. A slab from Carbonate Mass 3, the largest mass collected from the quarry, containing a very heterogeneous matrix (as highlighted across transect line A). Transect line A intersects the red-stained matrix and a sparry calcite-filled vug. A partial phosphate nodule is embedded more than 1 inch below the carbonate mass surface, below the sparry rind, as well as a partial phosphate nodule embedded in the outer chert layer.

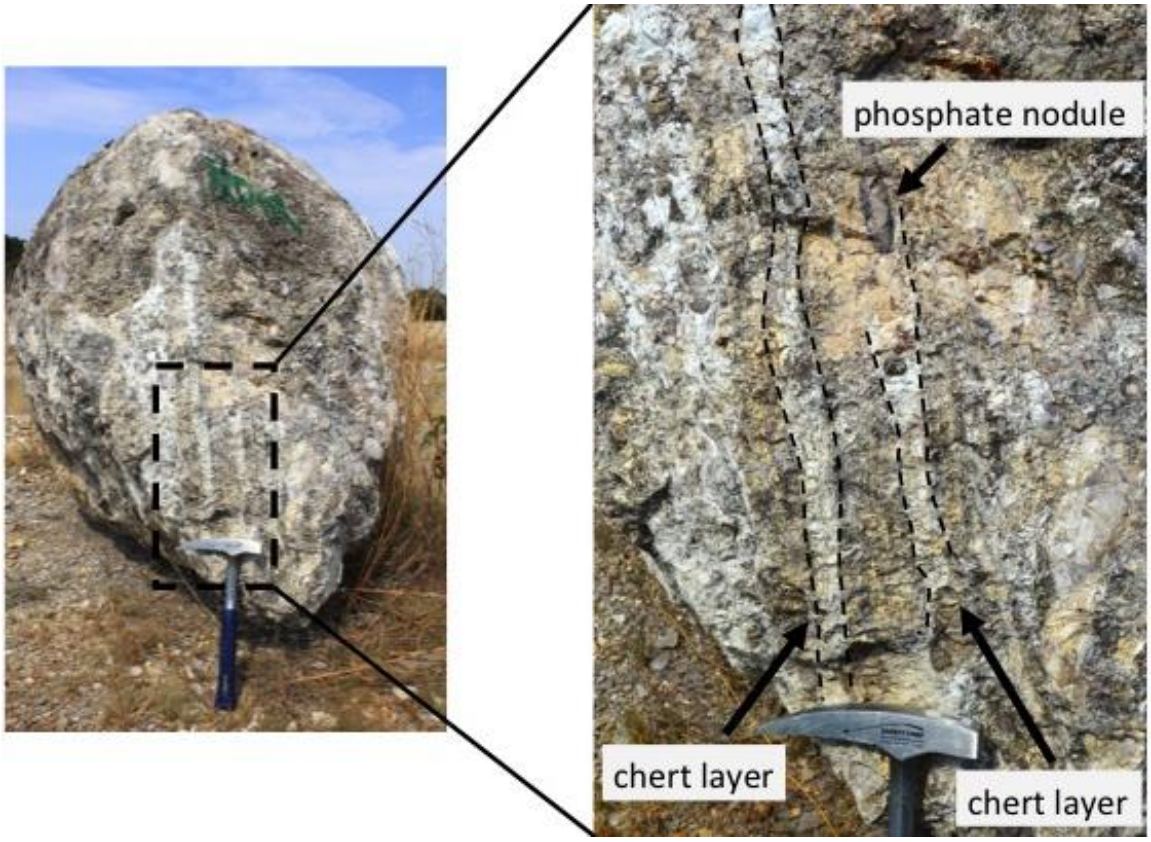

Figure 18. Large carbonate mass with bedded chert. Note that the chert layers become slightly divergent towards the heart of the mass. Located on the highwall (lat. 34.078131°, long. -97.155499°)

Figure 19. Large carbonate mass with chert bed in a depressed linear feature that spans the exposed surface of the large carbonate body. Located on the perimeter of the pond (lat. 34.078367°, long. -97.155019°)

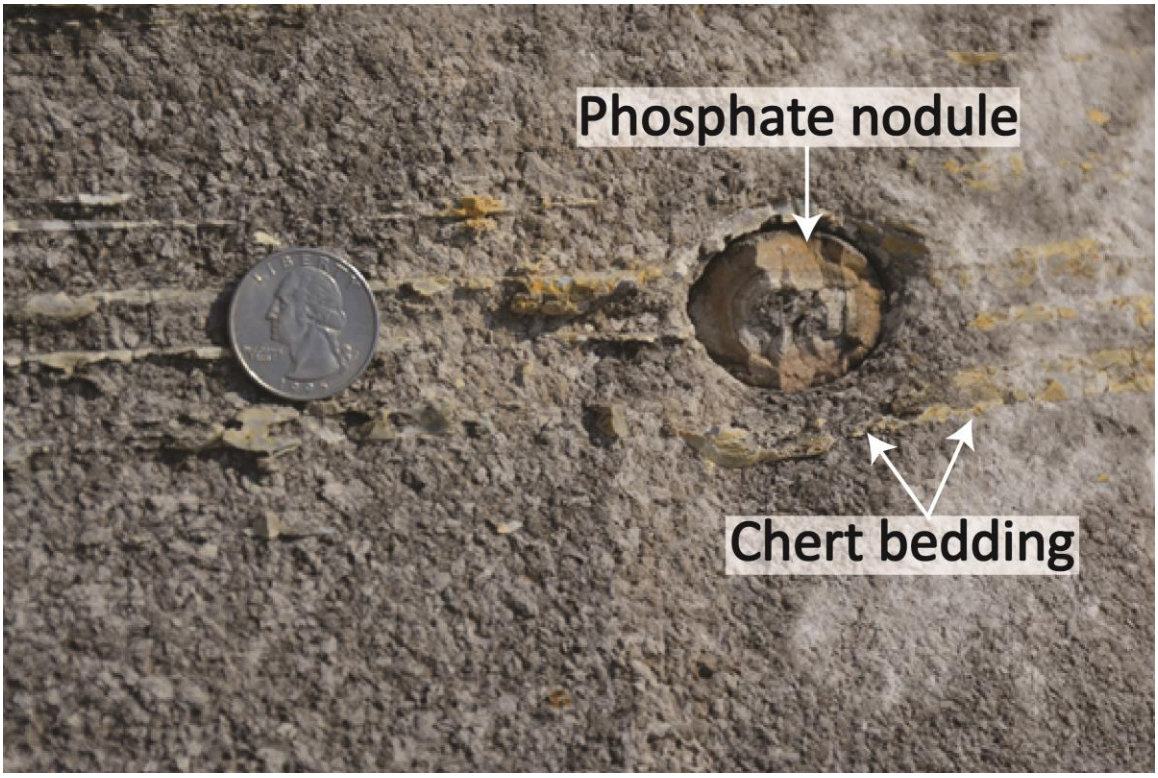

Figure 20. In-situ phosphate nodule embedded in surface of large carbonate mass with chert bedding. Internal chert layers terminate at phosphate nodule, while lower most layer curves around phosphate nodule. Located on perimeter of pond (lat. 34.078367°, long. -97.155019°).

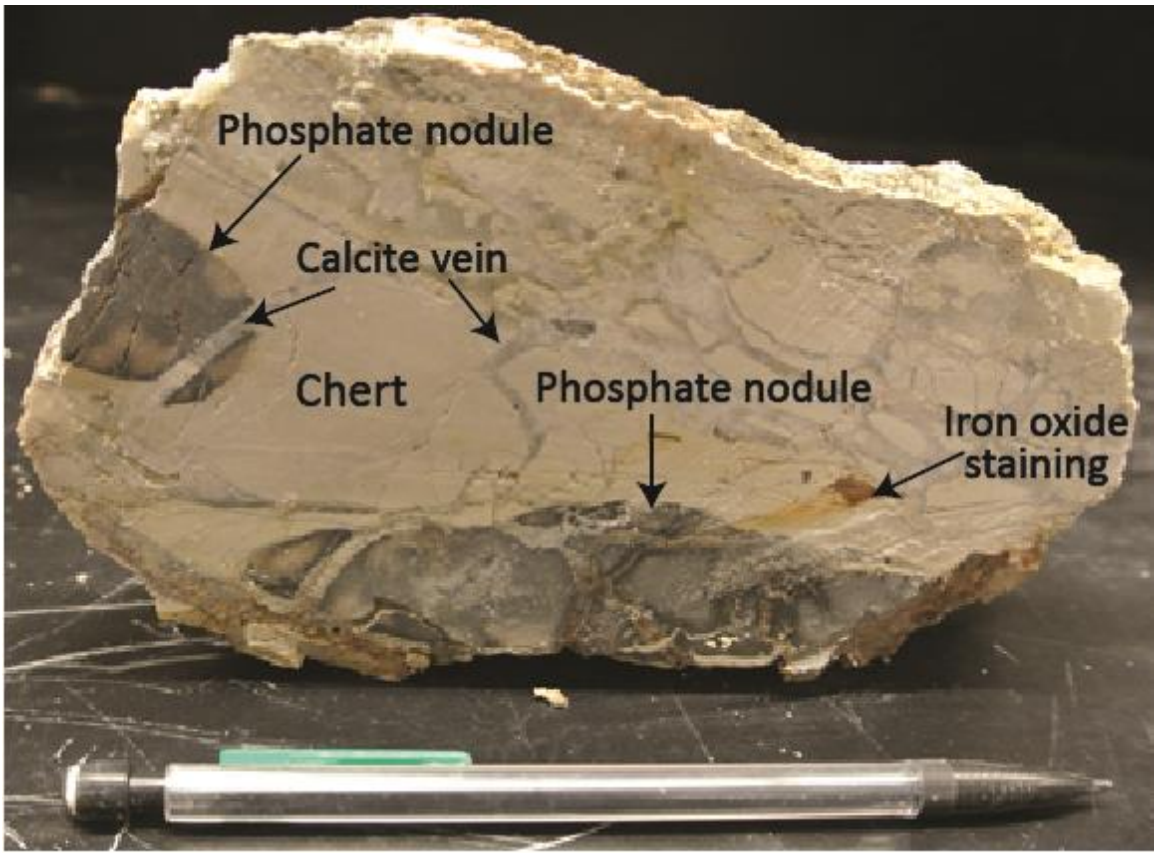

Figure 21. Phosphate nodules and chert containing calcite veins. Sample taken from surface of a large carbonate mass.

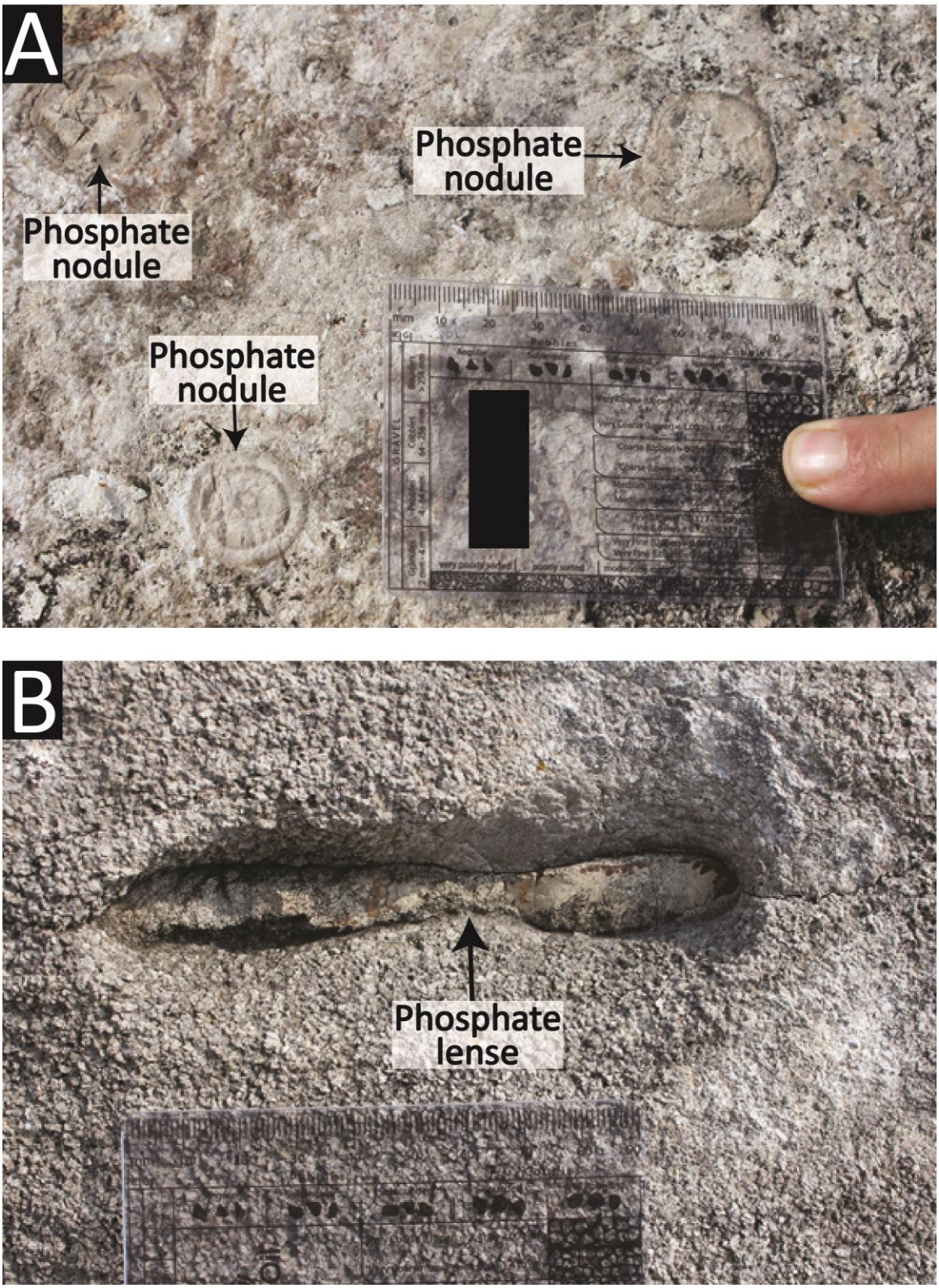

Figure 22. Phosphate nodules in large limestone masses. (A) Spherical to subspherical nodules with concentric banding. (B) Irregular discoidal lens.

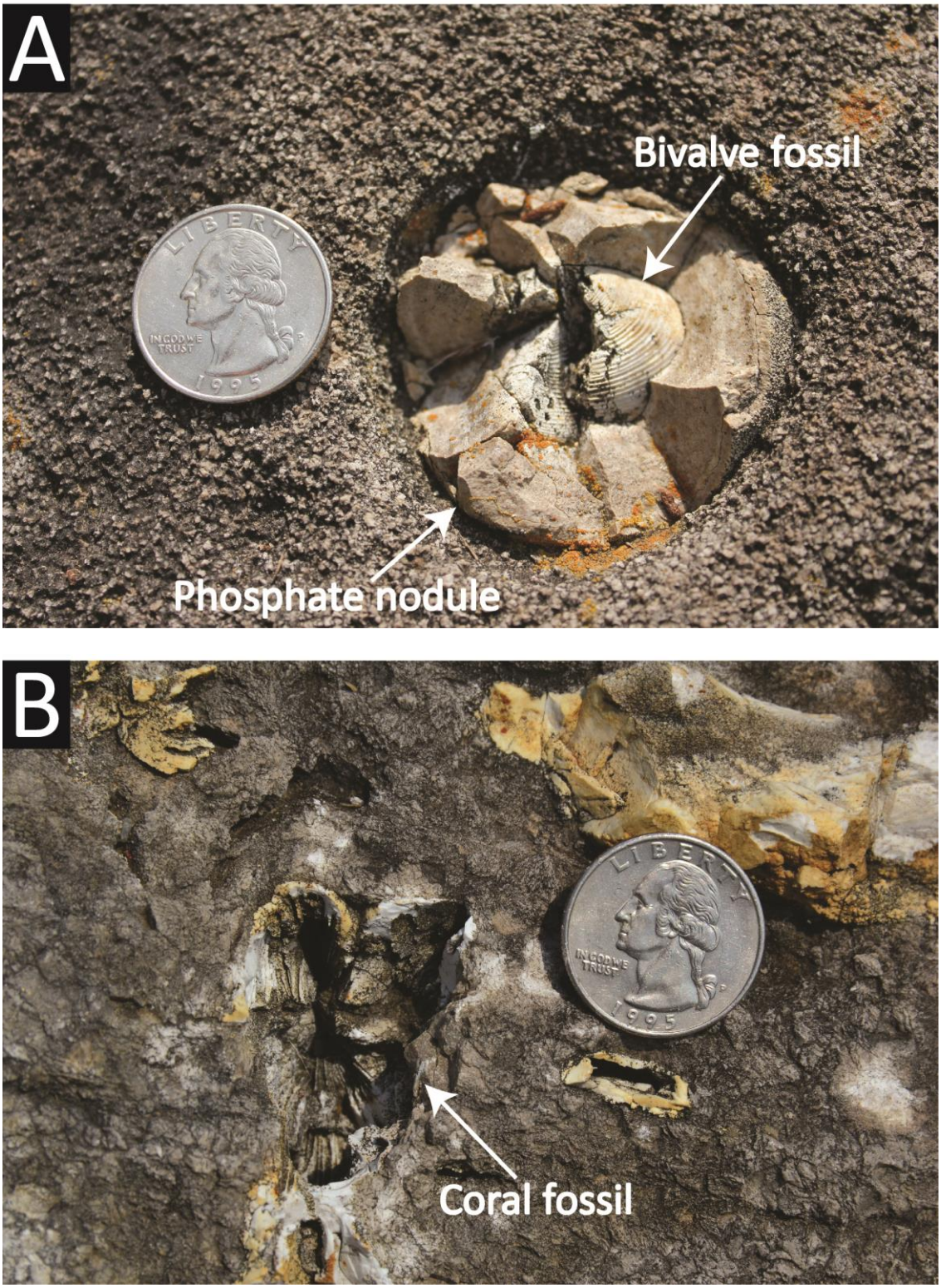

Figure 23. Marine fossils in large carbonate masses. (A) bivalve within phosphate nodule. (B) solitary rugose coral.

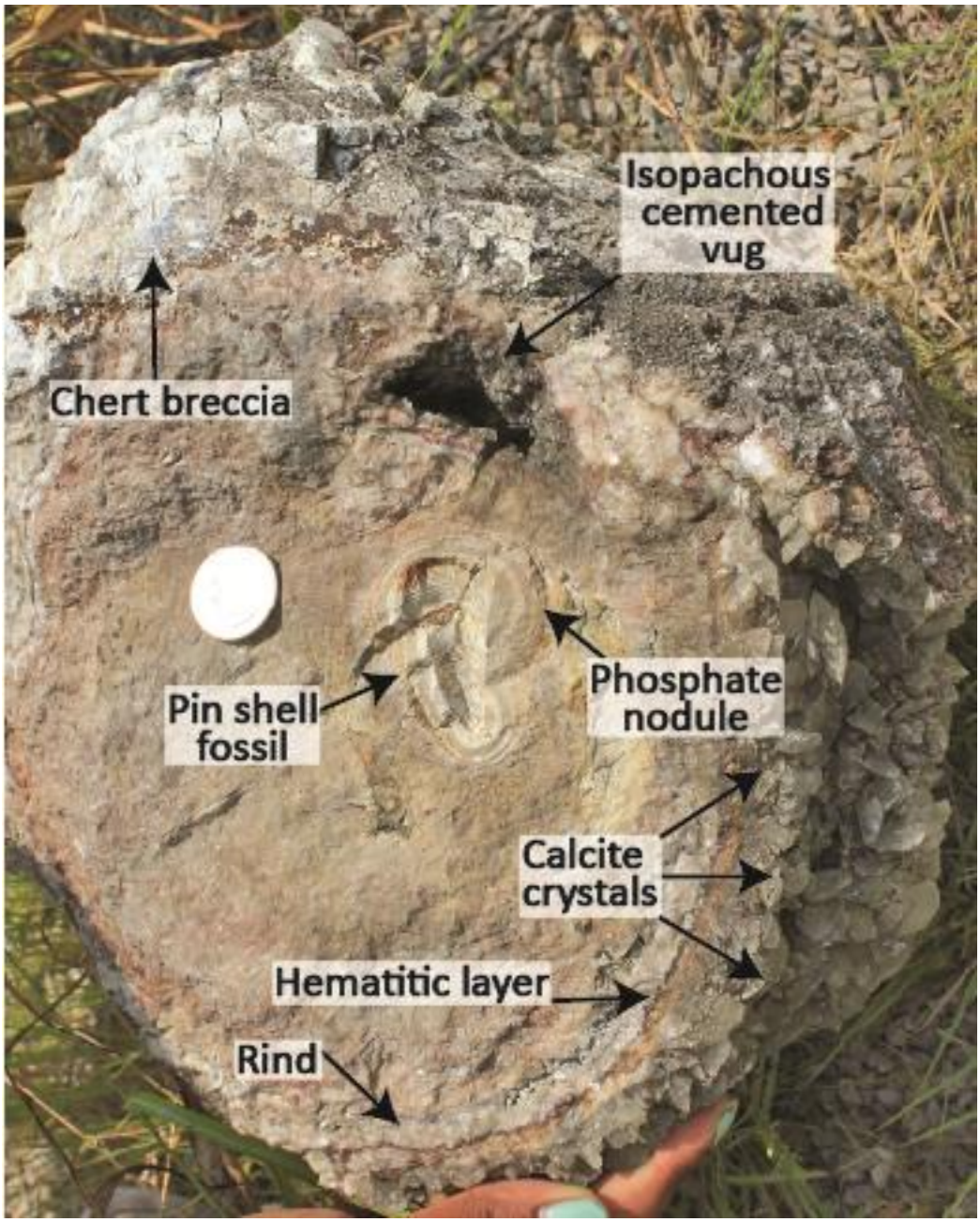

Figure 24. Small limestone concretion showing various components of Woodford Shale Devonian carbonate masses, with a pin shell fossil (cf. *Pinna* sp.), an isopachous cemented vug, isopachous outer rind, course calcite crystals and chert breccia.

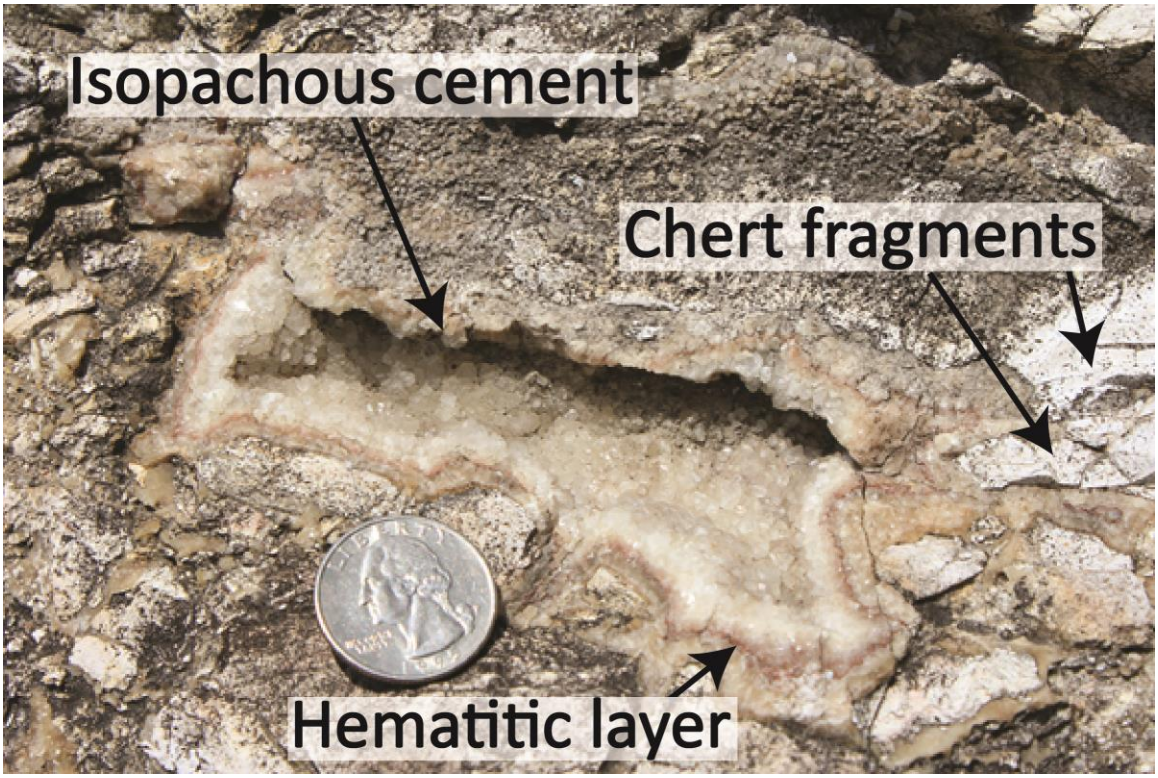

Figure 25. Large vug on surface of large carbonate mass. Isopachous cement with a hematitic layer lining vug. Chert fragments are also in the mass.

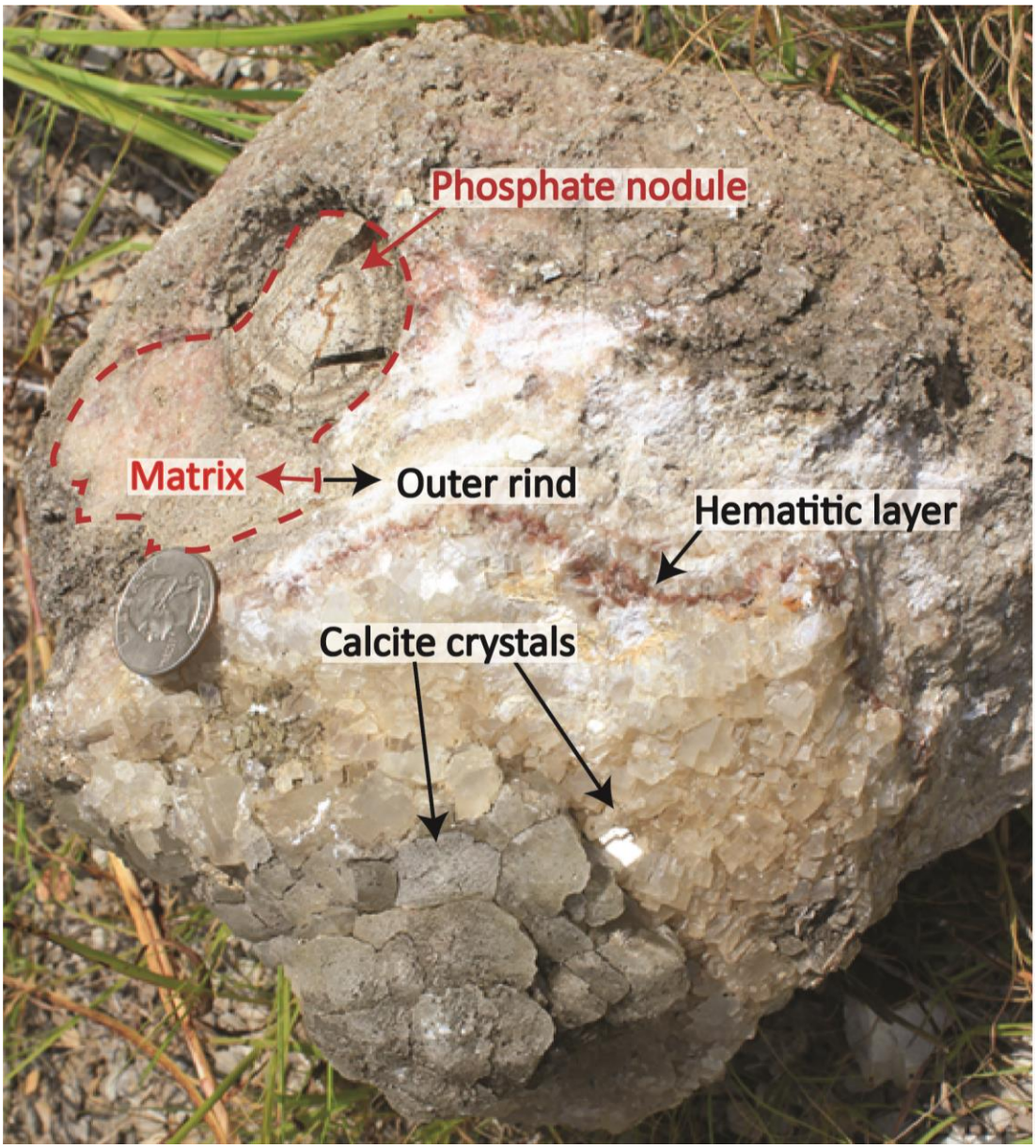

Figure 26. Small carbonate limestone mass with a phosphate nodule, hematitic banding and coarse calcite crystals. The exposed matrix is within the red-dotted enclosure; the outer rind is outside of the red-dotted enclosure.

IV. 2 Lithologic Descriptions: Thin Section

Thin sections of the limestone reveal a matrix composed mostly of microcrystalline calcite with poikilotopic calcite containing radiolaria, *Tasmanites*, sparse organic particles, and hematitic stain (Figs. 27-29). Under cross-polarized light it is apparent the poikilotopic calcite crystals form larger subequant calcite crystals, some of which are twinned (Figs. 28). Well-preserved siliceous microfossils, including radiolaria, are best preserved in the phosphate nodules within the limestone masses (Fig. 30). Within the matrix, the best preservation of microfossils is seen in Mass 3, possibly due to the higher chert content that can be seen in hand sample (Figs. 17, 27). Conodont elements and the spore, *Laevigatosporites* sp., were also observed in thin sections of the limestone (Figs. 31, 32).

Iron staining, wheat-seed siderite crystals, and spherulitic apatite crystals were also were observed in the matrix (Figs. 33-35). The spherulitic apatite crystals are preserving what appear to be delicate radiolaria tests.

Chert is present in all three masses in various forms: botryoidal chert filling vugs, chalcedony and novaculitic chert (Figs. 36-39). Calcite rims can be seen on circular chalcedony-filled microfossil psuedomorphs that is in optical continuity with the microcrystalline limestone under crossed polars (Fig. 37). The novaculitic chert was only observed in Sample Group 2 (Fig. 10), which was taken from a cherty layer on the very outer portion of a large limestone mass in the field. It contains brecciated novaculitic chert in a poikilotopic limestone matrix with degraded circular microfossils and chert spherulites. Fractures are filled with calcite and silica. Botryoidal chert in fracture fills in limestone and bedded chert also were observed (Figs. 38, 39).

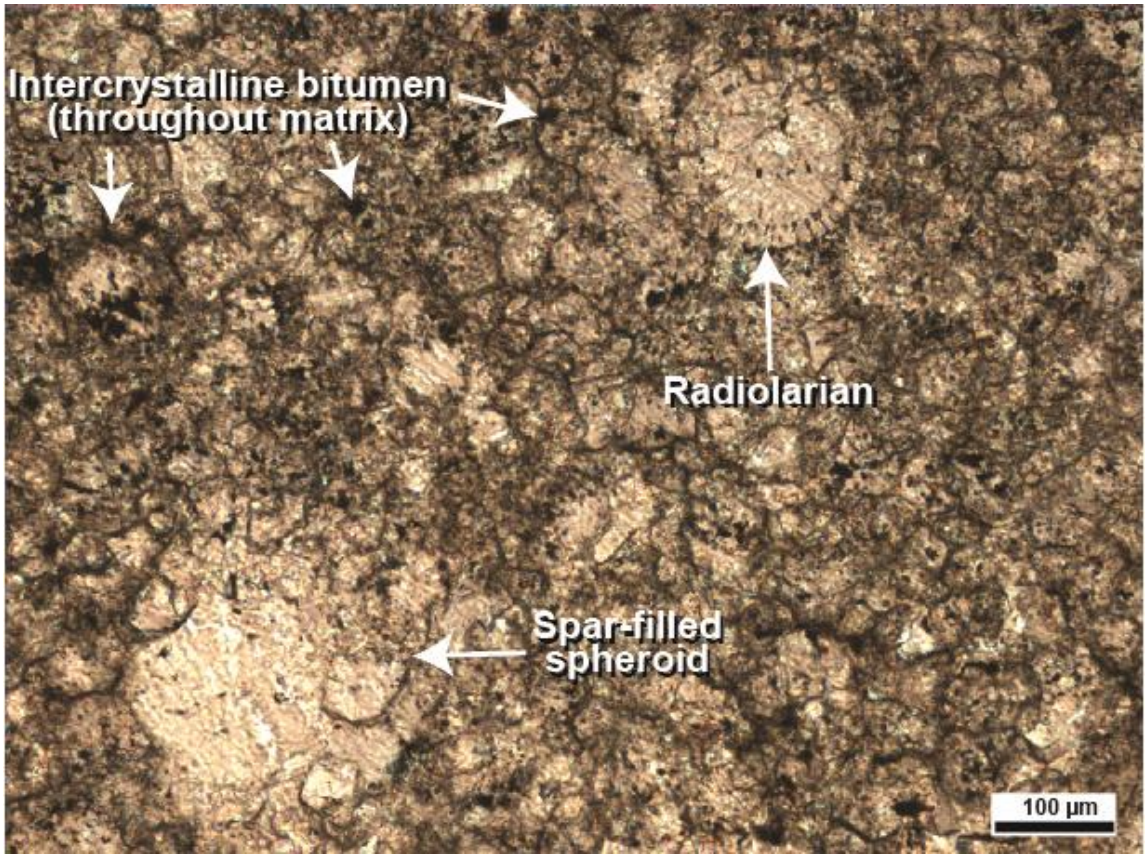

Figure 27. Thin section photomicrograph of microcrystalline calcite matrix containing spar-filled spheroids, which are microfossils, including radiolaria. This fabric represents one of the dominant fabrics observed in the masses. Note that this is the best preservation of a radiolarian seen in the calcite matrix of the limestone masses. This section was taken from the largest mass (Sample Group 1 in Fig. 10) which appeared to have a higher content of chert than the two smaller masses. The matrix also contains intercrystalline bitumen. Plane-polarized light.

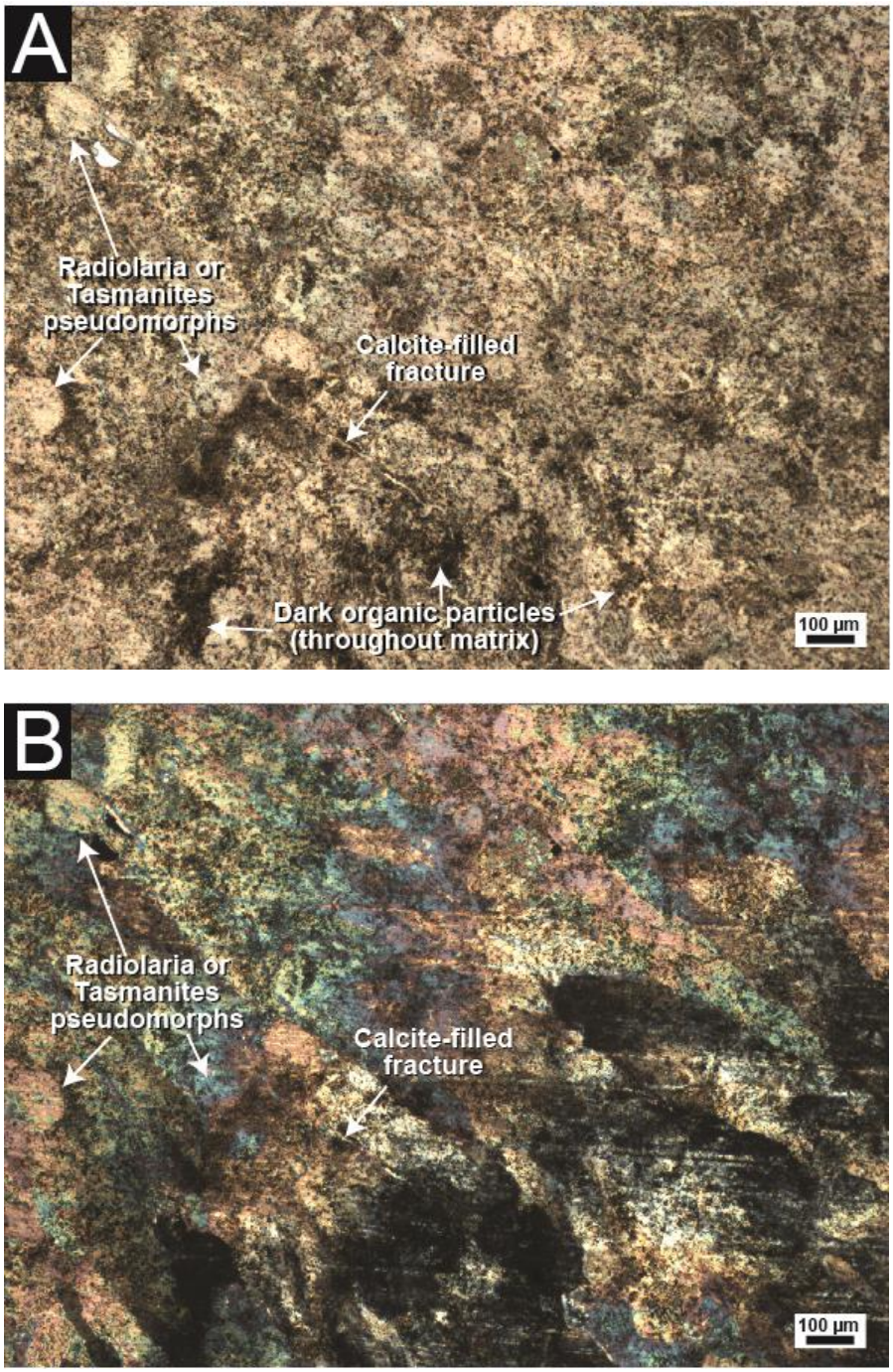

Figure 28. Thin section photomicrograph of microcrystalline calcite with circular bodies that are apparently radiolaria and *Tasmanites* fossils. This represents one of the two dominant fabrics seen in the matrix of the small carbonate masses (Sample Group 1 in Fig. 10). (A) Plane-polarized light. Note dark organic particles, probably bitumen, which are distributed throughout the sample. (B) Cross-polarized image showing birefringence of poikilotopic calcite.

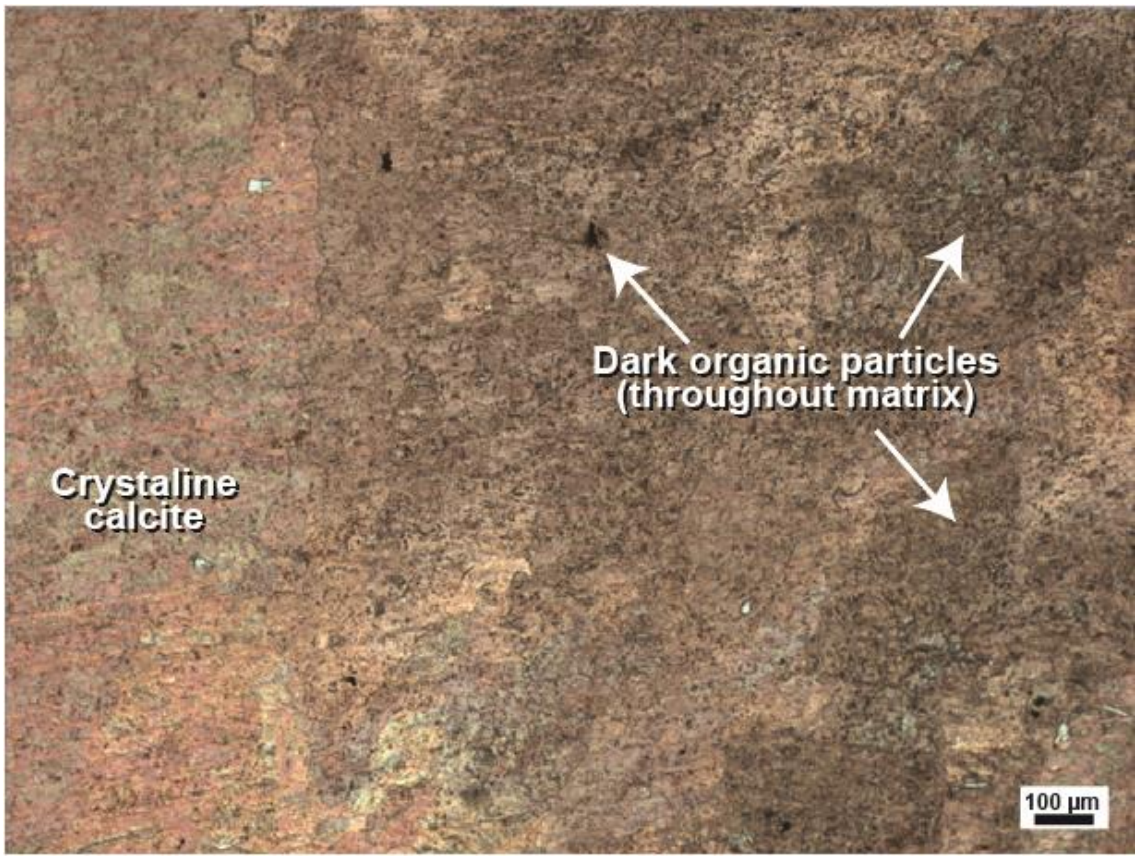

Figure 29. Thin section photomicrograph of crystalline calcite with dark organic particles representing one of the two dominant fabrics seen in the matrix of the small carbonate masses (Sample Group 1 in Fig. 10). When contrasted to the fabrics seen in Figs. 27 and 28, note the absence of spheroid pseudomorphs. Plane-polarized light.

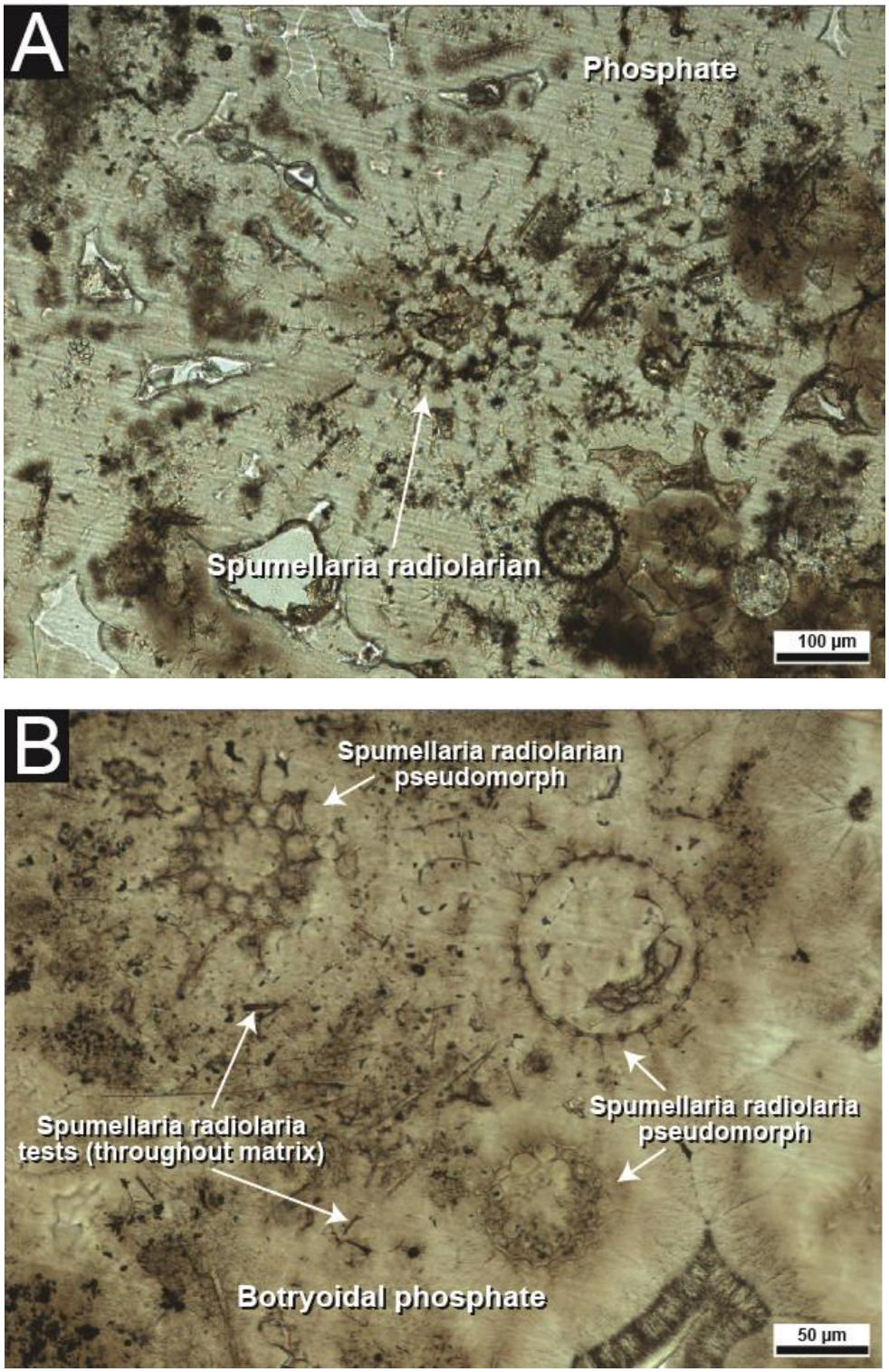

Figure 30. Thin section photomicrograph of radiolaria within phosphate nodules. (A) Spumellarian radiolarian test with spines intact. (B) Varied Spumellarian tests in botryoidal phosphate. Plane-polarized light.

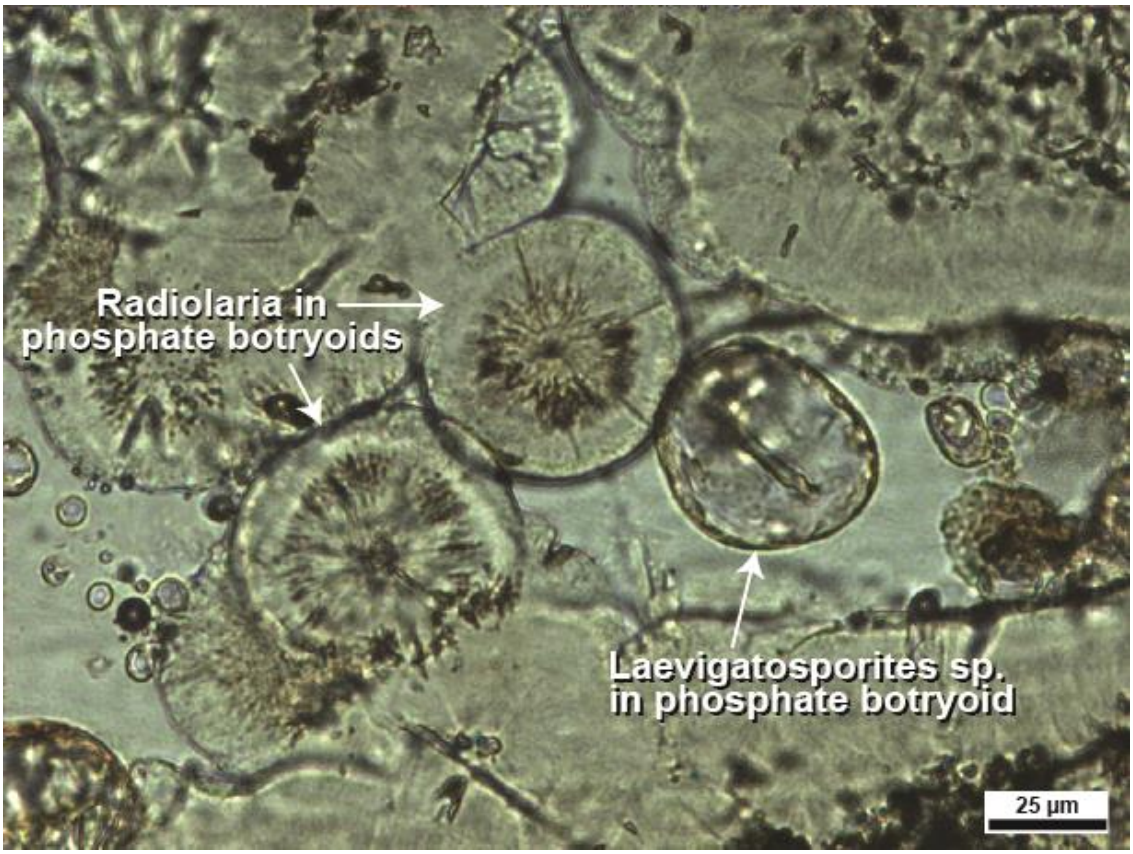

Figure 31. Thin section photomicrograph of radiolaria and *Laevigatosporites* sp. fossils preserved in phosphate botryoids within phosphate nodule. Plane-polarized light.

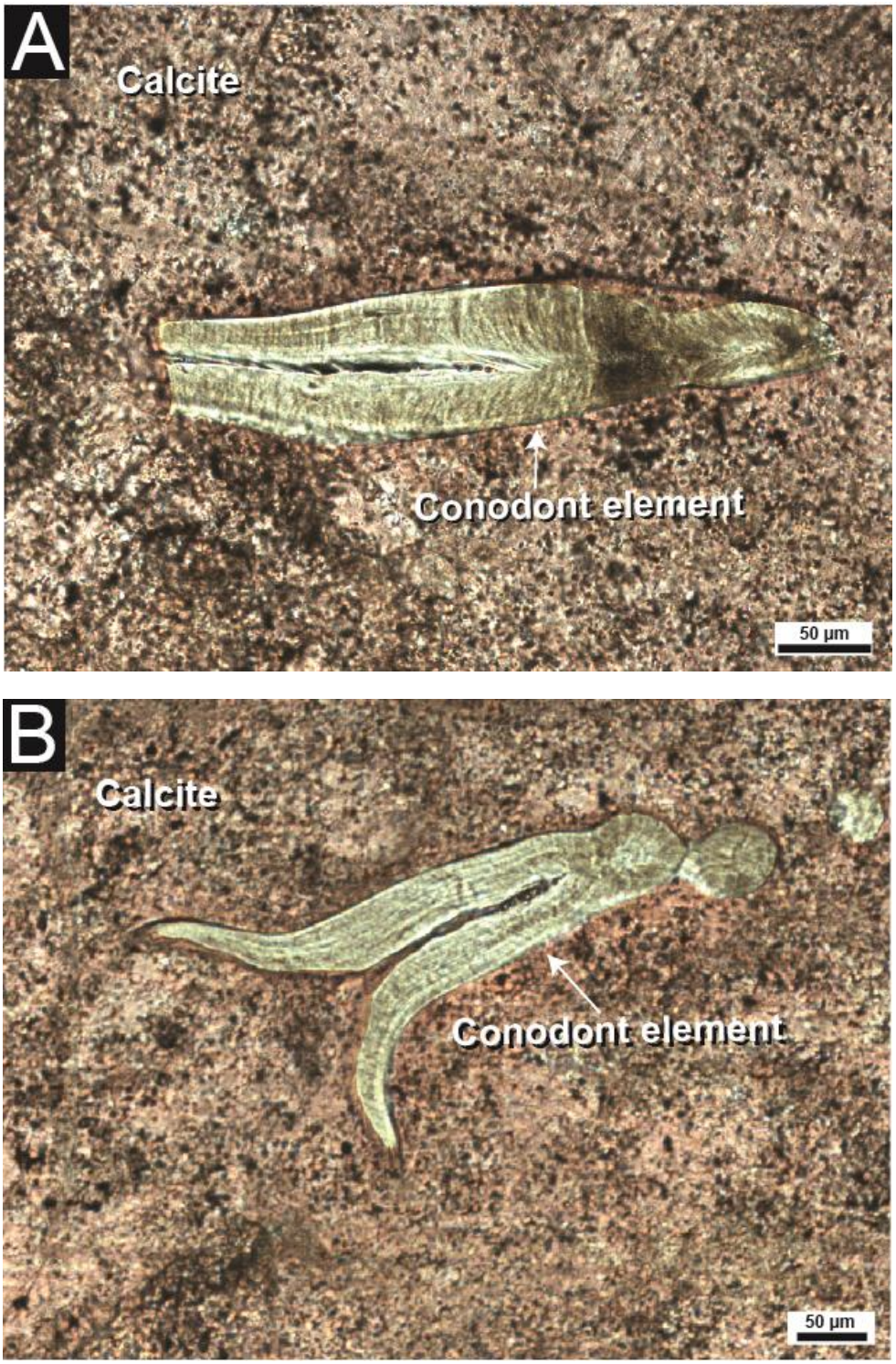

Figure 32. Thin section photomicrographs of conodont elements in limestone. (A) Platform or blade element displaying well-developed lamellar structure. (B) Oblique section of platform element. Plane-polarized light.

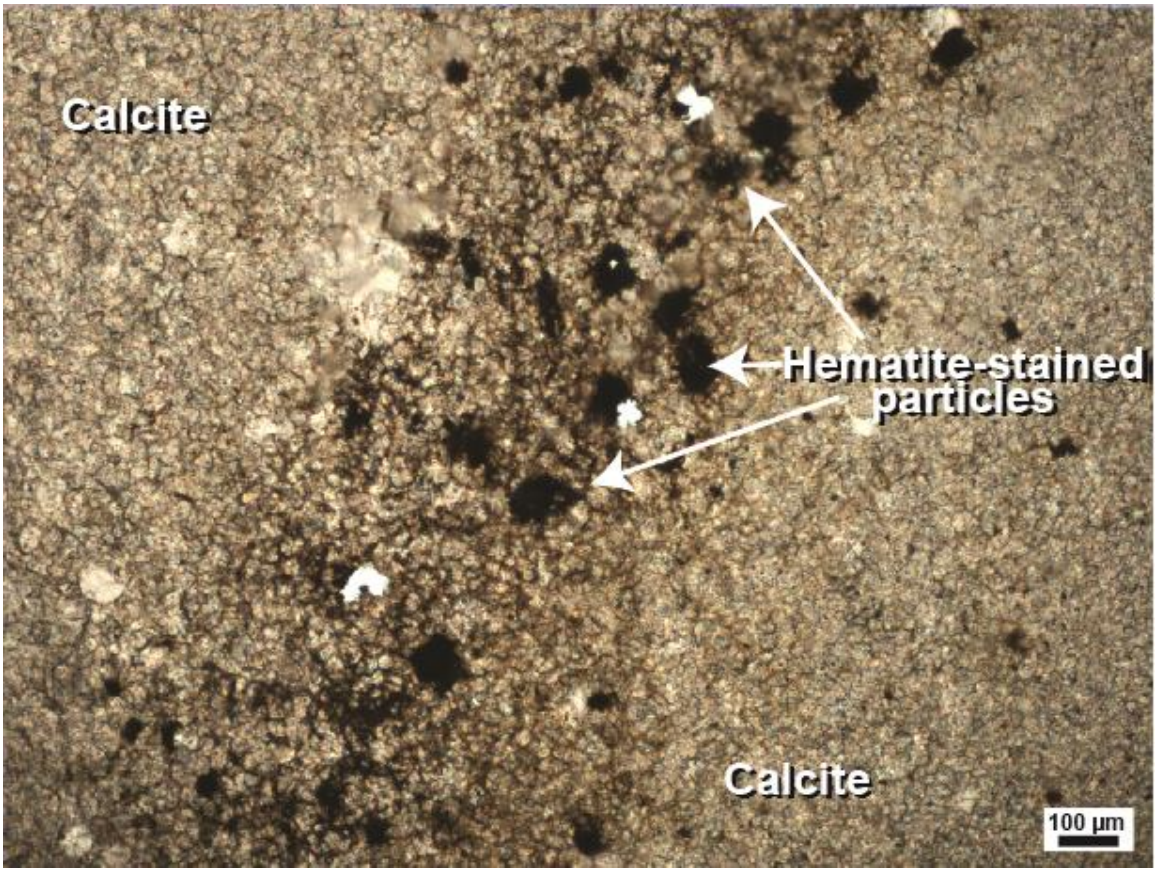

Figure 33. Thin section photomicrograph of microcrystalline calcite stained with opaque particles of hematite taken from Mass 3 (Fig.17). Plane-polarized light.

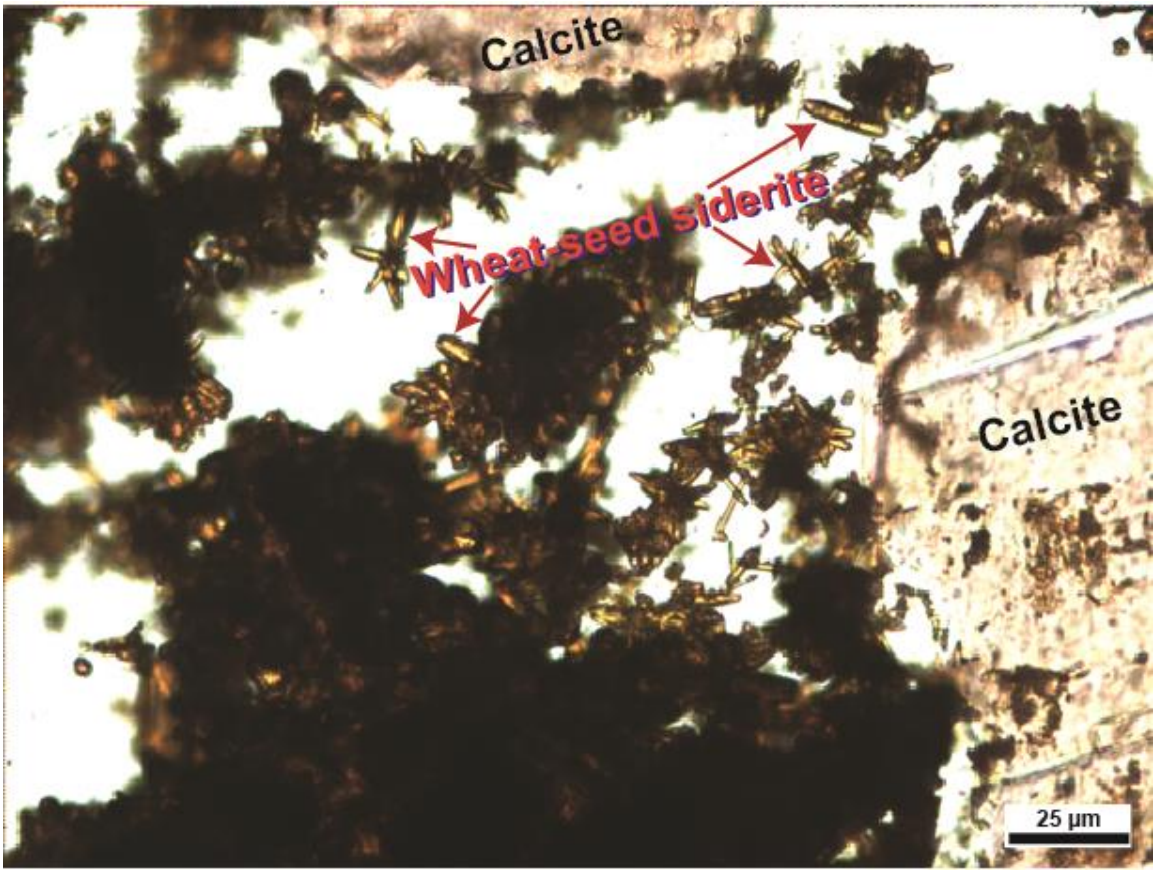

Figure 34. Thin section photomicrograph of wheat-seed siderite filling a vug in microcrystalline calcite. Plane-polarized light.

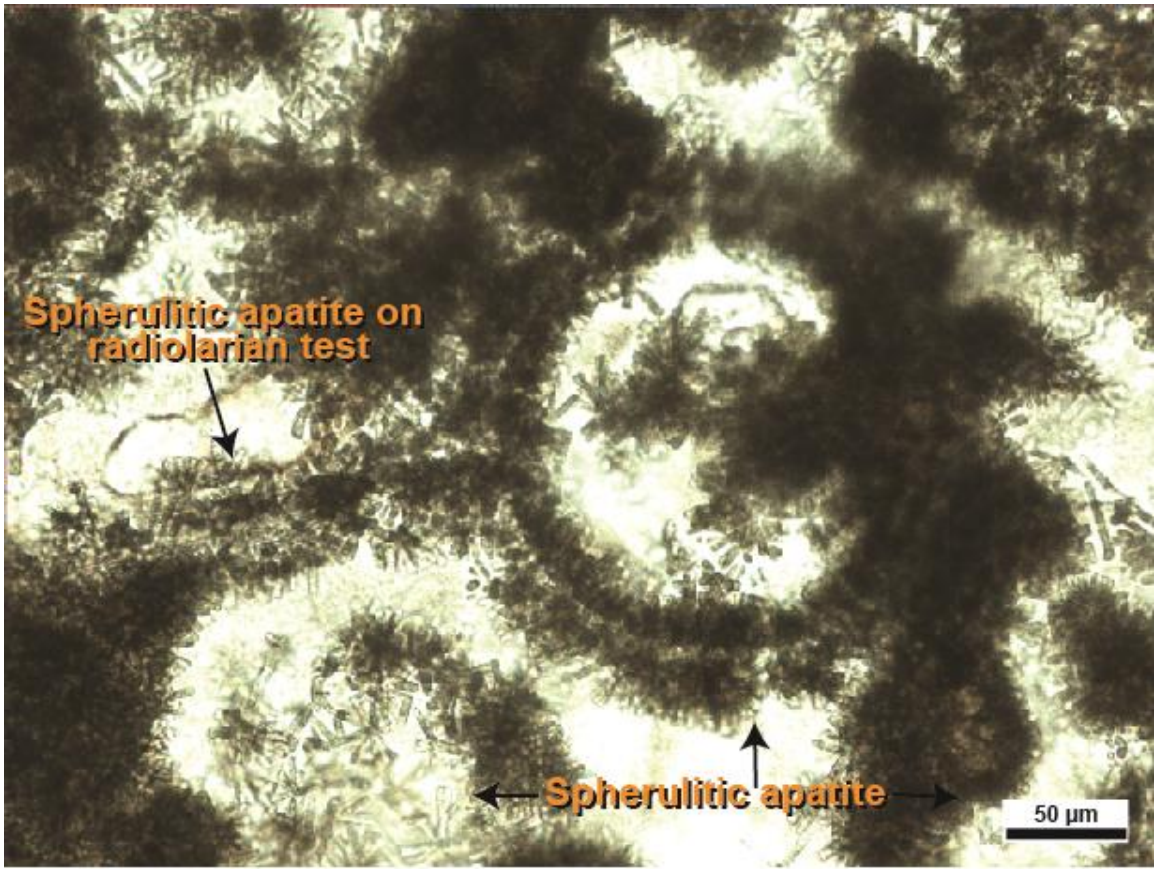

Figure 35. Thin section photomicrograph of phosphate nodule containing spherulitic apatite, some of which precipitated on a radiolarian test. Plane-polarized light.

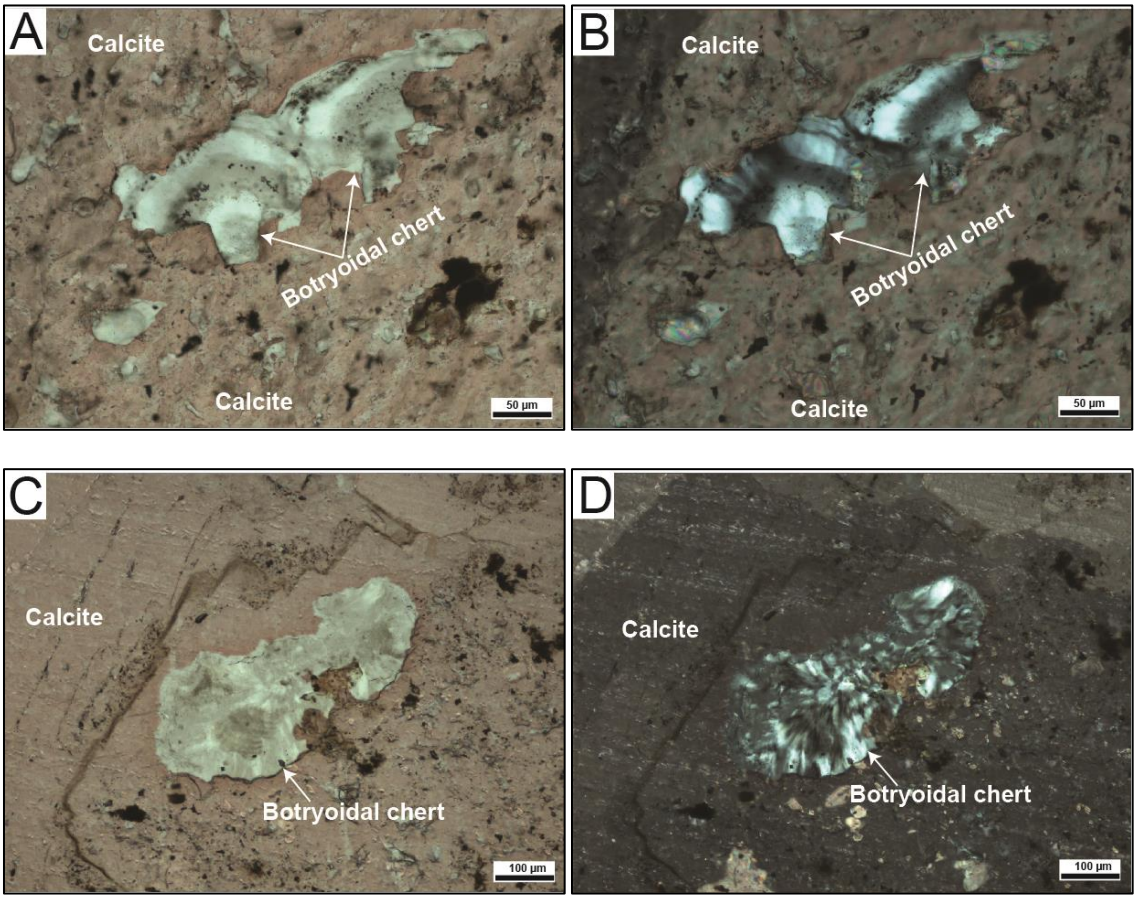

Figure 36. Thin section photomicrographs of botryoidal chert in limestone. (A, C) Plane-polarized light. (B, D) Cross-polarized light.

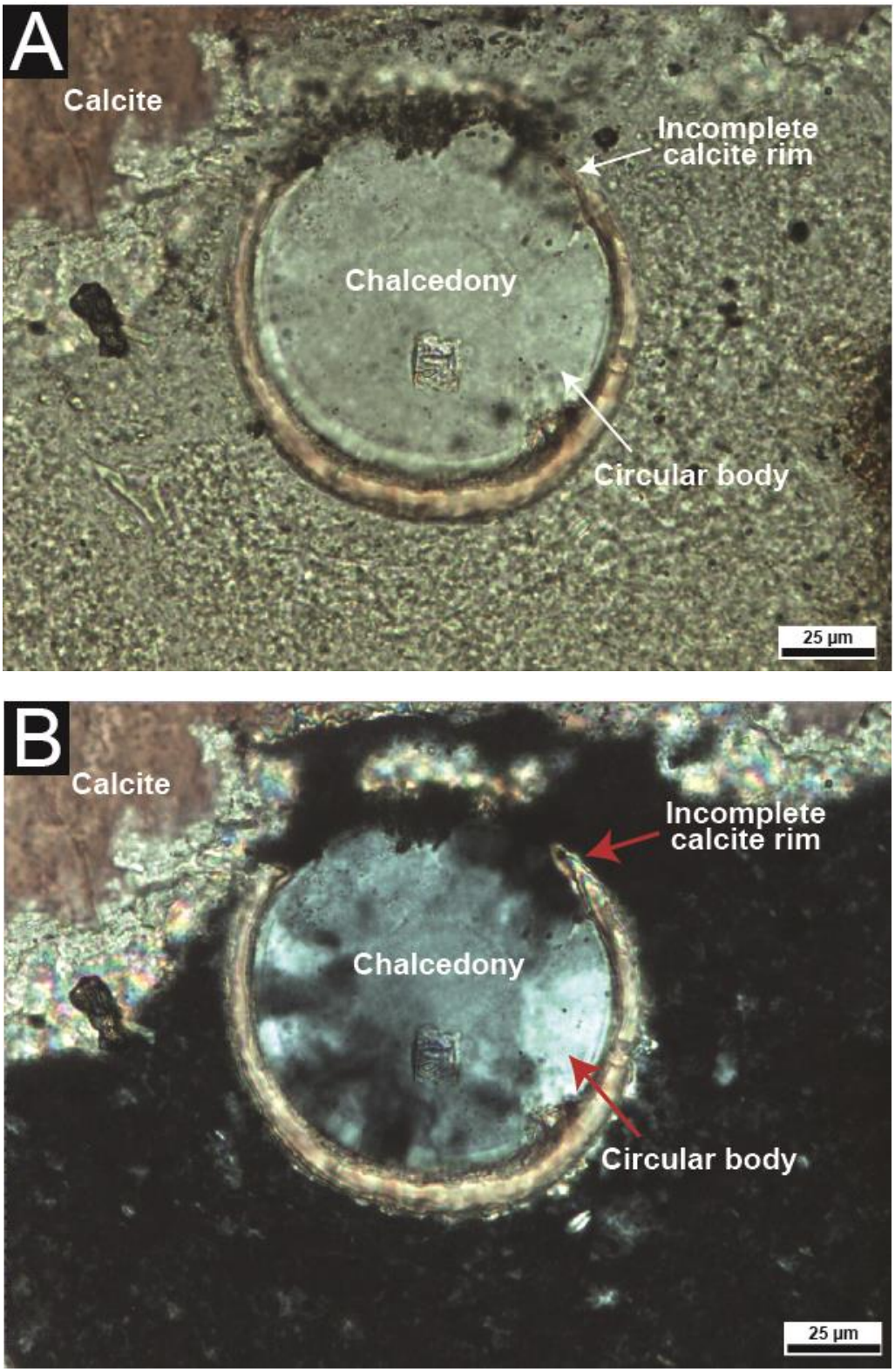

Figure 37. Thin section photomicrograph of incomplete calcite-rimmed circular body filled with chalcedony. (A) Plane-polarized light. (B) Cross-polarized light.

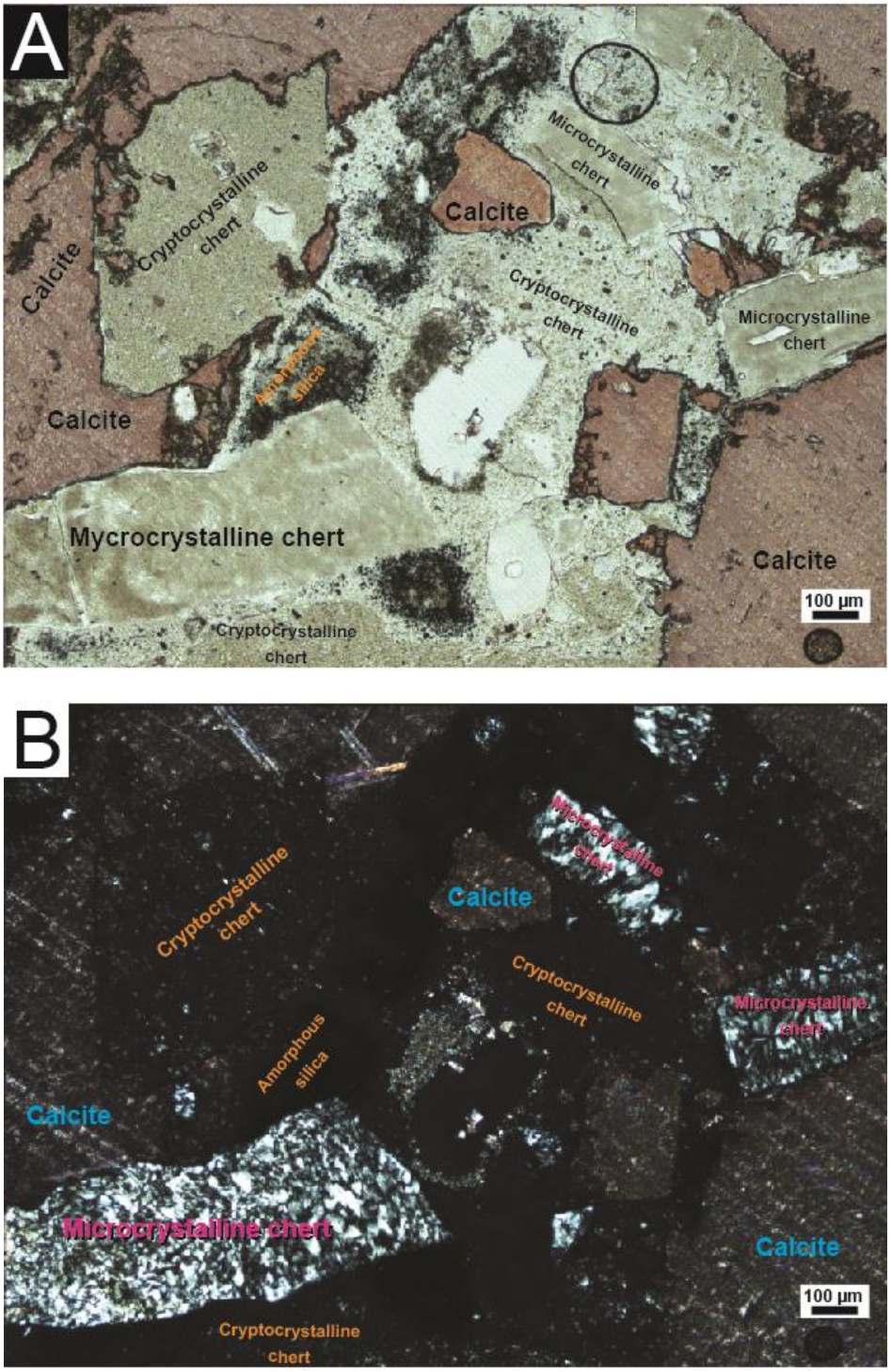

Figure 38. Thin section photomicrograph fractured bleached microcrystalline and cryptocrystalline chert, amorphous silica, and crystalline calcite. Sample taken from outer cherty layer of large carbonate mass (Sample Group 2 in Fig. 10). (A) Plane-polarized light. (B) Cross-polarized light.

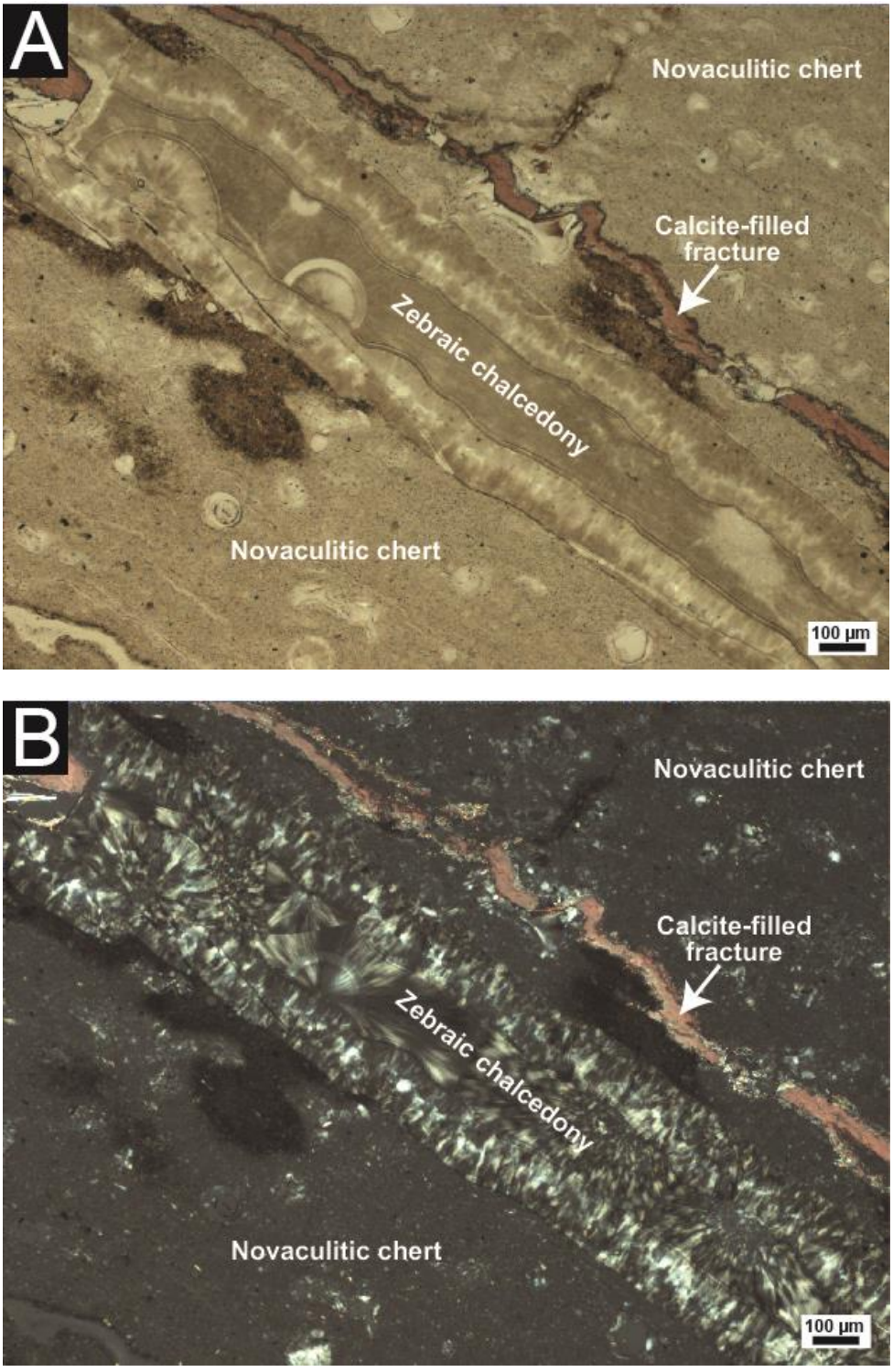

Figure 39. Thin section photomicrograph of zebraic chalcedony filling a fracture in novaculitic chert. Note calcite fracture fill (stained red). (A) Plane-polarized light. (B) Cross-polarized light.

Porosity is scarce in the crystalline limestone that forms the bulk of the spheroidal masses. Most pores are filled with chalcedony that cannot readily be observed in thin section (Fig. 41). Where porosity was observed, it tends to be highly irregular and may include open fractures, as well as interstitial porosity within microcrystalline limestone between the circular bodies associated with radiolarian and other microfossils (Fig. 40).

Angular to round clasts were identified in calcite spar. The rounded clasts resemble radiolaria (Fig. 41). Microscopic vug fills were observed in all masses and are filled with coarse equant calcite spar, in places showing two distinct stages of cementation (Fig. 42). A vug fill from the surface a large concretion (Sample Group 5, Fig. 10) contains coarse calcite crystals with possible zoning and some chert (Fig. 43).

The outer rind of the carbonate masses is composed of course calcite crystals. In hand sample, lamellae of alternating color can be seen (Figs. 14-16) and in thin section the same distinct lamellae of contains alternating calcitic and hematitic lamellae within the calcite can be seen (Fig. 44).

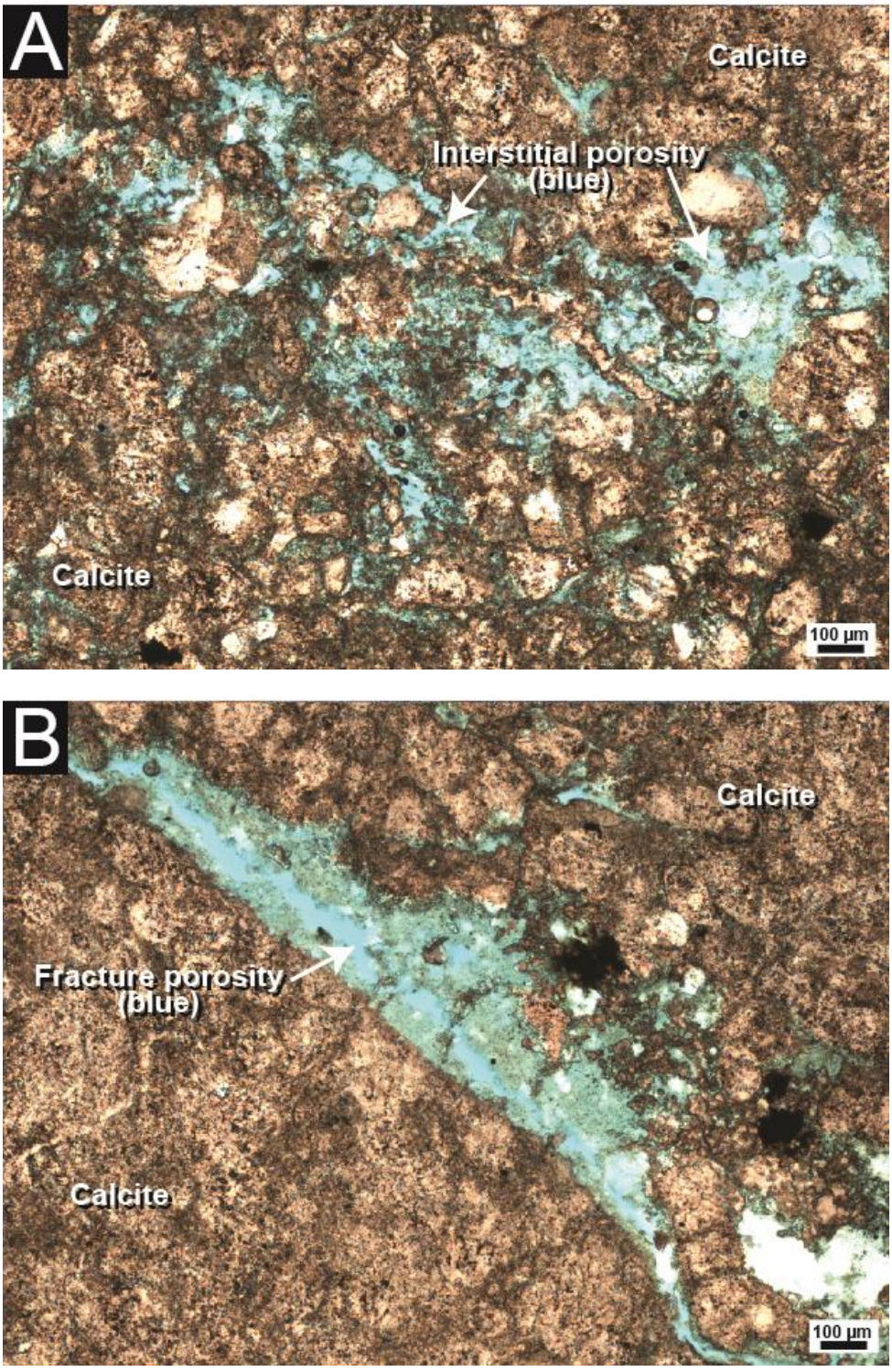

Figure 40. Thin section photomicrograph of porosity in the limestone masses. (A) Interstitial porosity in microcrystalline limestone. (B) Fracture porosity with associated interstitial porosity.

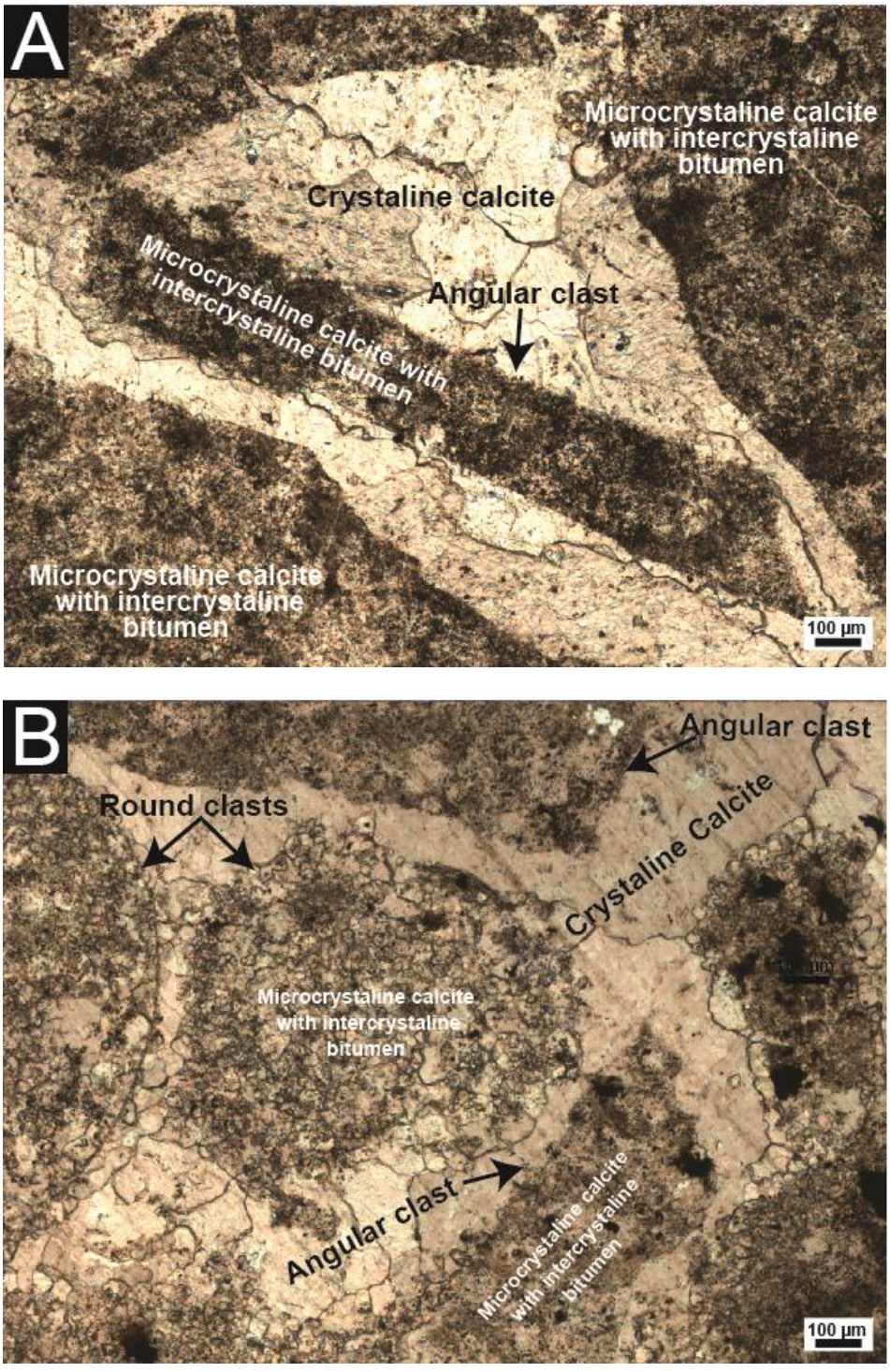

Figure 41. Thin section photomicrograph of (A) angular and (B) angular to round clasts of microcrystalline limestone in calcite spar. Circular bodies are possible radiolarian pseudomorphs. Note lining on left-most round body similar to Figure 42. Also note breccia-like habit of microcrystalline calcite angular clasts. Plane-polarized light.

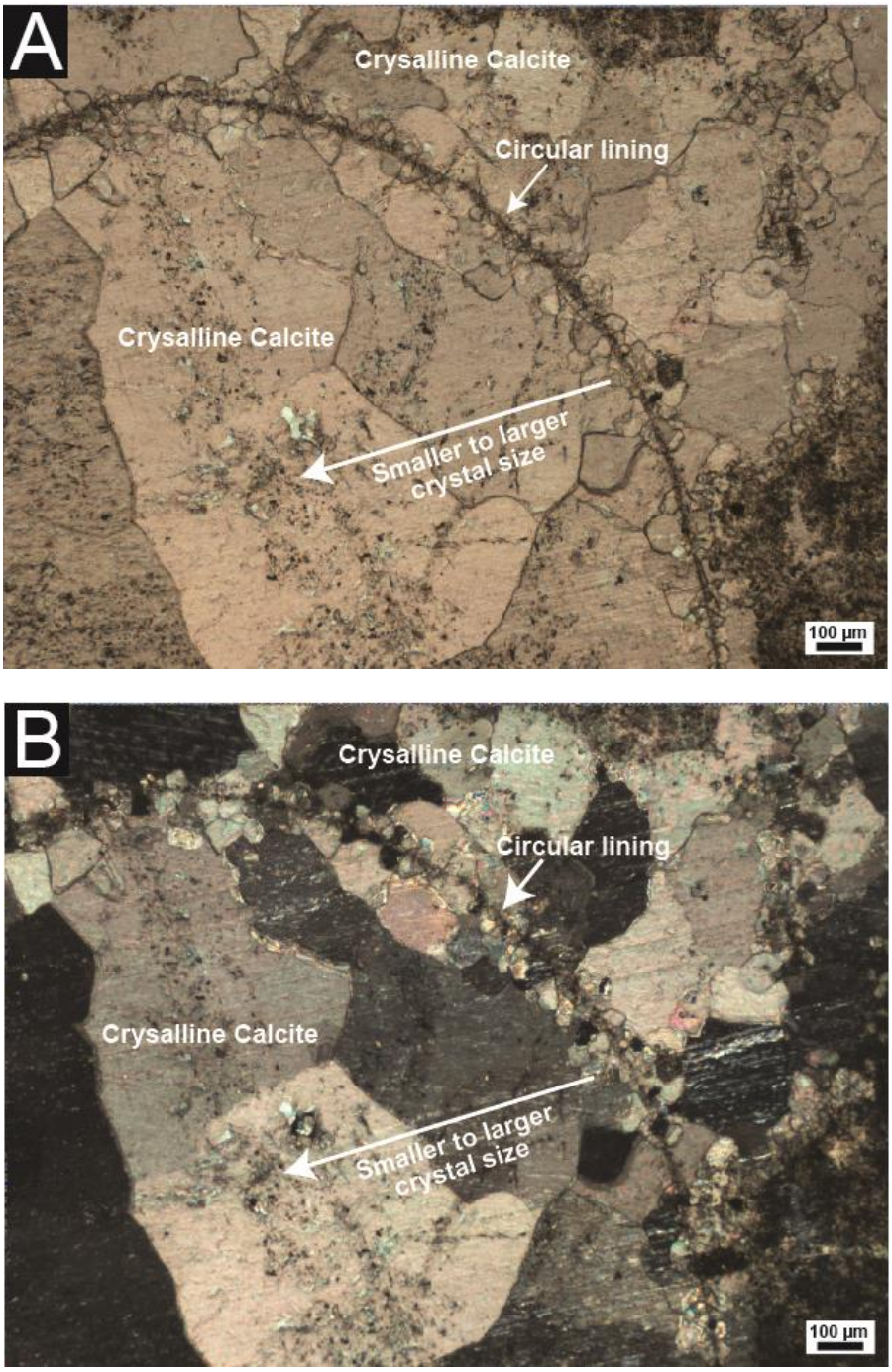

Figure 42. Thin section photomicrograph of sparry calcite-filled vug showing multiple phases of diagenetic replacement, the first stage of replacement being the circular lining and then branching outwards. Note the different groups of crystal sizes with the smallest crystals at the circular lining and the larger crystals inside the circular lining. (A) Plane-polarized light. (B) Cross-polarized light.

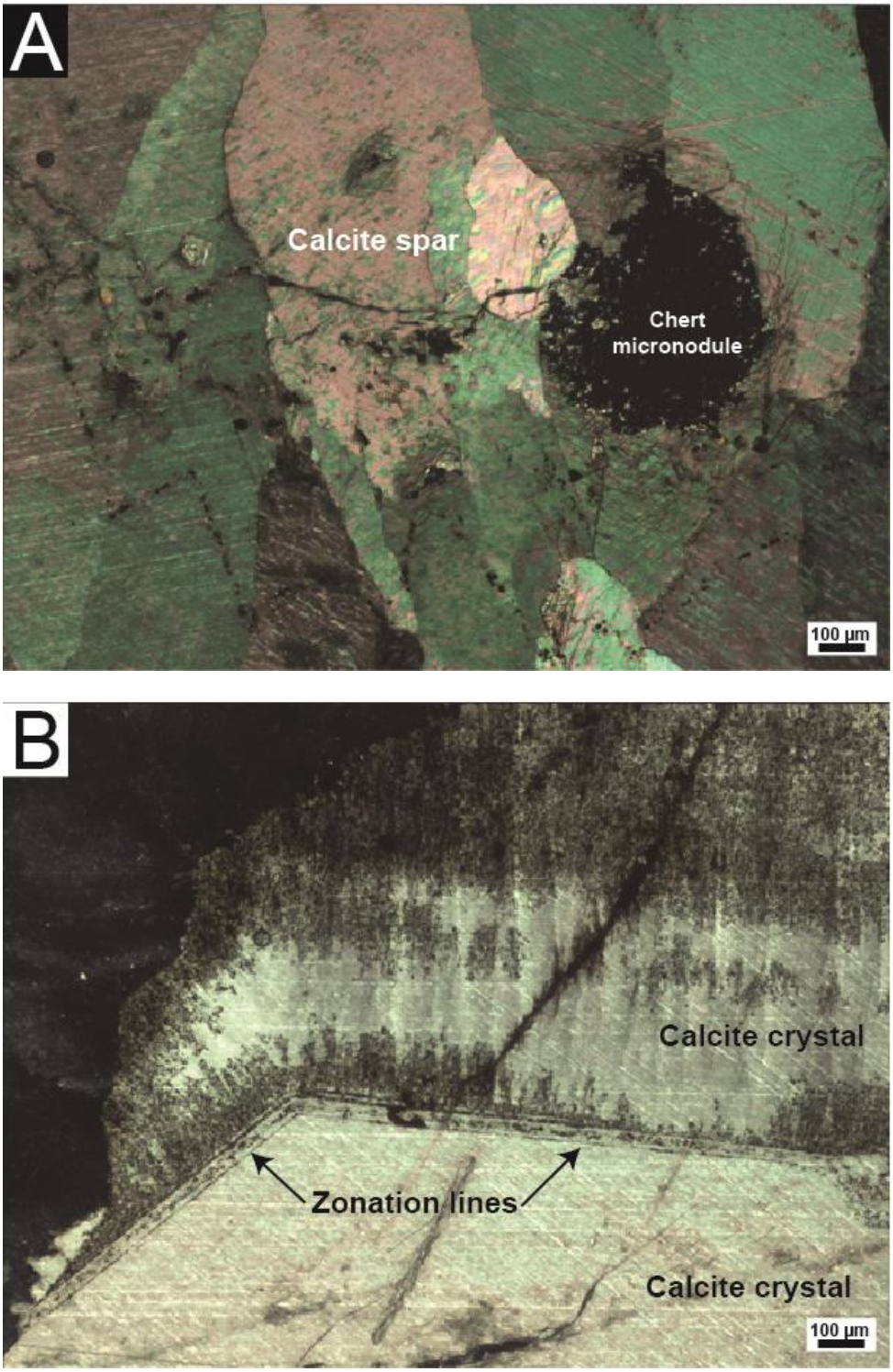

Figure 43. Thin section photomicrographs (crossed polars) of calcite crystals from large vug fill (Sample Group 5 in Fig. 10). (A) Micronodule of chert in calcite spar. (B) Zoned calcite crystals.

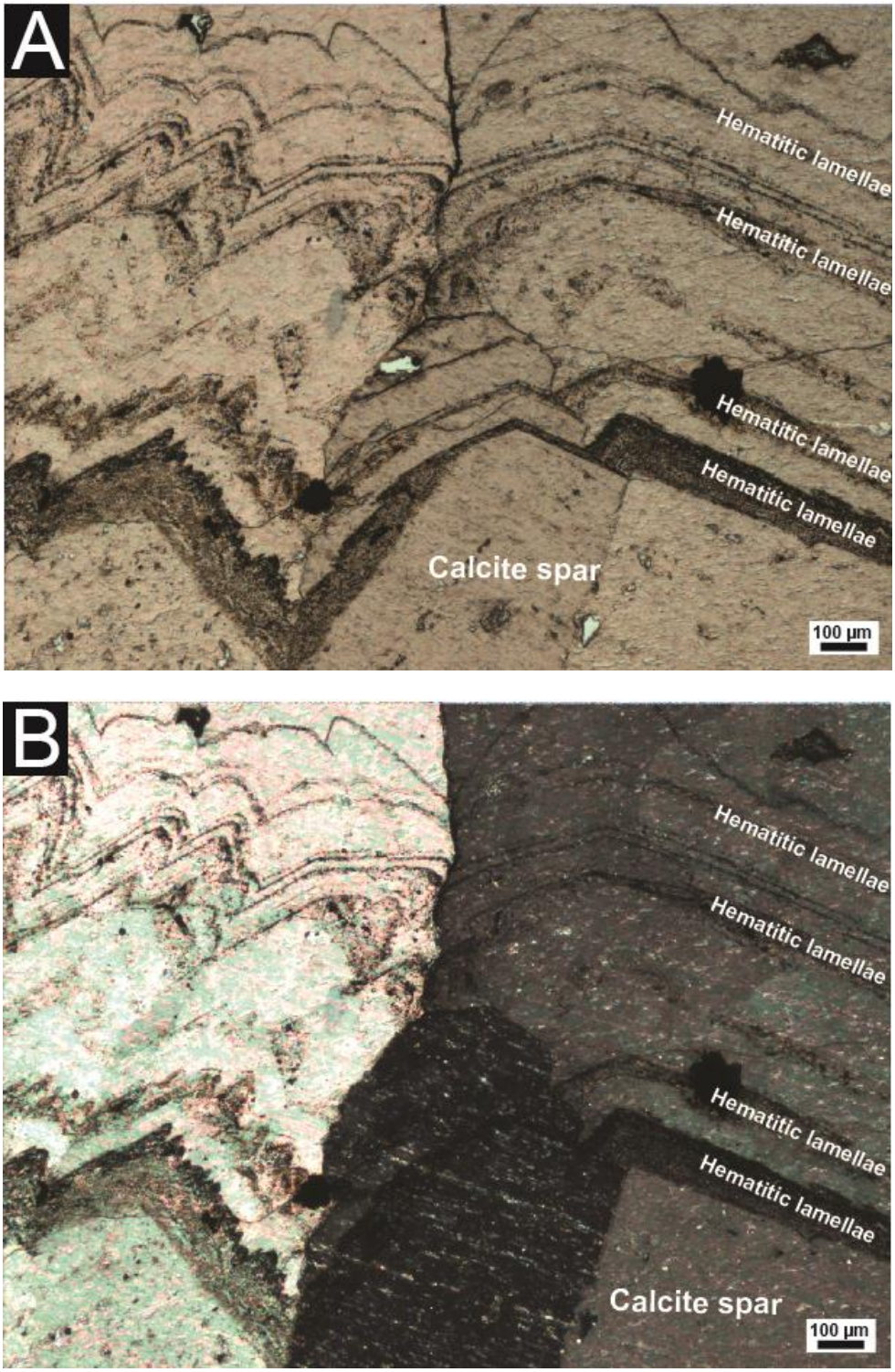

Figure 44. Thin section photomicrograph of calcite crystals in sparry rind. (A) Plane-polarized light image showing pale calcite spar and dark hematitic lamellae. (B) Cross-polarized light image showing optical discontinuity perpendicular to growth lamellae.

IV. 3 Cathodoluminescence Microscopy

Under CL both, the vug-fill from the inner concretion matrix and the outer rind show variation in crystal cathodoluminescence, the rind sample even more so (Figs. 45, 46). Cathodoluminescence is caused by the momentary trapping of electrons in impurities or structural defects in minerals, called extrinsic (impurity) and intrinsic (structural) luminescence (Boggs and Krinsley, 2006). Carbonate minerals often exemplify extrinsic cathodoluminescence due to activators (multi-valence ions such as Mn^{2+}) substituting for cations such as Ca^{2+} and Mg^{+} in the mineral structure. Activators ions enhance the cathodoluminescence of a mineral when used with CL. Some elements such as Fe^{2+} and Fe^{3+} are quenchers of this and when substituted into the crystal structure they suppress the cathodoluminescence by causing a decrease in CL emission (Machel et al., 1991; Tarashchan and Waychunas, 1995). This quenching effect was observed in the rinds of the carbonate masses (Fig 45). The highly cathodoluminescent calcitic bands can be clearly distinguished from the alternating dull hematitic bands. Concentric and sector zoning within the crystals was observed, which includes an erosional surface followed by uninterrupted zonation lines. The erosional surface is marked by highly irregular, rough-looking crystals, which suggest that the mineral formed under highly disturbed conditions. The smooth crystal faces indicate natural uninterrupted conditions for crystal growth. The vug-fill shows very little variation in cathodoluminescence (Fig. 46).

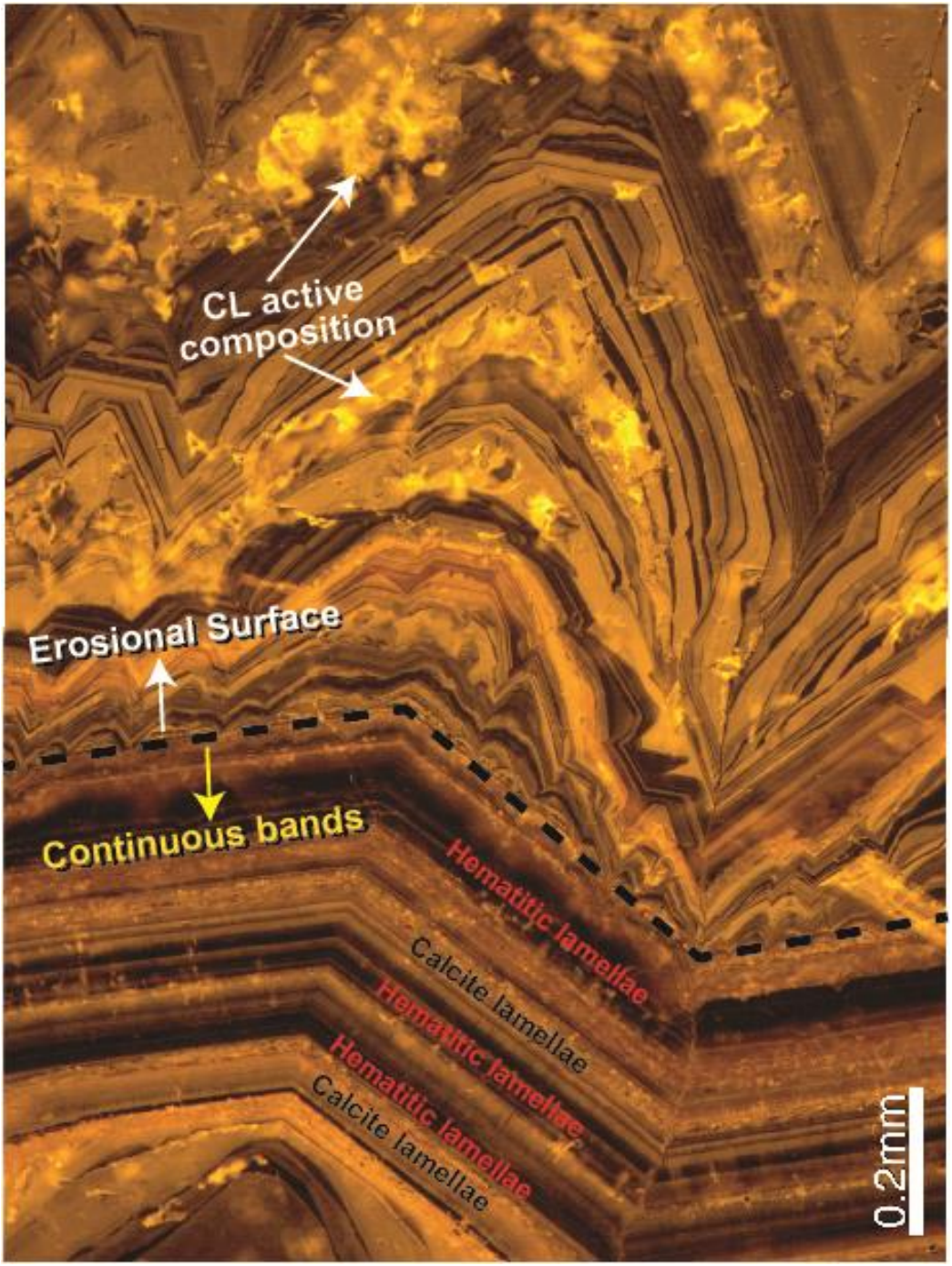

Figure 45. Cathodoluminescence image of zoned calcite spar in the outer rind of a carbonate mass. Note variability of crystal morphology and the presence of multiple arrest and solution discontinuities. The more calcite-rich bands luminesce more than the hematitic-rich bands which contain luminescence quenching ions of iron.

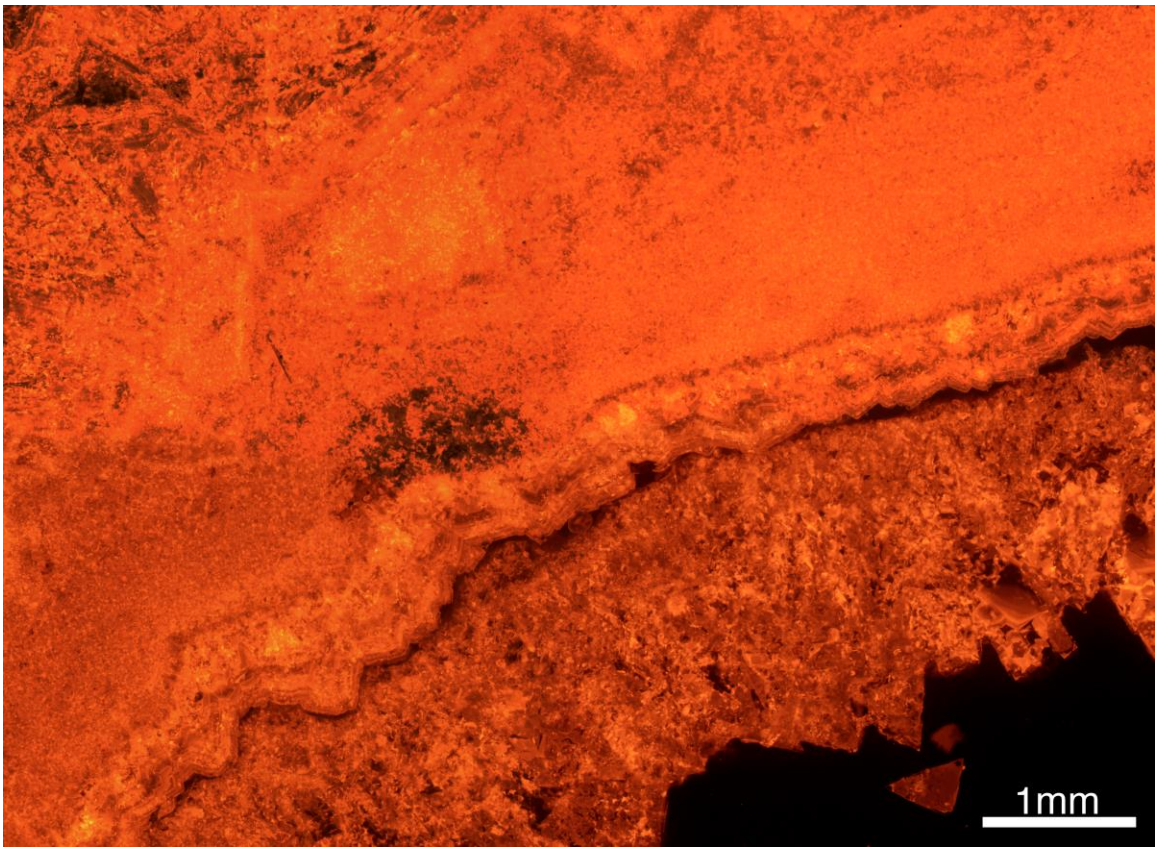

Figure 46. Cathodoluminescence image of calcite spar in vug of Mass 3 from outer rings (Fig. 17). Note that much less variation in luminescence can be seen when compared to the sparry rind in Figure 45.

IV. 4 Fluid Inclusion Microthermometry

One fluid inclusion plate from the outer rind of limestone Mass 3 was examined. Primary inclusions (i.e., single-phase inclusions) predominate in the calcitic-rich bands, which precluded the collection of freezing-point and bubble-point temperature data. Primary inclusions are formed during formation or recrystallization of a mineral when irregularities on the surface of the crystal trap fluid, which are subsequently sealed in the crystal body during continued crystal growth. These are different from secondary inclusions, which form when fluid enters the crystal body during the healing of a fracture in the mineral (Roedder, 1984). A few inclusions appear to contain a vapor bubble, but they are too small to analyze (up to 3 μm). These inclusions have an elongate shape (Fig. 47. A). Some possible three-phase (water, oil, vapor) inclusions (10 to 22 μm) also were identified and they have a more broad and regular shape than the single phase inclusions (Fig. 47. B). The presence of a solid phase within an inclusion suggests that solid material was suspended in the medium fluid when the crystal was forming or recrystallizing (Roedder, 1984).

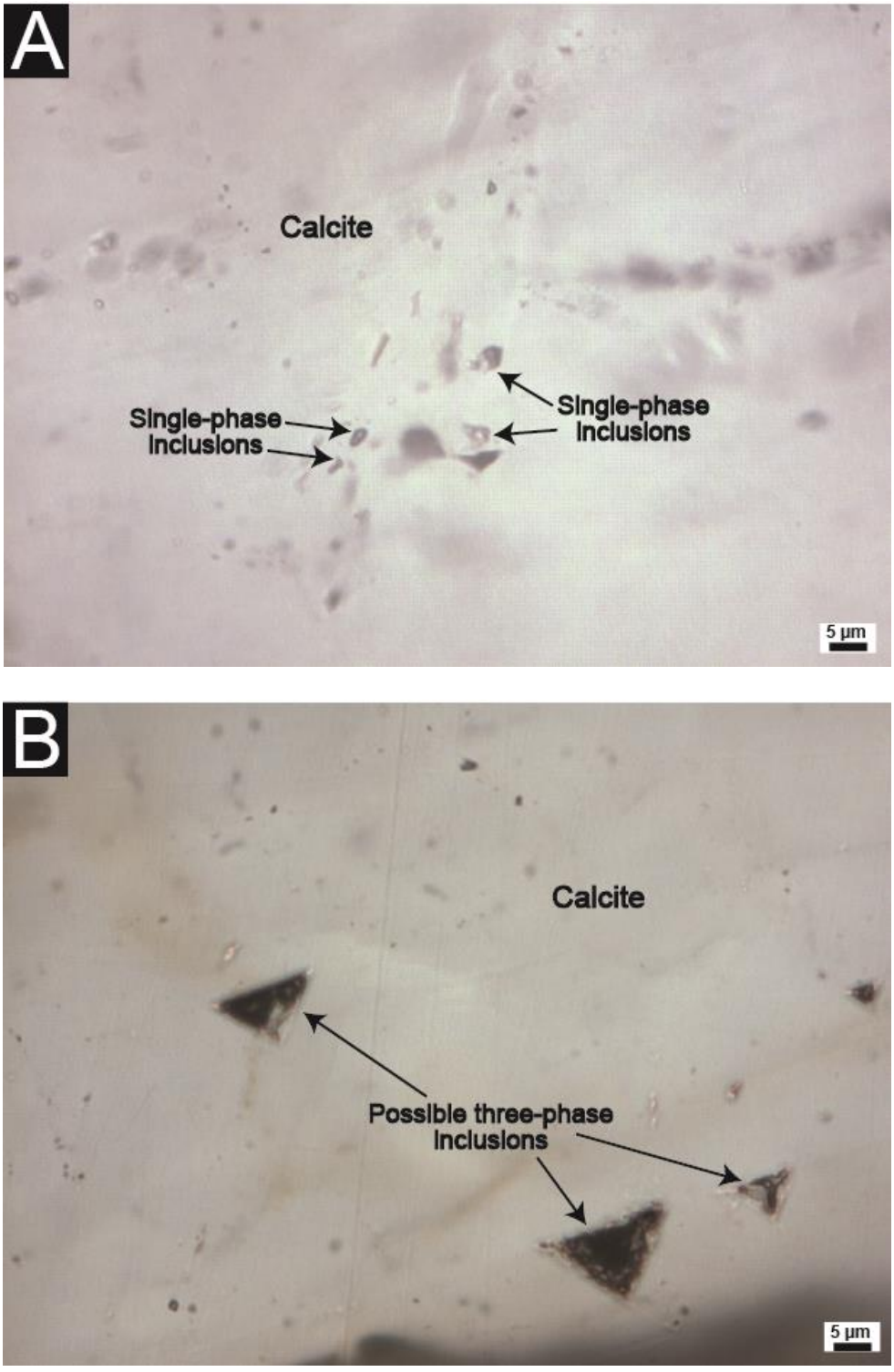

Figure 47. Thin section photomicrographs of sparry calcite in outer rind showing fluid inclusions. (A) Single-phase fluid inclusions containing water (B) Possible three-phase inclusions containing oil, water, and vapor.

IV. 5 Isotope Geochemistry

Stable $\delta^{13}C$ values for all masses range from -20.09 to 13.59 ‰ V-PDB and show an overall consistent trend of enrichment in all three carbonate masses. Isotopic values are most depleted in ^{13}C closest to the nucleus (-18.35 to -14.28 ‰) and become more enriched in the outer rings (-20.09 to -7.40 ‰) and then become more enriched in the sparry rind (-3.95 to +13.59 ‰). A noticeable spike (>11 ‰) occurs between the last two rind samples in all concretions.

Stable $\delta^{18}O$ values of all concretions range from -0.8 to -6.1 ‰ V-PDB, showing an overall consistent trend of depletion in all three carbonate masses. Isotopic values are most enriched in ^{18}O closest to the nucleus (-0.86 to -1.46‰) and become more depleted in the outer rings (-1.01 to -5.99‰) and then become slightly more enriched in the sparry rind (-3.06 to -5.47‰).

Stable $\delta^{15}N$ values range from -12.0 to +16.8‰ relative to air, showing an overall trend of depletion from the nucleus to outer rings (with one outlier in Mass 1 outer rings) and then an overall enrichment in the sparry rind. Isotopic values are most depleted in the nucleus (+0.51 to +3.09 ‰) and the outer rings (-7.82 to 10.59‰), with values becoming more enriched in the sparry rind (-6.92 to +16.78‰). $\delta^{15}N$ values of Mass 2 and Mass 3 are most enriched in the sparry rind, while Mass 1 has the greatest enrichment in the outer rings.

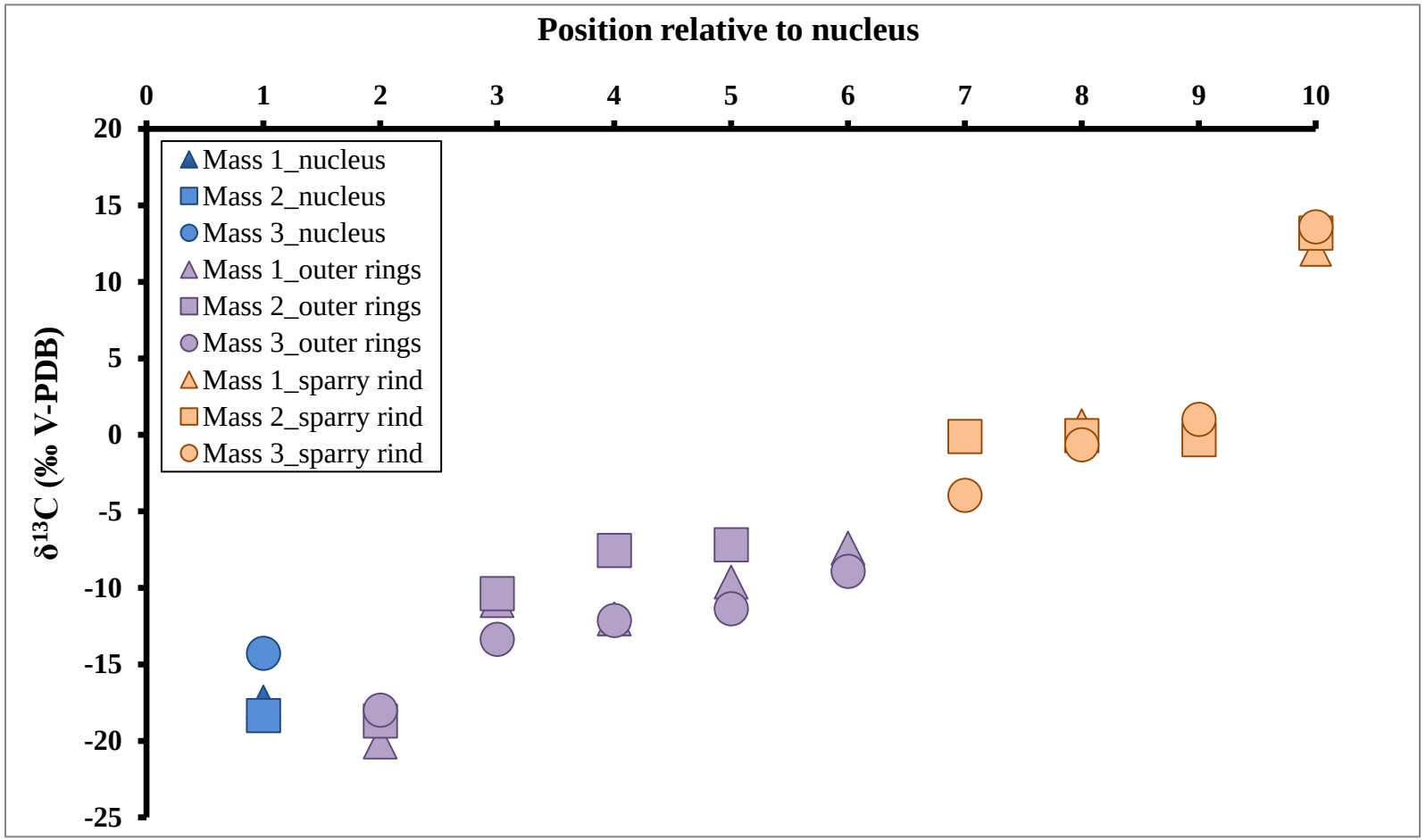

Figure 48. Stable isotope $\delta^{13}C$ values (‰ relative to V-PDB) for Small Carbonate Masses 1, 2 and 3 showing overall enrichment in $\delta^{13}C$ from the nucleus to sparry rind. Note the consistency of the isotopic signatures between the three masses. See Figures 14-16 for location of sample points.

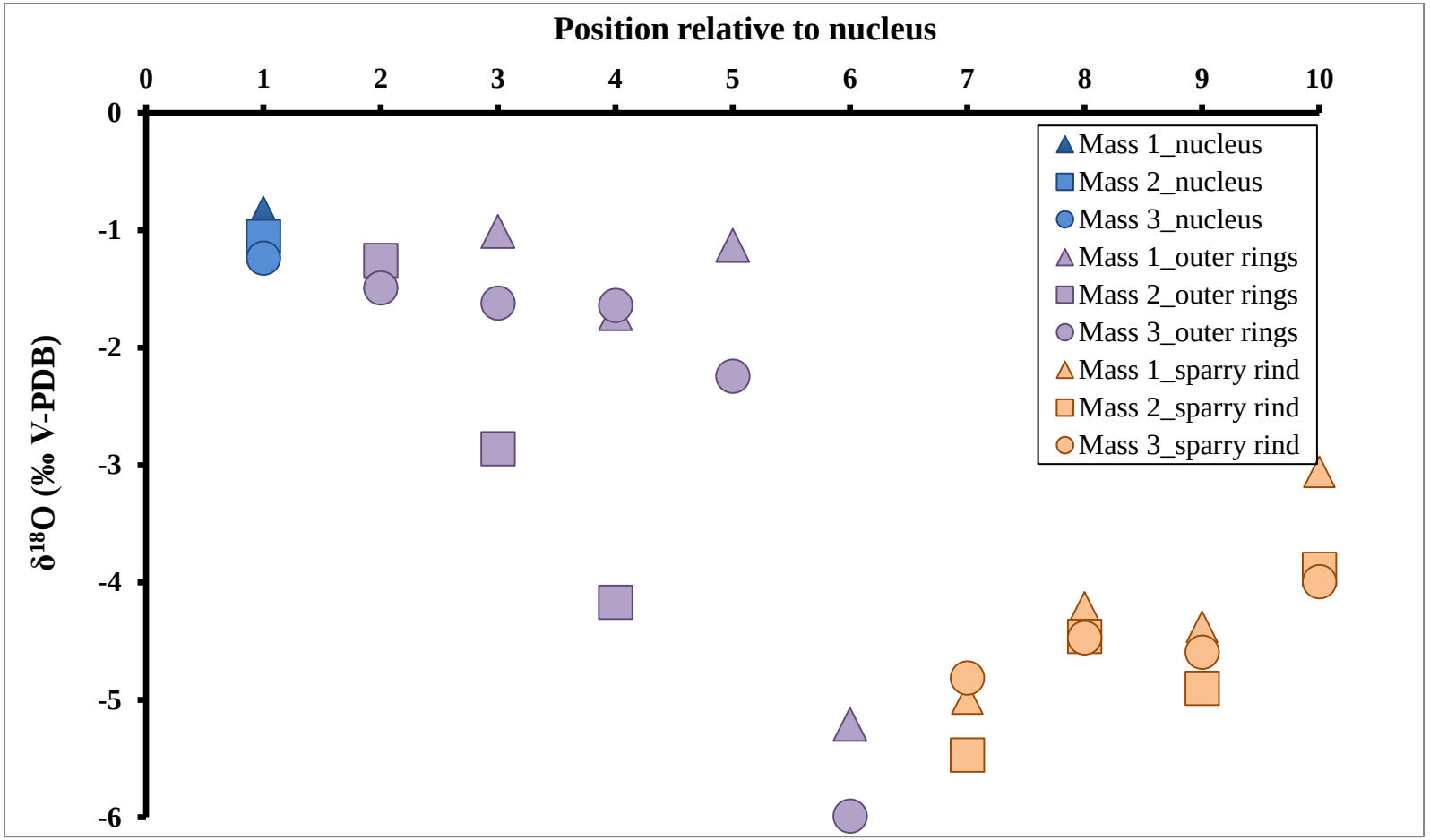

Figure 49. Stable isotope $\delta^{18}O$ values (‰ relative to V-PDB) for Small Carbonate Masses 1, 2 and 3 showing overall depletion in $\delta^{18}O$ from the nucleus to sparry rind. Note the consistency of the isotopic signatures between the three masses. See Figures 14-16 for location of sample points.

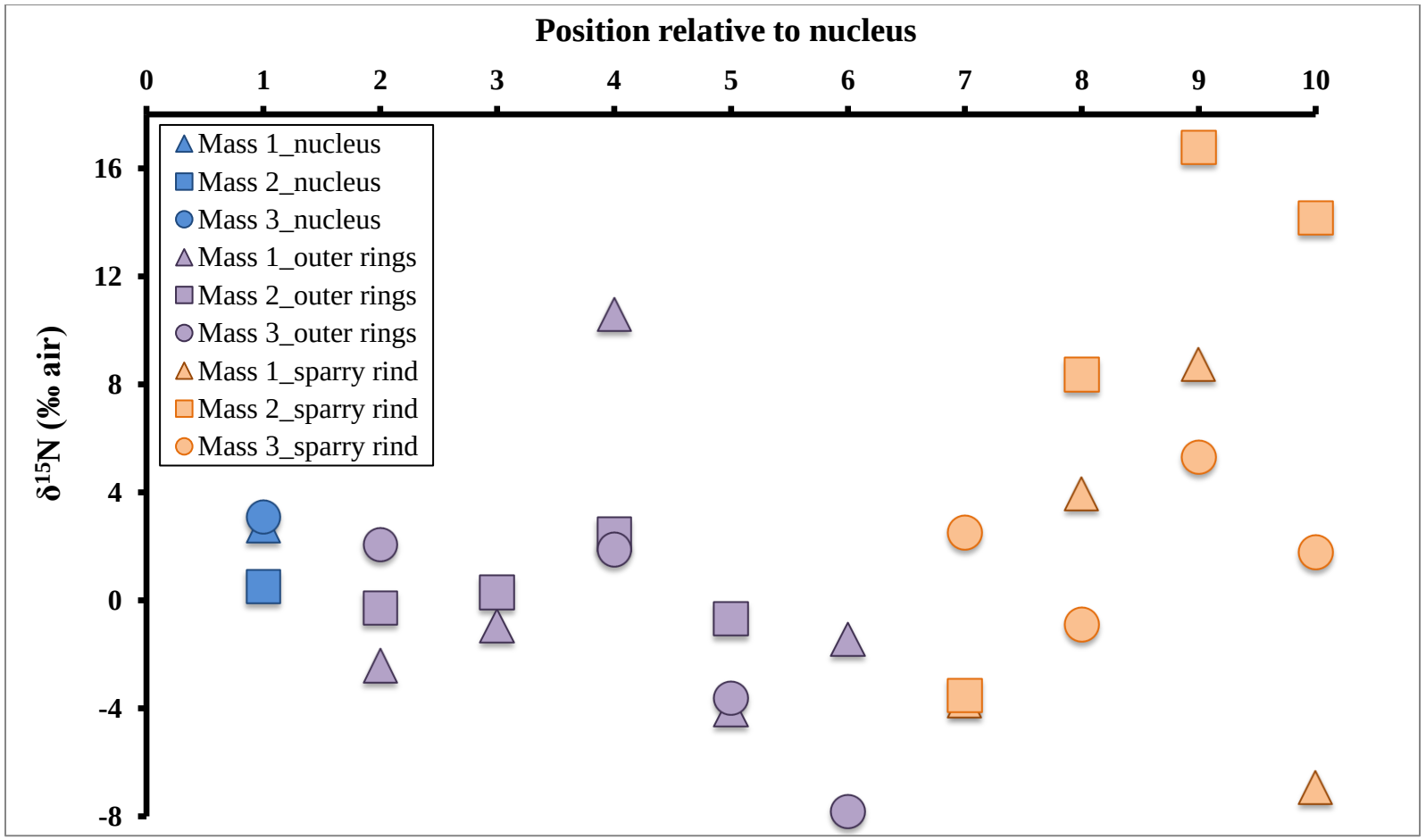

Figure 50. Stable isotope $\delta^{15}N$ values (‰ relative to air) for Small Carbonate Masses 1, 2 and 3 showing overall depletion in $\delta^{15}N$ from the nucleus to sparry rind. See Figures 14-16 for location of sample locations.

IV. 6 Trace Metal Analysis

Three trace elements (V, Ni and Mo) were highlighted because of their paleoredox implications. Vanadium concentrations for all masses range from 14 to 366 ppm (Fig. 51). One value of 366 pm from the edge of the outer rings of Mass 3 was not plotted to highlight trends in all three masses. Masses 1 and 2 show an overall negative trend from the nucleus to the edge of the rind (87 to 14 ppm), with one outlier (164 ppm) in the outer rings of Mass 1. Mass 3 shows an overall positive trend from the nucleus (71 ppm) to the outer rings (61 to 366 ppm) and then values fluctuate within the rind not showing any clear trend (126 to 20 ppm).

Ni concentrations for all masses range from 52 to 117 ppm and show an overall consistent trend, increasing in concentration from the nucleus to the edge of the outer rings (4 to 117 ppm) and then decreasing in concentration from the start of the rind to the outer rind (97 to 2 ppm) (Fig. 52). There were some outlier samples from Mass 3 that did not follow the positive and negative trends, one value (52 ppm) from the nucleus and two values (40 and 6 ppm) from the rind. Values from masses 1 and 2 were more consistent. Mo concentrations for all masses range from 41 to 866 ppb and show a slight positive trend from the nucleus to the outer rings (171 to 476 ppm), and there was no clear trend in the rind (866 to 134 ppm) (Fig. 53).

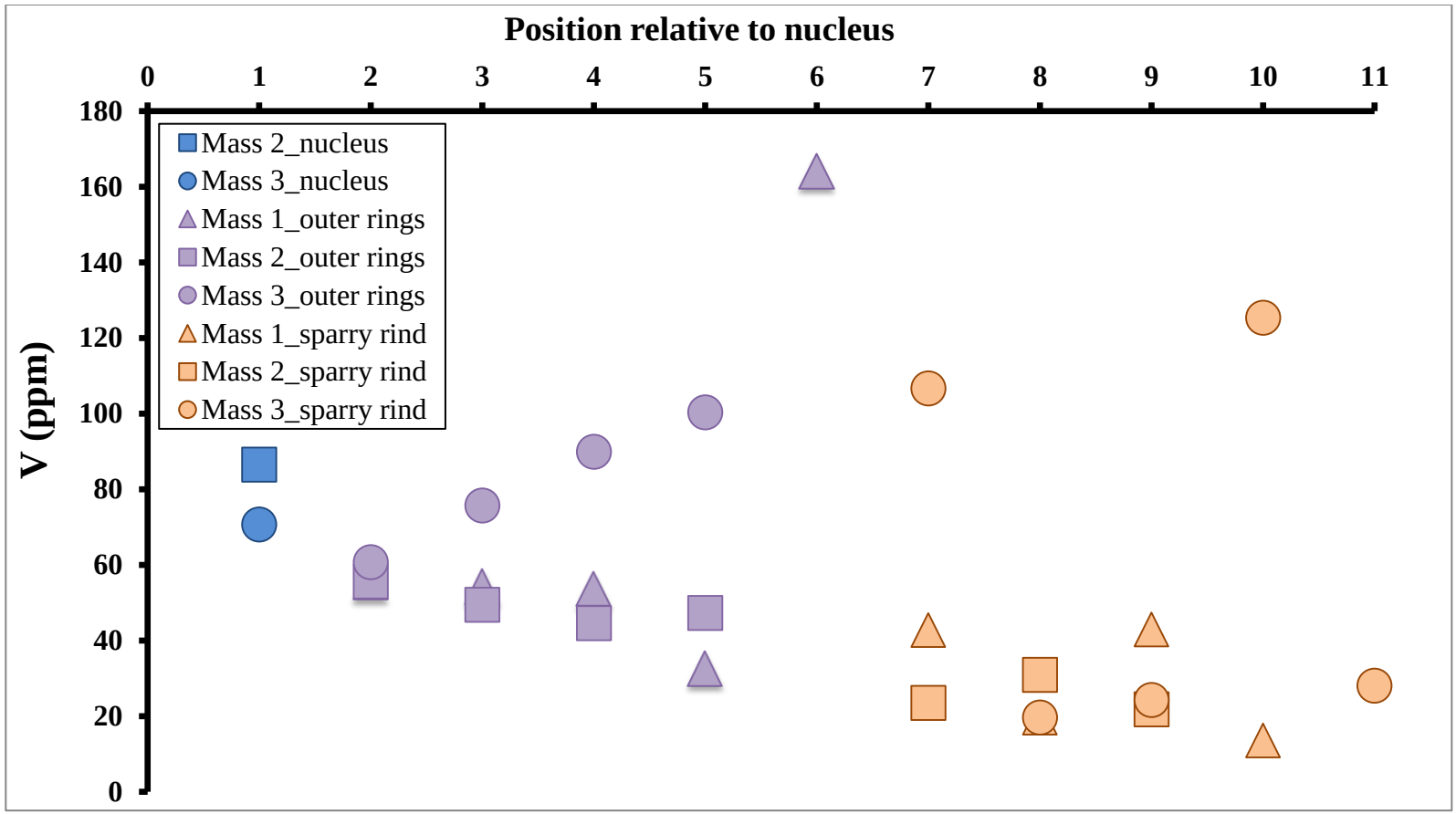

Figure 51. Trace metal analysis results for V in all three carbonate masses (concentrations reported in ppm). See Figures 14-16 for location of sample points.

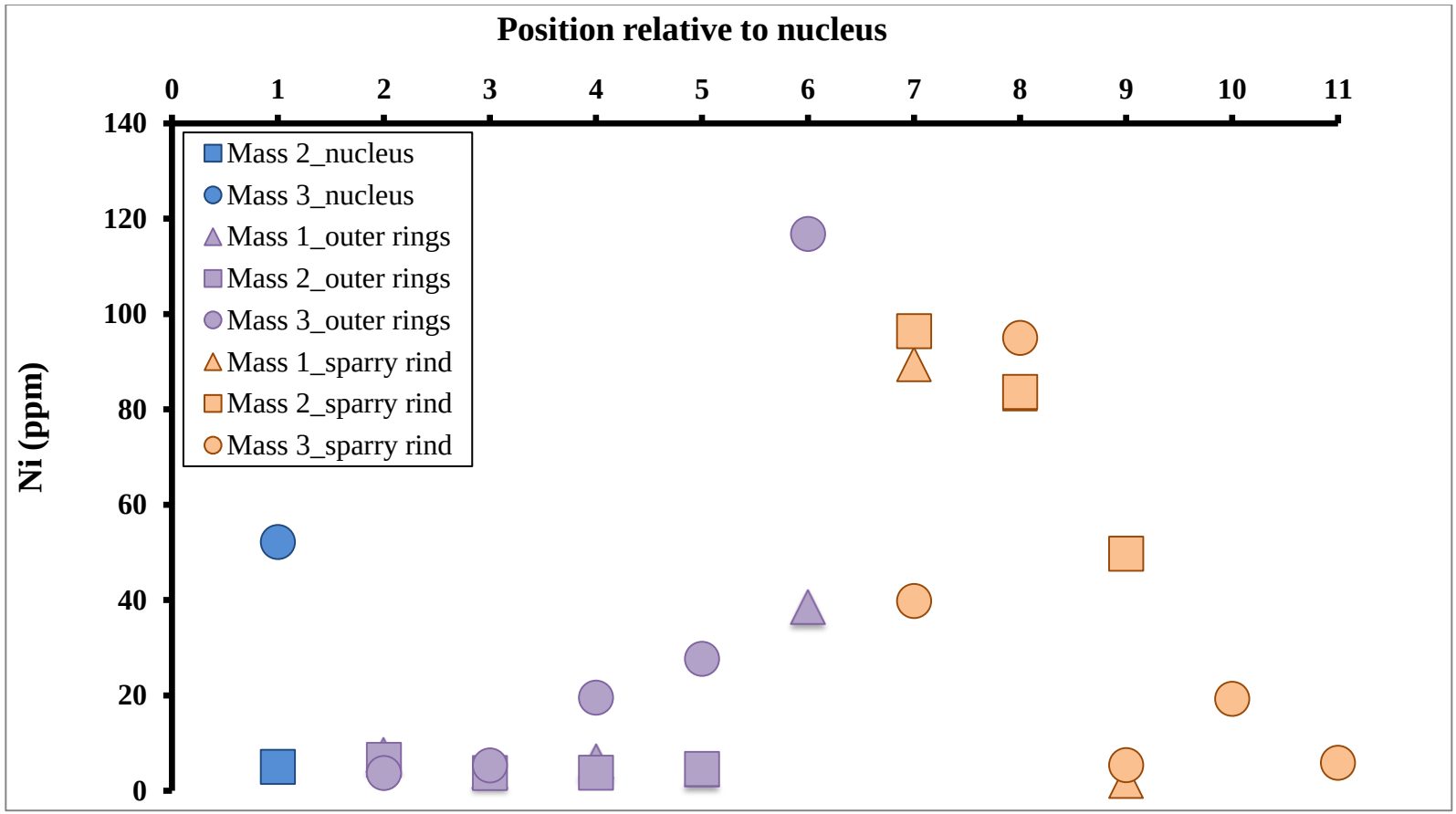

Figure 52. Trace metal analysis results for Ni in all three carbonate masses (concentrations reported in ppm). See Figures 14-16 for location of sample points.

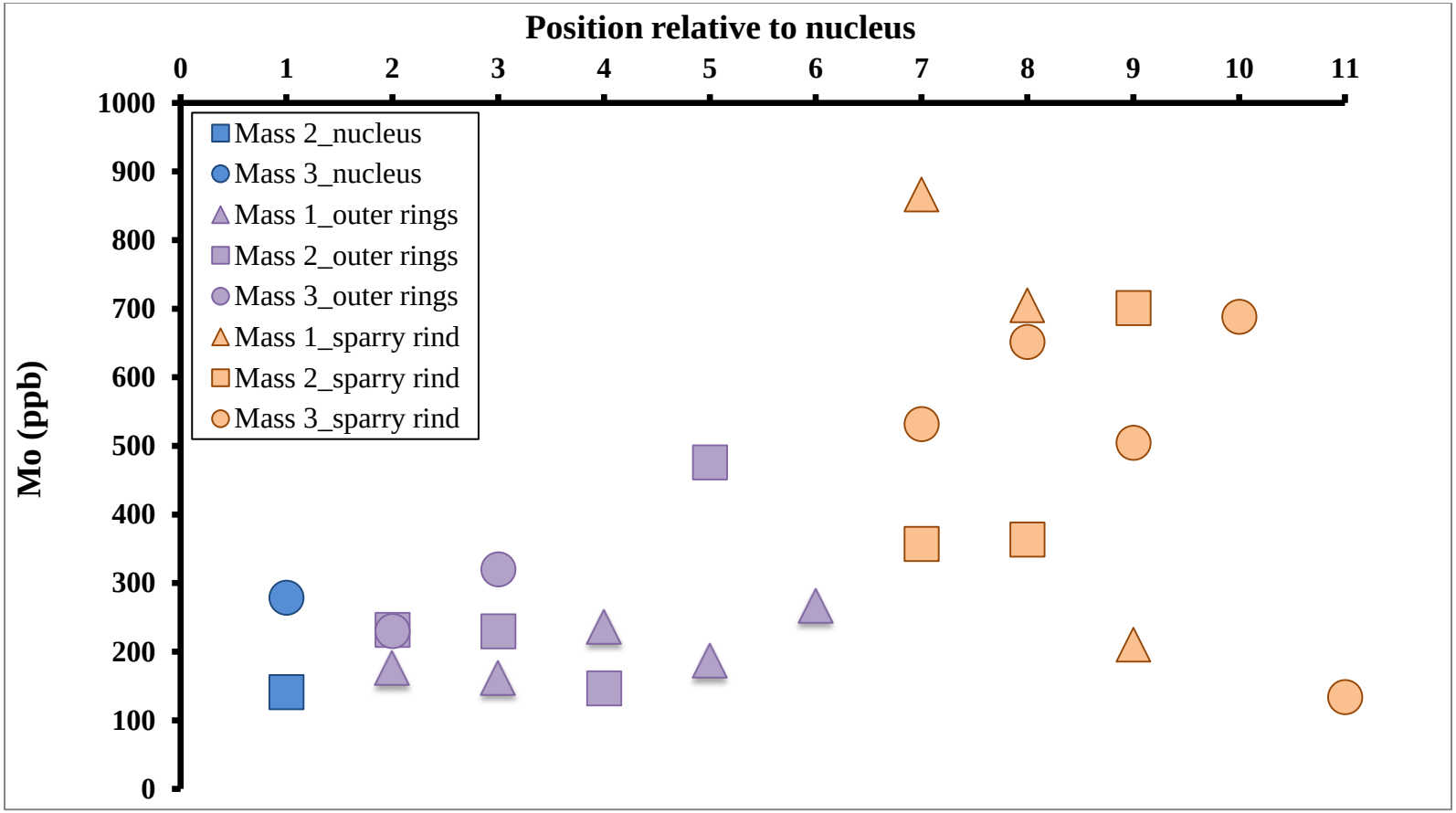

Figure 53. Trace metal analysis results for Mo in all three carbonate masses (concentrations reported in ppb). See Figures 14-16 for location of sample point

CHAPTER V

DISCUSSION

Field, petrologic, and geochemical results suggest a marine origin for the carbonate masses. This is supported primarily by marine fossils, including radiolarians, conodonts, rugose corals, and bivalves (Figs. 23, 24, 30-32). Vugs completely filled with isopachous cement further support a marine origin, as opposed to partial cements of a meniscus shape between grains, which indicate a vadose environment that was possibly karstic (Figs. 24, 25). Radiolaria are a hallmark of the Woodford Shale and the associated novaculitic chert in Oklahoma and indicate a major contribution of planktonic sediment (Sullivan, 1985; Kirkland et al. 1992; Cecil, 2016). Preservation of the delicate features of these microfossils supports our initial hypothesis that these masses preserve the precompactional fabric of the host sediment. The occurrence of abundant radiolaria and phosphate nodules indicates that, like the enveloping Woodford Shale, the limestone formed in an area influenced by marine upwelling (Figs. 13, 22, 27). Concentration of rugose corals and pin shells in the limestone masses, however, is unusual for the Woodford Shale. Rugose corals and *Pinna*-type bivalves indicate that the sea bottom supported epibenthos, yet no evidence for infauna, such as feeding burrows, was identified. The corals, moreover, indicate that sediment was either deposited in or was transported from an area with marine conditions (i.e., normal salinity and oxygenation). Broken phosphate nodules and blocks of limestone within the masses, moreover, indicate that at least some of the limestone was reworked (Fig. 17). This could have occurred shortly after formation of the outer rings but before formation of the sparry rind, such as during Late Pennsylvanian or pre-Cretaceous exposure and supports one of our initial

hypotheses of the carbonate masses being altered by soil forming processes during this tectonically active time.

Although fossil content was an important part of the original fabric of the carbonate masses, a broad range of field, petrologic, and geochemical evidence points toward a complex diagenetic and burial history. In hand sample, concentric banding defined by reddening in polished slabs is most likely a product of weathering over time, and this banding contributes to the concretionary appearance of the masses (Figs. 14-16). The optical fabric of the masses is dominated by microcrystalline calcite, and examination under crossed polars reveals that the calcite forms much larger poikilotopic crystals (Fig. 28). Vugs are common, and their shape and size (round to sub-angular, up to 8 cm) suggest they formed primarily by dissolution of limestone (Fig. 25) and, to a lesser extent by mechanical reworking of the masses (Fig. 17). Highly angular clasts may have formed by brecciation of the limestone and subsequent filling of the voids with calcite spar (Fig. 41) during uplift and exposure. Intercrystalline porosity may have formed by dissolution (Fi. 40). Cement stratigraphy indicates multiple generations of rind growth but only one generation of calcite vug fill (Figs. 45-46). Alternating smooth bands in the outer rind with rough crystal faces indicate periods of disturbed mineral growth possibly due to exposure and dissolution of the outer rind.

A consistent trend of $\delta^{13}C$ enrichment was observed from the nucleus to the to the outer rind (-20.09 to +13.59 ‰) in all three carbonate masses (Fig. 48). This trend is consistent with carbonate concretion values reported in the literature (Hudson 1978; Astin and Scotchman 1988; Coniglio and Cameron 1990; Scotchman 1991, Mozley and Burns, 1993) and supports part of the initial hypothesis that these are concretionary masses (Fig. 48). The $\delta^{13}C$ isotopic values from the nucleus and outer rings (-20.09 to -7.40 ‰) are consistent with limestone formed in marine waters with periods of meteoric alteration (Nelson and Smith, 1996;) (Fig. 54). $\delta^{13}C$ values become much higher in the rind (-3.95 ‰ to +13.59 ‰) and suggest burial and CO2 reduction

cement that is consistent with calcite precipitated in a methanogenic environment below the sulfur-methane transition zone (SMTZ), where CO_2 is reduced (Nelson and Smith, 1996). A positive trend in $\delta^{13}C$ from the core to the outer rings was also noted in the Devonian carbonate masses in the Ohio Shale (-19.5 to 11.2‰) (Clifton, 1957). These masses are seen as somewhat analogues for the Woodford carbonate masses, except that they like as sparry rind. Kirkland et al. observed a $\delta^{13}C$ values of -7.2 to -26‰ in the mass core and +5.8‰ in the sparry rind of a large Woodford carbonate mass in the quarry.

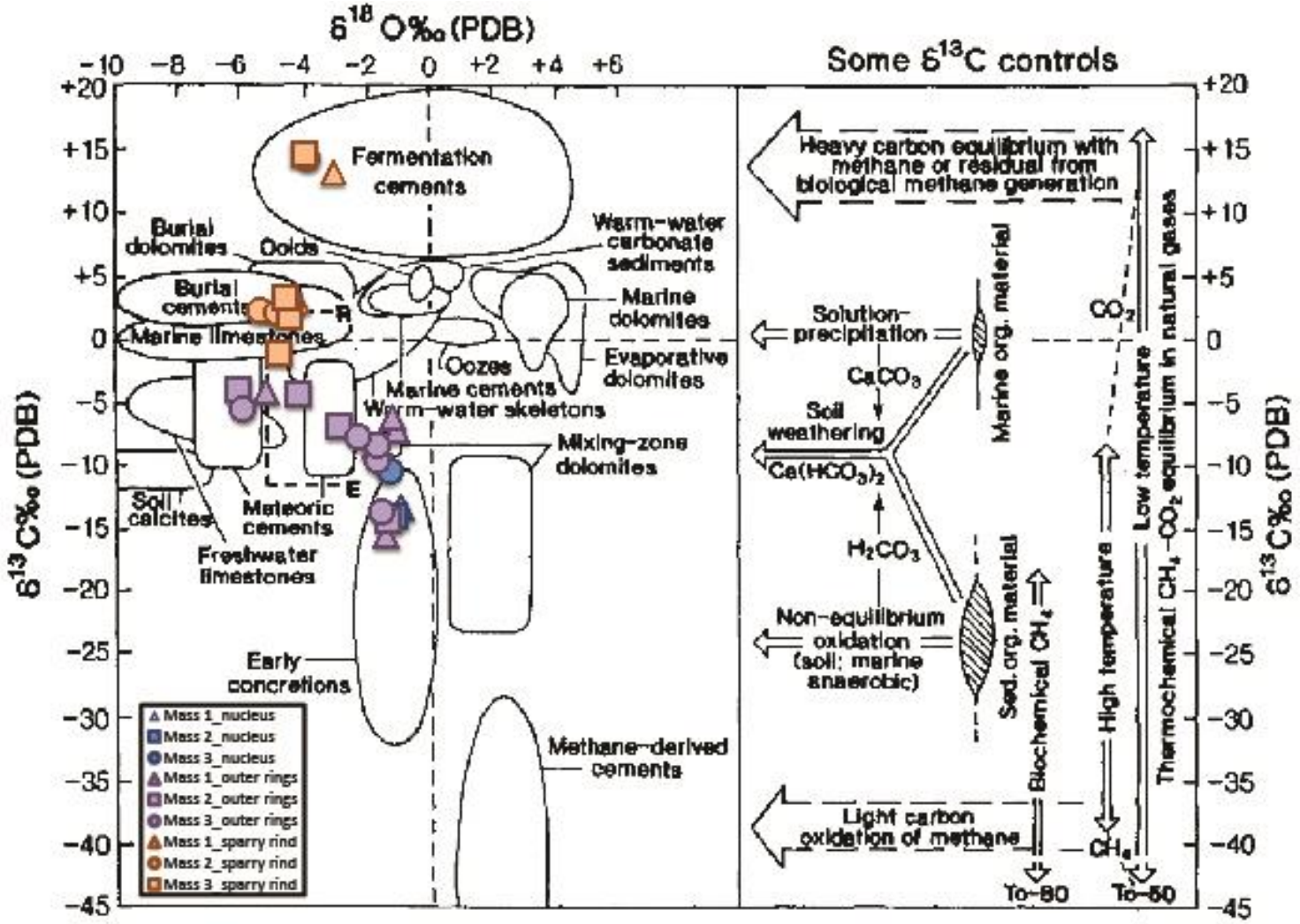

Figure 54. Diagram of generalized $\delta^{18}O$ and $\delta^{13}C$ cross plot fields for carbonate (After Nelson and Smith, 1996). Isotope values for the three small carbonate masses from the McAlister Cemetery Quarry are plotted on the diagram.

Although carbon isotope results from the outer rind indicate enrichment in ^{13}C due to minerals precipitated in the zone of methanogenesis, the presence of hematite in the outer rind indicates an increase in oxygen availability. One explanation for this geochemical zoning is fluctuation of redox conditions during rind formation. Accordingly, most calcite appears to have been precipitated under conditions favorable to microbially mediated CO_2 reduction. The hematitic rinds may suggest occasional oxidation, as evidenced by discontinuities in growth lamellae (Figs. 14-16). Moreover, both the degradation of Woodford organic matter, which facilitated microbial methanogenesis, and the uplift of the Criner Hills Uplift from the Late Pennsylvanian into the Cretaceous (i.e., angular unconformity in Pennsylvanian section, pre-Early Cretaceous unconformity, and post-Cretaceous exhumation) may have oxidized the carbonate mass matrix and hematitic layers in the rind.

Oxygen isotope values of carbonate minerals typically reflect the isotopic composition and temperature of the pore fluids in which they precipitated (Epstein et al., 1953). The $\delta^{18}O$ values of the carbonate masses show a consistent trend throughout all three samples that correlate to the layers (nucleus, outer rings and sparry rind) seen within the samples and further suggest that these masses are a consistent record of the change in pore fluid chemistry in the depositional environment from the initial formation of these carbonate masses until the end of their growth (Fig. 49). The isotopic trends cannot be analyzed independently of the basic lithologic observations. Recrystallization of carbonate minerals is a possibility, which would subject the $\delta^{18}O$ to isotopic overprinting and thus unable to be directly compared to temperature indicators of known first generation carbonate minerals. Although extensive replacement of microfossils were observed in the Woodford carbonate masses, the original radiolarian-rich host shale fabric is still preserved in most part of the masses so we can most likely rule out recrystallization (Hudson and Friedman 1974; Carpenter et al. 1988; Coniglio and Cameron 1990). Two sets of trends were observed in the data of the Woodford Shale carbonate masses: 1) a progressive depletion in $\delta^{18}O$

from the nucleus to the outer rings (- 0.86 to -5.99‰) and 2) a progressive enrichment in $\delta^{18}O$ from start of the rind to it's outer perimeter to (-5.47 to -3.06‰). This distinction indicates a change in pore fluid chemistry from the onset or rind formation, one in which O was sourced from a more $\delta^{18}O$-rich environment (Mozley and Burns, 1993). The Ohio carbonate masses, conversely, show a positive trend in $\delta^{18}O$ from the mass core to the outer rings (-10.4 to 3.6‰). Kirkland et al. 1992 observed $\delta^{18}O$ values of -2.3 to -0.3‰ in the mass core and -13.3‰ in the sparry rind of a large Woodford carbonate mass from the quarry.

Nitrogen is a biologically driven geochemical parameter that requires redox reactions in order to incorporate N gas into molecules. A correlation between oxygen availability in bottom waters and $\delta^{15}N$ has been observed where $\delta^{15}N$ is lowest in anoxic and oxic waters and higher in suboxic waters (Quan et al., 2008). The Woodford carbonate masses have the lowest $\delta^{15}N$ values in the edge of the outer rings, transitioning to the rind, and highest closer to the nucleus and within the rind (Fig. 50). One explanation could be that initial concretion formation occurred just below the sediment-water interface and then less oxygen became available in the pore waters with deeper burial of the masses as the outer rings and rind were forming, followed by increased oxygen availability as the Criner Hills were uplifted. Bulk $\delta^{15}N$ values for Woodford carbonate masses (-12.0 to +16.8‰) have a wider range of values than observed in the host Woodford Shale (1.5‰ to 3.5‰) (Quan et. al, 2013).

V, Ni and Mo were chosen to highlight for their paleoredox implications. The average elemental concentrations of the Woodford carbonate masses (Figs. 51-53) (V_{Avg}= 640 ppm, Ni_{Avg}=37 ppm, Mo_{Avg}= 66 ppb) were average for V concentration and low for Ni and Mo concentrations when compared to concentrations in Devonian-Mississippian black shales (V_{Avg}= 193 to 1166 ppm, Ni_{Avg}= 83 to 282 ppm, Mo_{Avg}= 82 to 297 ppm) (Rimmer, 2003). Molybdenum has been suggested to indicate anoxic conditions (Dean, 1997). The trends of the Mo results for the masses suggest that less oxygen became available in the pore waters with continued initial

concretion formation and then decreased, with some fluctuation, from the onset of rind formation.

One way of looking at metal input into a system is by analyzing the trace metal concentration relative to Al concentration (Al is a proxy for detrital clay and other aluminous silicates). Plots of trace metal ratios show an enrichment of all metals within the sparry rind relative to the core of the masses, suggesting that there was an increase in metal availability during formation of the calcitic rind (Figs. 56-58).

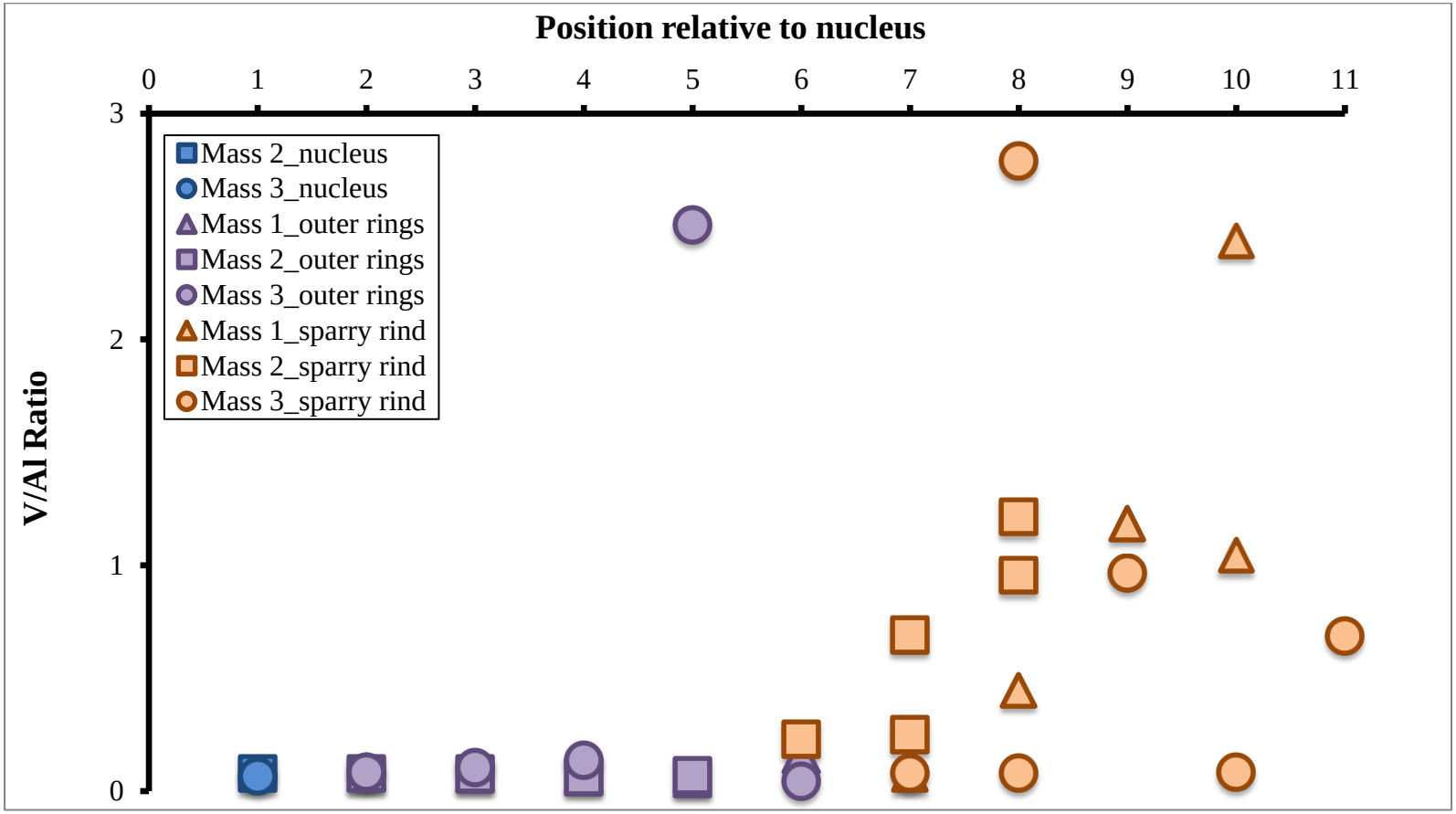

Figure 56. Plot of V/Al ratio in the limestone masses. Note increase in the ratio within the outer rind.

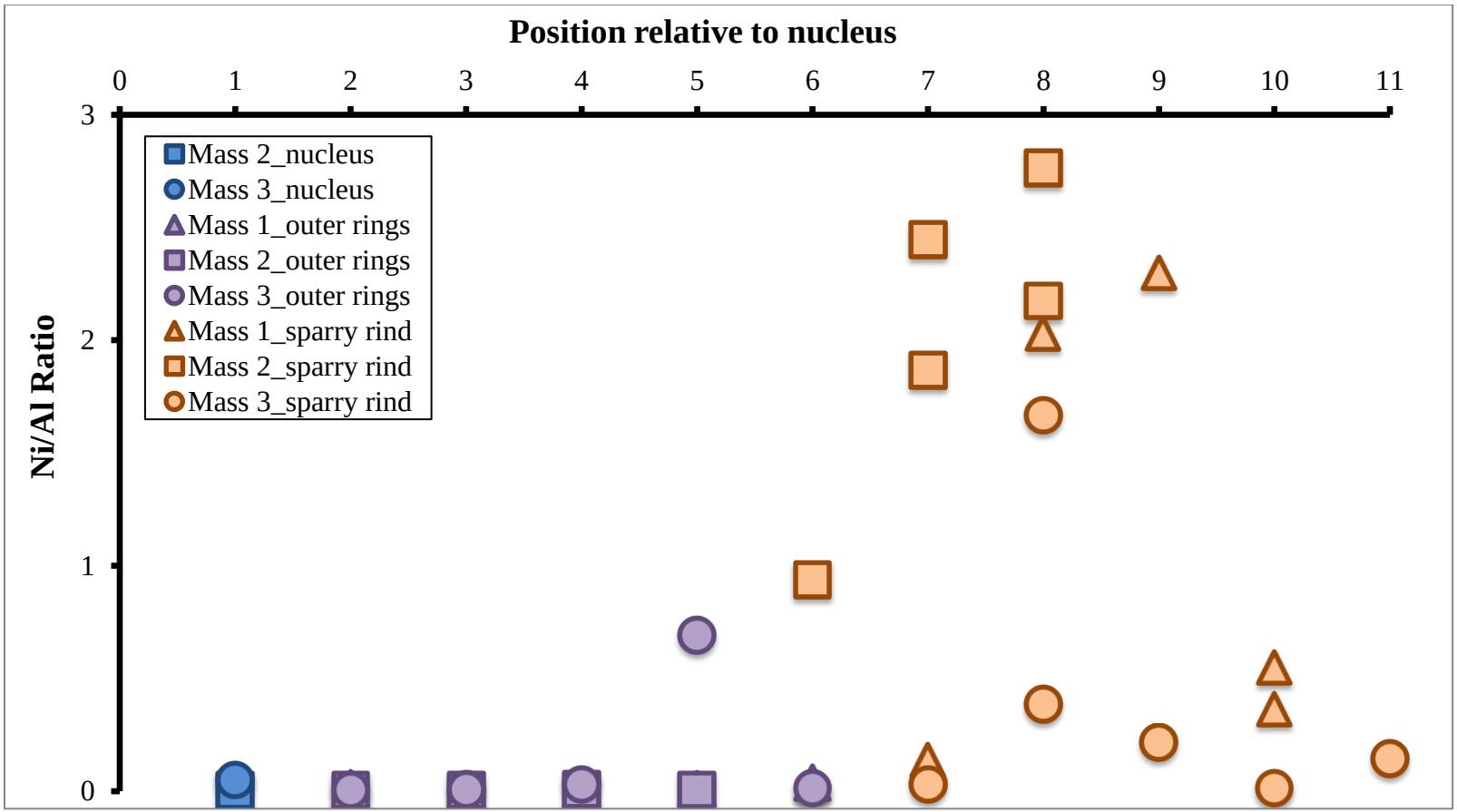

Figure 57. Plot of Ni/Al ratio in the limestone masses. Note increase in ratio within the outer rind.

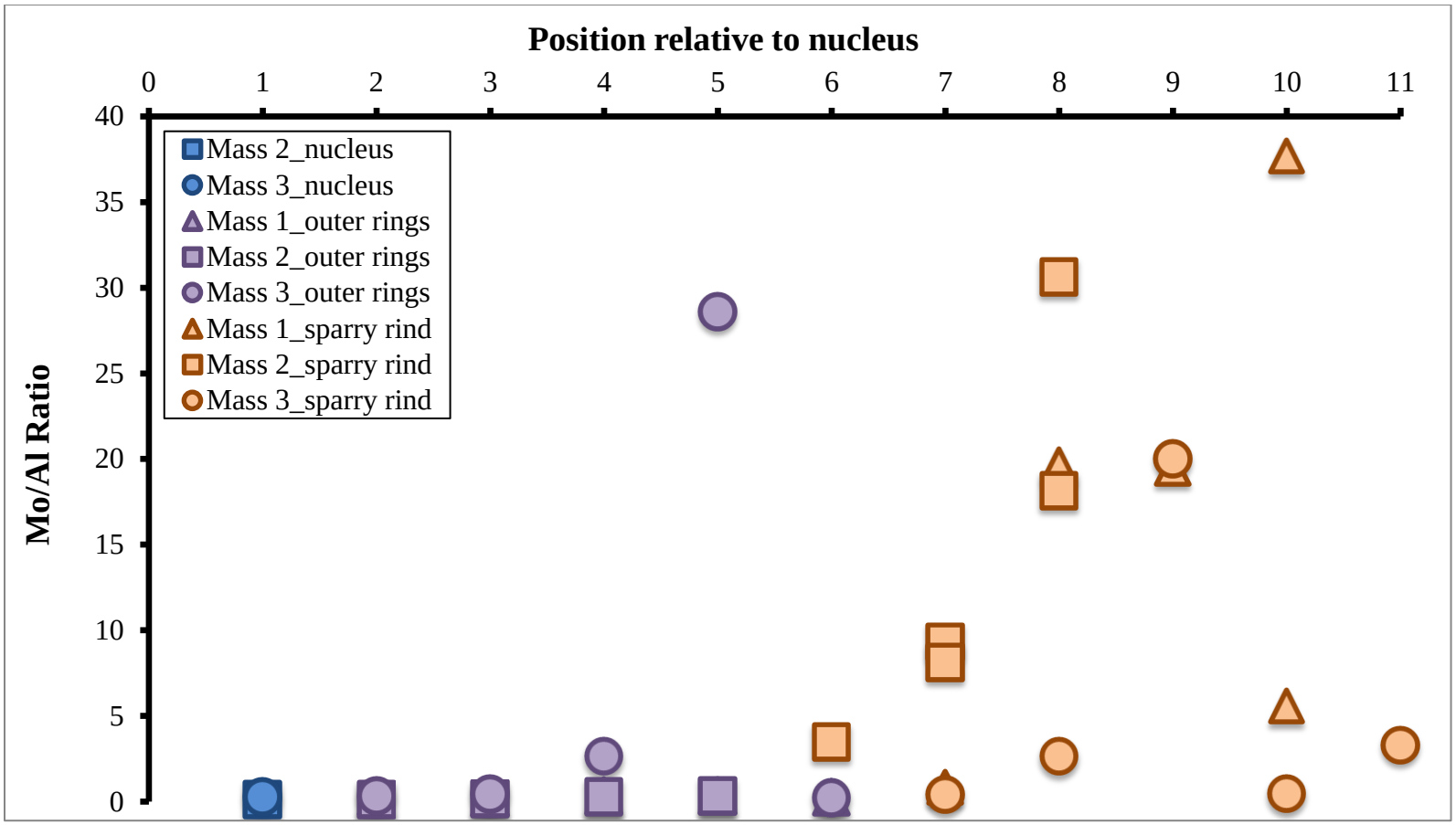

Figure 58. Plot of Mo/Al ratio in the limestone masses. Note increase in the ratio within the outer rind.

Table 1. Paragenetic Model of formation and subsequent diagenetic alteration of Woodford Shale carbonate concretions.

Depositional and Diagenetic Events	Initial Burial	Deeper Burial	Late Pennsylvanian		Cretaceous
Black shale (chert)					
Phosphate nodules					
Authigenic carbonate					
Reworking of limestone					
Meteoric alteration					
Calcitic rind, hematite					

CHAPTER VI

SUMMARY AND CONCLUSIONS

The goal of this thesis research was to characterize the depositional environment, diagenetic history, and mechanisms by which the mysterious Woodford Shale carbonate masses formed using the following tools: (1) descriptions of the external and internal sedimentologic, biologic, and diagenetic fabrics and structures of the limestone masses (2) analyzing petrological and geochemical indicators preserved in the host rock and cements, and (3) synthesizing the results into a conceptual model of the origin of the carbonate masses. The initial hypotheses were that the masses are (1) concretions preserving the precompactional fabric of the shale in a manner similar to coal balls, or alternatively, (2) remnants of a primary carbonate unit that was deposited as part of the Woodford Shale, and (3) have been altered by soil-forming processes, perhaps in association with development of a Late Pennsylvanian angular unconformity and a sub-Cretaceous disconformity in the Criner Hills area. Previous research conducted on the carbonate concretions in the McAlister Cemetery Quarry suggests that these masses are simple concretions, having accreted in response to early diagenetic processes within the black shale and chert. Results of this study reveal a much more complex diagenetic history than discussed in previous research, one in which they formed in pore waters with varying paleoredox conditions and involves the complete geologic history of the Woodford Shale in the Criner Hills Uplift.

Petrographic evidence (marine fossils, isopachous cement) and geochemical results ($\delta^{13}C$ and $\delta^{18}O$) indicate that initial concretion formation occurred just below the sediment water interface with normal Devonian waters above and early diagenetic processes having preserved the precompactional fabric of the Woodford Shale, as seen through preserved delicate features of microfossils (radiolaria, *Tasmanites)*. Early concretion nucleus growth began just below the sediment water interface. With an increase in burial depth the mass continued to form the outer rings with gradual heavier isotopic signatures (C, O and N isotopes) trends and trends in trace metal enrichment (V, Ni and Mo trace metals). Microbial mediated methanogenesis gave way for creating a very isotopically heavy C pore water environment in which the calcitic sparry rind of all three masses formed ($\delta^{13}C_{Rind=}$ -3.95 ‰ to +13.59‰). Possible three-phase inclusions observed in the rind suggest suspension of organic matter in medium fluid during concretion formation. Evidence for oxidation of the carbonate masses (red-stained matrix, hematitic bands) may furthermore give evidence for uplift of the Woodford Shale in the Criner Hills area associated with the sub-Cretaceous unconformity suggested in literature. Tectonic activity could possibly explain the conglomerate nature of the largest concretion studied in the lab. Erosional surfaces are clearly seen in CL images to support intermittent disturbed crystal growth during rind formation. Complex replacement of concretion fabric and evidence for reworked limestone is also seen (multi-generation vug cement and chert, broken phosphate nodules, blocks of limestone in Mass 3). All evidence supports initial hypotheses of these masses being true concretions but with a complex diagenetic history, which records all paleoactivity that took place during the Woodford Shale deposition and subsequent uplift in the Criner Hills Area.

REFERENCES

Allen, R., 2000, Complex structural features of the Ardmore Basin: Stratigraphy, Mountain Building and Complex Geological Structures of the Ardmore Basin: Shale Shaker, v. 51, p. 10.

Alvi, K., and Winterhal, B., 2001, Authigenic mineralisation in the temporally anoxic Gotland Deep, the Baltic Sea: Baltica, v. 14, p. 74–83.

Amsden, 1975, Hunton Group (Late Ordovician-Silurian and Early Devonian) in the Arkoma Basin of Oklahoma: Oklahoma Geological Survey Bulletin 121, p. 11-14.

Astin, T.R., and Scotchman, C., 1988, The diagenetic history of some septarian concretions from the Kimmeridge Clay, England: Sedimentology, v. 35, p. 349-368.

Boggs, S. and Krinsley, D., 2006, Applications of cathodoluminescence imaging to the study of sedimentary rocks, p. 5-37.

Callner, S. A., 2014, An integrated approach to understanding sedimentary structures and depositional processes in Devonian-Mississippian black shale: The Woodford Shale and associated strata in the southern Midcontinent: Stillwater, Oklahoma State University, unpublished Master's thesis, 94 p.

Calvert, S.E., & Pederson, T.F., 1993, Geochemistry of recent oxic and anoxic marine sediments: implications for the geological record, in Marine Geology, v. 113, p. 67-88.

Cardott, B., 2012, Thermal maturity of Woodford Shale gas and oil plays Oklahoma USA: International Journal of Coal Geology, v. 103, p. 109–119.

Cardott, B., and Chaplin, J., 1993, Guidebook for selected stops in the Western Arbuckle Mountains, Southern Oklahoma: Oklahoma Geological Survey Special Publication 93, p. 1-10.

Carpenter, S.J., Erikson, J.M., Lohmann, K.C. and Owen, M.R., 1988, Diagenesis of fossiliferous concretions from the Upper Cretaceous Fox Hills Formation, North Dakota: Journal of Sedimentary Petrology, v. 58, p. 706-723.

Cecil, K. A., 2016, Origin and characteristics of Silurian-Mississippian Novacultic Chert in the southern Midcontinent: Stillwater, Oklahoma State University, unpublished Master's thesis

Clifton, H., 1957. The carbonate concretions of the Ohio Shale: Ohio Journal of Science, v. 57, no. 2, p. 113-124.

Comer, J.B., 1992, Organic geochemisty and paleogeography of Upper Devonian formations in Oklahoma and western Arkansas, in K.S. Johnson and B.J. Cardott, eds., Source rocks in the southern Midcontinent, 1990 symposium: Oklahoma Geological Survey Circular, 93, p. 70-93.

Comer, J.B., 2005, Facies distribution and hydrocarbon production potential of Woodford Shale in the southern Midcontinent, *in* Cardott, B. J., ed., Unconventional Energy Resources in the Southern Midcontinent, 2004 Symposium, Oklahoma Geological Survey, Circular 110, p. 51-62.

Comer, J.B. and Hinch, H., 1987, Recognizing and quantifying expulsion of Oil from the Woodford Formation and age-equivalent rocks in Oklahoma and Arkansas: American Association of Petroleum Geologists Bulletin, v. 71, p. 844-858.

Conoligio, M. and Cameron, J.S., 1990, Early diagenesis in a potential oil shale: evidence from calcite concretions in the Upper Devonian Kettle Point Formation, southwestern Ontario: Bulletin of Canadian Petroleum Geology, v. 38, p. 64-77.

Criss, R.E., Cook, G.A. and Day, S.D., 1836, An organic origin for the carbonate concretions of the Ohio Shale, in U.S. Geological Survey Bulletin, p. 1-21.

Dean, W.E., Gardner, J.V., Piper, D.Z., 1997, Inorganic geochemical indicators of glacial–interglacial changes in productivity and anoxia on the California continental margin, in Geochimica Cosmochima, Acta. 61, 4507–4518.

Edwards, A.B. and Baker, G., 1951, Some occurrences of supergene iron sulphides in relation to their environments of deposition: Journal of Sedimentary Petrolology, v. 21, p. 34-46.

Epstein, S., Buchsbaum, R., Lowenstam, H.A., and Urey, H.C., 1953, Revised carbonate-water isotopic temperature scale: Geologocal Society of America Bulletin, v. 64, p. 1315-1326.

Ettensohn, F.R., and Lierman, R.T., 2012, Chapter 4, Large-scale tectonic controls on the origin of Paleozoic, dark-shale, source-rock basins: Examples from the Appalachian foreland-basin region, eastern United States, *in* Gao, D., ed., Tectonics and

sedimentation: Implications for petroleum systems: American Association of Petroleum Geologists Memoir 100, p. 95–124.

Ham, W.E., 1975, Regional Geology of the Arbuckle Mountains Oklahoma, *in* Ham, W.E., eds., Guidebook for field trip no. 5: The Geological Society of America 1973 Annual Meeting: Oklahoma Geological Survey, p. 1-17.

Hass, W., Huddle, J., 1965, Late Devonian and Early Mississippian age of the Woodford Shale in Oklahoma as determined from Conodonts, *in* Geological Survey research: U.S. Geological Survey Professional Paper 525-D, p. 125-132.

Hatch, J.R. and Leventhal, J.S., 1992, Relationship between inferred redox potential of the depositional environment and geochemistry of the Upper Pennsylvanian (Missourian) Stark Shale Member of the Dennis Limestone, Wabaunsee County, Kansas, U.S.A, in Chemical Geology, v. 99, p. 65-82.

Hansen, M.C., Ohio Shale Concretions, in GeoFacts: Ohio Department of Natural Resouces Division of Geological Survey, no. 4.

Hudson, J.D., and Freedman, I., 1974, Carbon and oxygen isotopes in concretions: relationship to pore-water changes during diagenesis, in Cadek, J. and Paces, T., eds., Proceedings, International Symposium on Water-Rock Interaction, Czechoslovakia: Geological Survey, Prague, p. 331-339.

Johnson, K., Amsden, T., Denison, R., Dutton, S., Goldstein, A., Rascoe, B., Sutherland, P., and Thompson, C., 1988, Geology of the Southern Midcontinent: Oklahoma Geological Survey Special Publication 89, p. 1-9.

Johnson, K., Cardott, B., 1992, Geologic framework and hydrocarbon source rocks of Oklahoma, *in* K.S. Johnson and B.J. Cardott, eds., Source Rocks in the Southern Midcontinent, 1990 Symposium: Oklahoma Geological Survey Circular 93, p. 21-37.

Jones, B., & Manning, D. (1994). Comparison of geochemical indices used for the interpretation of paleoredox conditions in ancient mudstones, in Chemical Geology, p. 111- 129.

Kirkland, D., Denison, and Gormly, J., 1992, Geology and organic geochemistry of the Woodford Shale in the Criner Hills and Western Arbuckle Mountains Oklahoma, *in* K.S. Johnson and B.J. Cardott, eds., Source Rocks in the Southern Midcontinent 1990 Symposium: Oklahoma Geological Survey Circular 93, p. 38-69.

Kvale, E. P., and Bynum, J., 2014, Regional upwelling during Late Devonian Woodford deposition in Oklahoma and its influence on hydrocarbon production and well

completions (abstract): AAPG Technology Workshop Proceedings, unpaginated CD-ROM.

Lambert, M., 1993, Internal Stratigraphy and organic facies of the Devonian-Mississippian Chattanooga (Woodford) Shale in Oklahoma and Kansas, *in* Source Rocks in a Sequence Stratigraphic Framework: AAPG Studies in Geology 37, p. 163-176.

Machel, H. G. and E. A. Burton, 1991. Factors governing cathodoluminescence in calcite and dolomite, and their implications for studies of carbonate diagenesis, *in* Luminescence Microscopy and Spectroscopy: Qualitative and Quantitative Applications, SEPM Short Course 25, pp. 37–57.

Machel, H.G., R.A. Mason, A.N. Mariano, and A. Mucci, 1991, Causes and emission of luminescence in calcite and dolomite, *in* Luminescence Microscopy and Spectroscopy: Qualitative and Quantitative Applications, SEPM Short Course 25, pp. 9–25.

Mozley, P.S., and Burns, S.J., 1992, Oxygen and carbon composition of marine carbonate concretions: An overview, in Journal of Sedimentary Petrology: Society for Sedimentary Geology, v. 63, n. 1, p. 73-83.

Pashin, J. C., McIntyre-Redden, M. R., Mann, S. D., Kopaska-Merkel, D. C., Varonka, M., and Orem, W., 2014, Relationships between water and gas chemistry in mature coalbed methane reservoirs of the Black Warrior Basin: International Journal of Coal Geology, v. 126, p. 92-105, http://dx.doi.org/10.1016/j.coal.2013.10.002.

Pitman, J. K., Pashin, J. C., Hatch, J. R., and Goldhaber, M. B., 2003, Origin of minerals in joint and cleat systems of the Pottsville Formation, Black Warrior basin, Alabama: implications for coalbed methane generation and production: American Association of Petroleum Geologists Bulletin, v. 87, p. 713-731.

Puckette, J., Boardman D.R., Watney, W.L., 2013, Woodford Shale, correlating rock properties in outcrop and core with Wireline log characteristics: Search and Discovery Article #50885, p. 46.

Quan, T.M., van de Schootbrugge, B., Field, M.P., Rosenthal, Y., Falkowski, P.G., 2008. Nitrogen isotope and trace metal analyses from the Mingolsheim core (Germany): evidence for redox variations across the Triassic-Jurassic boundary, in Global Biogeochemical Cycles 22, GB2014.

Quan, T.M., Adigwe, E.N., Riedinger, N., Puckette, J., 2013, Evaluating nitrogen isotopes as proxies for depositional environmental conditions in shales: Comparing Caney and Woodford Shales in the Arkoma Basin, Oklahoma, in Chemical geology, v. 360-361, p. 231-240.

Rimmer, S., 2004, Geochemical paleoredox indicators in Devonian-Mississippian black shales, Central Appalachian Basin, USA, in Chemical Geology, v. 206, 373-391.

Roedder, E., 1984, Fluid inclusions, *in* Ribbe, P., ed., Reviews in mineralogy and geochemistry: Mineralogical Society of America, v. 12, p. 6-46.

Scotchman, I.C., 199 I, The geochemistry of concretions from the Kimmeridge Clay Formation of southern and eastern England: Sedimentology, v. 38, p. 79-106.

Siesser, W.G., 1978, Petrography and geochemistry of pyrite and marcasite in DSDP Leg 40 sediments: Initial Reports of the Deep Sea Drilling Project, Supplement to Volumes 38, 39, 40, and 41, p. 767–775.

Smith, A., Nelson, C., 1996, Stable oxygen isotope compositional fields for skeletal and diagenetic components in New Zealand Cenozoic nontropical carbonate sediments and limestones a synthesis and review: New Zealand Journal of Geology and Geophysics, v. 39, p. 93-107.

Sullivan, K.L., 1985, Organic facies variation of the Woodford Shale in western Oklahoma: Shale Shaker, v. 35, p. 76-89.

Tarashchan, A.N. and G. Waychunas, 1995. Interpretation of luminescence spectra in terms of band theory and crystal field theory. Sensitization and quenching, photoluminescence, radioluminescence, and cathodo-luminescence, *in* Marfunmin, A. S. (ed.), Advanced Mineralogy 2, Methods and Instrumentations: Results and Recent Developments, Berlin, Springer-Verlag, pp. 124–35.

Walker, W.M., 2006, Structural Analysis of the Criner Hills, South-Central Oklahoma: Baylor University, unpublished Master's thesis.

Wilson, L., 1958. Oklahoma's oldest fossil trees: Oklahoma Geology Notes, v. 18, p. 172-177.

VITA

Danielle P. Martin

Candidate for the Degree of

Master of Science

Thesis: GEOLOGIC CHARACTERIZATION OF ENIGMATIC CARBINATE MASSES IN THE WOODFORD SHALE, CRINER HILLS AREA, OKLAHOMA

Major Field: Geology

Biographical: Danielle Martin was born in Miami, Florida and grew up in Maplewood, New Jersey, graduating high school with a strong interest in math and science.

Education:

Completed the requirements for the Master of Science in Geology at Oklahoma State University, Stillwater, Oklahoma in May 2017.

Completed the requirements for the Bachelor of Arts in Earth and Environmental Science at Wesleyan University, Middletown, CT/USA in 2014.

Experience: Held a petroleum geology internship at WPX Energy in Tulsa, OK and an environmental consulting internship at Tierra Consulting Group Inc in Fort Lauderdale, FL.

Professional Memberships:

American Association of Petroleum Geologist (AAPG)
Geological Society of America (GSA)
National Association of Black Geoscientists (NABG)
Oklahoma City Geological Society (OCGS)